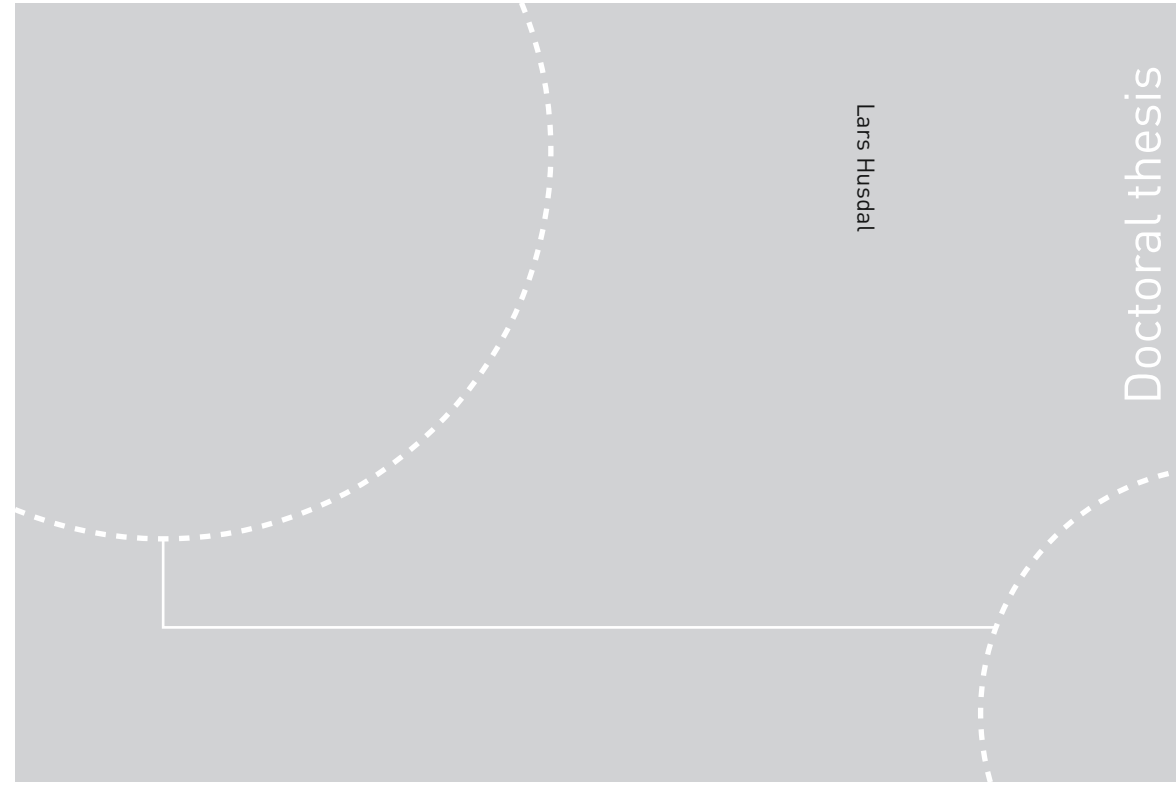


ISBN 978-82-326-2466-9 (printed ver.)
ISBN 978-82-326-2467-6 (electronic ver.)
ISSN 1503-8181



Doctoral theses at NTNU, 2017:197

Lars Husdal

Viscous Phenomena and Entropy Production in the Early Universe

 **NTNU**
Norwegian University of
Science and Technology

 NTNU

Doctoral theses at NTNU, 2017:197

NTNU
Norwegian University of Science and Technology
Thesis for the Degree of
Philosophiae Doctor
Faculty of Natural Sciences
Department of Physics

 **NTNU**
Norwegian University of
Science and Technology

Lars Husdal

Viscous Phenomena and Entropy Production in the Early Universe

Thesis for the Degree of Philosophiae Doctor

Trondheim, June 2017

Norwegian University of Science and Technology
Faculty of Natural Sciences
Department of Physics



Norwegian University of
Science and Technology

NTNU
Norwegian University of Science and Technology

Thesis for the Degree of Philosophiae Doctor

Faculty of Natural Sciences
Department of Physics

© Lars Husdal

ISBN 978-82-326-2466-9 (printed ver.)
ISBN 978-82-326-2467-6 (electronic ver.)
ISSN 1503-8181

Doctoral theses at NTNU, 2017:197

Printed by NTNU Grafisk senter

Abstract

This thesis looks at some phenomena in the early universe — the stage of the Universe from when it was populated by all the particles in the Standard Model, until the last positrons disappeared. More specifically from when the Universe was 10^{-12} seconds old until a few minutes after the big bang.

The first paper addresses the degrees of freedom related to the elementary particles, and show the evolution of these as the universe expands and cools. As the temperature decreases the particles will go from relativistic velocities to semi- and non-relativistic velocities, before finally disappearing. The temperature at which this happens depends on the particles masses. One important difference between relativistic and non-relativistic particles is that they cool at different rates ($T \propto a^{-1}$ vs. $T \propto a^{-2}$). If we have a mixture of both types a bulk viscous effect will arise, resulting a heat transfer between the two components. My second and third paper discuss these phenomena.

Bulk viscosity and entropy production are at their highest at the end of the lepton era, just before the neutrinos decouple at $T = 10^{10}$ K. At this time the neutrinos have a very long mean free path, resulting in large momentum transfers and heat exchange. Many previous works have concentrated their work on just the lepton era ($T = 10^{12}$ K \rightarrow 10^{10} K), a time where most of the Universe consisted of electrons, positrons, neutrinos, and photons. At higher temperatures, hadrons and eventually quarks and gluons make up a significant contribution to the particle soup. I have made a model universe where all particles except the leptons and photon are excluded. I can thus include the heavier cousins of the electron — the muon and tau. By doing this, we get a more qualitative picture of what happens as particle species goes from relativistic velocities to semi- and non-relativistic temperatures and finally disappears one by one.

Preface

This thesis is submitted to the Norwegian University of Science and Technology (NTNU) as a partial fulfillment of the requirements for the degree of Philosophiae Doctor. It is the result of six years of research at the Department of Physics at NTNU under the supervision of professors Kåre Olaussen and Iver H. Brevik.

The first part of my thesis gives a short introduction to the field of cosmology and more importantly to the subjects of viscosity and entropy in the early Universe. This part is also meant to motivate and elucidate my three papers which make up the second part of this thesis. I have tried to make this introduction fairly basic, making it accessible to people new to the field or from a related field.

Lars Husdal
Trondheim, March 2017

Acknowledgements

First, I would like to thank professor Kåre Olaussen for accepting me as his student, and your guidance and fruitful discussions during the majority of my stay here at NTNU. Secondly, thanks to professors Iver Brevik and Jens O. Andersen for helping me in my final stages of my Ph.D., their help is highly appreciated, and really accelerated my publication rate. I would also thank professor Jan Myrheim for his help.

A big shoutout to my fellow Ph.D. students, post-docs and friends whom I got to know here at NTNU: Arturo Amador Opsetmoen, Marius Eidsaa, William R. Naylor, Severin Sadjina, Lars E. Leganger, Lars T. Kyllingstad, Alireza Qaiumzadeh, Camilla Espedal, Hans Skarsvåg, Peder N. Galteland, Therese Frostad, Eva Mørtsell, Erlend Gryten, André Kapelrud, Sverre Gulbrandsen, Eirik L. Fjærbu, Stefan Rex, Dag-Vidar Bauer, Manu Linares Alegret, Fredrik Nicolai Krohg, Øyvind Johansen, Marina Jorge, and all the rest at the Department of Physics for making life here in Trondheim so enjoyable. Thanks for great discussions, cabin-trips, and other social events.

I final thanks to my family: my grandmother, my mother and father, and my brother, all of whom has been very supportive, both for my Ph.D. and life in general.

List of Papers

Paper I

Lars Husdal:

On Effective Degrees of Freedom in the Early Universe,
Galaxies 4 (2016) no. 78 [1].

Paper II

Lars Husdal:

Viscosity in a Lepton-Photon Universe,
Astrophysics and Space Science **361** (2016) no. 8 [2].

Paper III

Lars Husdal and Iver Brevik:

Entropy in a Lepton-Photon Universe,
Astrophysics and Space Science **362** (2017) no. 2 [3].

Contents

I	Thesis Part	1
1	Introduction	3
1.1	Chronology of the Universe	3
1.1.1	The very early universe	4
1.1.2	The early universe	6
1.1.3	Structure formation	9
1.2	Cosmological parameters	10
2	Particle Physics Summary	13
2.1	Standard Model of elementary particles	13
2.2	Baryon-to-photon-ratio	15
2.3	Chemical potential	16
3	Statistical Mechanics	17
3.1	Distribution function	17
3.2	Particle velocities in Maxwell-Boltzmann and Maxwell-Jüttner distributions	19
3.3	Ideal quantum gases in thermodynamic equilibrium	20
3.3.1	Thermodynamic functions	21
3.3.2	From momentum to energy integrals	22
3.3.3	Massless particle contributions	24
3.3.4	Effective degrees of freedom	24
4	The Friedmann Equations and Expansion of the Universe	29
4.1	Newtonian gravity	29
4.1.1	Deriving the Friedmann equations classically	29
4.1.2	The fluid equation	30
4.1.3	The acceleration equation	31
4.2	Friedmann equations from general relativity	31
4.3	Equations of state and the evolution of our Universe	32
4.4	Adding viscosity to the Friedmann equations	34
4.5	Viscosity by numbers and illustrations	36
4.6	The deceleration parameter	37

5 Kinetic Theory	41
5.1 Four-vectors, velocities and momenta	41
5.2 Cross sections and mean free paths	41
5.3 Weinberg-Salam model for weak interactions	42
5.3.1 Mandelstam variables	43
5.3.2 Weak currents	44
5.4 Relativistic kinetic equation	47
5.4.1 Kinetic equation without collisions	48
5.4.2 Kinetic equation with collisions	48
A Short history of Modern Cosmology	53
B Big Bang Nucleosynthesis	57
C Gamma matrices	59
II Papers	67
Paper I	69
Paper II	99
Paper III	113

Part I
Thesis Part

1 Introduction

In 1964, the two radio astronomers Arno Penzias and Robert Wilson accidentally discovered the cosmic microwave background (CMB) radiation — a clear evidence that the Universe began as a hot dense ball which has been expanding ever since. Further studies of the CMB have shown us that the early universe was in a state of almost perfect thermal equilibrium, being both isotropic and homogeneous. This is what we normally would say was a state of maximum entropy. However, as we clearly know, that was not the case, and the total entropy is continuing to increase as time goes by (the arrow of time is by many physicists related to the increase of entropy. So how could a state which is in perfect thermal equilibrium still increase its entropy? One reason has to do with the fact that a non-relativistic gas cools down at a different rate than a relativistic gas, and if we have a mixture of the two phases, entropy will increase. During the early universe era, all the massive particles of the Standard Model went from being relativistic to non-relativistic to essentially disappearing completely. One would thus assume that an increase in the total entropy would occur. Before heading into the physics, a short history of the Universe from the Big Bang to today is in order.

1.1 Chronology of the Universe

According to the latest results from the Planck satellite and other experiments, the age of the universe is 13.799 ± 0.021 billion years old [4]. Throughout this time its overall characteristics have changed significantly. There are several ways to categorize the different phases, and it all comes down to context. We will later see that one option is to distinguish them according to how the geometry of the Universe evolves due to the dominating energy contributor. This gives us radiation, matter, and dark energy dominated eras, we being in the latter era now. An illustration of these eras are given later in Figure 4.1. This is important when it comes to the geometry of the Universe as a whole.

If we are more interested in what is going on the smaller scales, a better way would be to divide the evolution into three main different phases, namely the *very early universe*, the *early universe*, and *structure formation* (and if we want, we can add another phase for the future and fate of the Universe). All three phases have distinct characteristics.

The first phase began at the earliest time we can imagine, namely the Big Bang. During this period the four forces we know today separated out one by one from what

we think was one unified force. The other main point here is that the theories we have for this period are, to some extent, speculative. By that I mean that temperatures and energies during this phase were higher than what we can produce in any accelerators today — it involves physics beyond the Standard Model.

The next phase is the early universe and begins at temperatures “low” enough to be recreated in experiments here on Earth (e.g. the LHC). We are now talking about Standard Model physics. During this phase, the Universe went from being populated by all the known particles in the Standard Model of particle physics, to essentially being dominated by the photons and neutrinos.

The third and current phase is that of structure formation. This phase started with the photon decoupling which made the Universe transparent and is the theoretical limit for how far back in time we can see using observational astronomy. During this period matter cooled down and started to clump together, thus starting to form stars, galaxies, and other structures — hence the name.

Each of these three phases consists of shorter periods, which we call *eras*, or epochs and deserves a closer look. For the early universe, I will distinguish these eras by number contribution (other sources might use mass domination).

1.1.1 The very early universe

Planck era ($0 \text{ s} \rightarrow 10^{-43} \text{ s}$). According to the classical Big Bang theory, the Universe began as a singularity with infinite density and temperature. Quantum effects, however, are not taken into account. Our understanding of quantum theory only makes sense in a certain range, that below the Planck scale. For time this is called the Planck time and is defined as $\sqrt{\hbar G/c^5} = 5.39 \times 10^{-44} \text{ s}$) Everything before this is what we call the *Planck era*. Although we know very little about this era, we believe that the gravitational force will be as strong as the other fundamental forces and they will behave as one unified force. A theory describing this era should unite quantum field theory (QFT) and general relativity (GR). Until such a theory comes about, we are not able to make any predictions about what was happening in that era.

The first step towards such a theory is to find a quantum description of gravity. General Relativity is formulated using classical physics, while the other three forces are formulated using quantum mechanics. Coupling together a classical and a quantum mechanical system might lead to trouble, which is the case here [5]. We say that it is not renormalizable. One popular theory for this quantization is *loop quantum gravity*. If a theory also unifies gravity with the other three forces it is also a so-called *theory of everything* (ToE). String theory, for example, is one such theory.

Grand unification era ($10^{-43} \text{ s} \rightarrow 10^{-36} \text{ s}$). As the Universe cooled down, gravity splits out as a separate force, while the other three forces: the strong, weak and electromagnetic forces (collectively called the gauge forces) are still united as one

force. Theories trying to explain and unify the strong and electroweak forces are called *Grand Unified Theories*. There are many grand unification models. The simplest of these uses SU(5) and was proposed by Howard Georgi and Sheldon Glashow in 1974 [6]. Common for all models is the inclusion of some heavy bosons with masses around 10^{15} GeV/ c^2 . These are like analogies to the W and Z particles, but couples quarks to leptons. In the Georgi-Glashow model, there are 12 of these, named X and Y bosons, respectively. When the temperature decreases below this at around 10^{-36} s it will result in a symmetry breaking splitting the strong force from the electroweak force. In some theories baryogenesis is caused by the decay of these heavy bosons (X, Y, or something equivalent), as they may violate baryon number [7].

Inflationary era (10^{-36} s \rightarrow 10^{-32} s). After the grand unification era, the Universe is thought to have gone through a phase of rapid exponential expansion called inflation. The linear size of the Universe is thought to have increased by a factor of at least 10^{26} and volume by 10^{78} [8]. The actual mechanism behind inflation is speculative but is thought to have started around the time of the GUT transition by a scalar field called the inflaton (field). This field is thought to be quite similar to dark energy or the Higgs field, but involving much higher energies.

The idea of an early inflationary epoch was proposed by a number of physicist around 1980. Among them was Starobinsky who looked at non-singular cosmological models, and saw the importance of quantum corrections to Einsteins Field Equations [9, 10]. Guth is often credited for seeing the importance of inflation, and in his original theory, the inflaton field would be in what we call a false vacuum — a kind of positive energy (as opposed to the negative energy of gravity), which according to general relativity would accelerate the expansion of space at an exponential rate [11]. More modern versions (e.g. Linde [12]) of inflation have abandoned the false vacuum part, but rather assuming that the inflaton field starts at a high energy state, from which it slow rolls down a potential well [13]. While the value of the inflaton field was dropping very slowly, the particle content in the Universe would cool down and dilute rapidly. As the potential start to drop more quickly, the inflation process stops and a reheating process starts. In this process the potential energy which is released results in the creation of particles, in a process we call reheating. In practice, everything in our observable universe results from this process. This era is thought to have ended at around 10^{-32} seconds.

Inflation theory has a lot of supporters as it solves several big questions in cosmology, the three biggest ones being the flatness problem, the horizon problem, and the magnetic monopole problem. *The flatness problem* has to do with the curvature of the Universe being so small. Without inflation, this would require the energy density in the Universe to be very fine-tuned to a special value (the critical density). If there was an inflationary era then the Universe we observe today is just a very small fraction of a bigger universe, which might very well be curved. *The horizon problem* has to do with why the horizon on the opposite sides of the Universe (relative to an

observer) have the same temperature. Classical theory says that they should never have been in contact with each other (causally separated). If the whole Universe went through an inflationary period, the whole observable universe was all very close and causally connected before inflation separated them with superluminal speeds. The last problem has to do with *magnetic monopoles*, which are a type of hypothetical particles with magnetic charge (just a north or south pole). These particles would make the connection between electricity and magnetism more symmetric. No magnetic monopoles have ever been observed, but they might be too massive to be produced from the potential energy of the inflaton field. In such case, the reason we haven't seen any magnetic monopoles isn't necessary because they don't exist, but because they are so diluted we just haven't seen them yet.

Cosmic inflation is the simplest theory which solves all the aforementioned problems. According to the theory the structure we see in the Universe today originate from quantum fluctuations in the inflaton field which would grow to macroscopic sizes during the exponential growth. The effects of the primordial fluctuations were studied by among others: Mukhanov and Chibisov [14, 15], and Hawking [16]

Electroweak era (10^{-32} s \rightarrow 10^{-11} s). After the symmetry breaking at the GUT scale, the strong force separated out from the what we call the electroweak force. The Universe is filled with hot quark-gluon plasma, leptons, and the gauge bosons of the electromagnetic and weak forces. In the electroweak era, these bosons were all massless and named the W_1 , W_2 , W_3 , and B bosons. The electroweak era lasted quite long (if we look at it from a logarithmic point of view). Then at around 100 GeV, when the Universe was around 10^{-11} s old, the Higgs mechanism caused a spontaneous symmetry breaking of the electroweak force. The four aforementioned bosons split into the three massive W^+ , W^- , and Z^0 particles; and the massless photon.

The electroweak energy scale of 100 GeV has been possible to recreate here on Earth for some decades now. The electroweak theory is thus well understood and verified by experiments. However, there is a big gap between the highest energies we can produce in accelerators today (13 TeV at the LHC) and the 10^{10} TeV at the end of inflation. Most of the electroweak era is still uncharted territory.

1.1.2 The early universe

Quark era (10^{-11} s \rightarrow 10^{-5} s). At this time all the four fundamental forces have settled down to their current form. The temperature is not high enough to create the heavier particles like W, Z, H, and t, so these will quickly annihilate. We are thus left with (the remaining five) quarks, gluons, leptons, and photons. The temperature is too high for quarks to form hadrons in the form of baryons and mesons. Instead, they are in a state together with gluons which we call a quark-gluon plasma, where they act as free elementary particles.

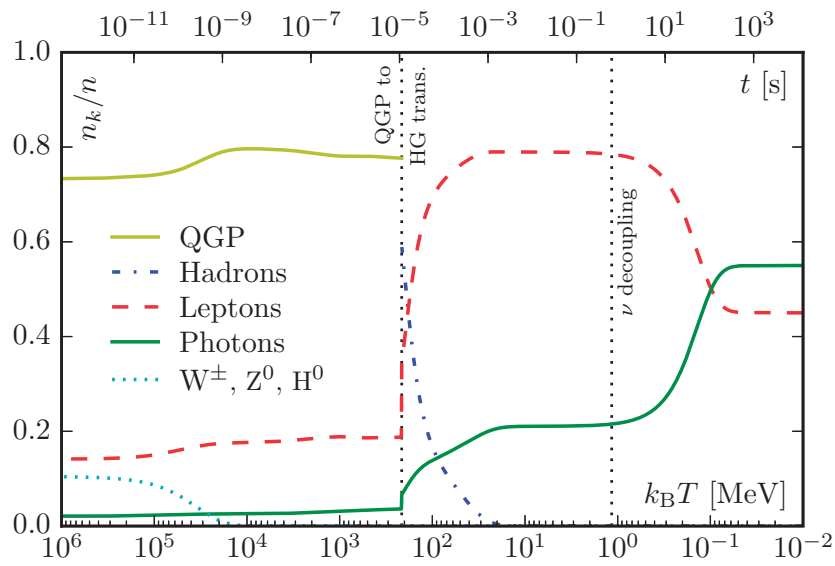


Figure 1.1: Relative number densities of the different particle types from $k_B T = 10^6$ to 10^{-2} MeV. We can categorize the different eras of the Universe according to the dominant particle species. From left to right (high to low temperature) we have the quark, hadron, lepton, and photon eras. From a number density (or energy density) point of view, the hadron era is very short.

Hadron era (10^{-5} s \rightarrow 10^{-4} s). Somewhere between 150 and 300 MeV, there is an important phase transition. The previously freely roaming quarks and gluons will clump together to form color-neutral hadronic particles like mesons and baryons (see Chapter 2 on particle physics). By number density or (kinetic) energy density (which does not include rest mass) this period does not last very long. The low temperature only allows for a small production of the heavier baryons like protons and neutrons. The lighter pions exist for a while longer. Eventually, all the anti-hadrons will annihilate and we are left with only a very small portion of hadrons.

Lepton era (10^{-4} s \rightarrow 100 s). When the temperature dropped to around 100 MeV the number and energy density of the Universe became dominated by the leptons (neutrinos, electrons, positrons and also some muons). At this time neutrinos were coupled with the charged leptons through the weak interaction and remained in equilibrium. At around $T = 1$ MeV the mean free path of neutrinos became greater than the Hubble distance (the distance to something receding by the speed of light and is defined as cH^{-1}), and decoupled directly from the electron-positrons and indirectly from the photons. From here on the neutrinos and the photon-coupled particles cool down independently from each other. Shortly after the neutrino decoupling the last numerous massive particles — the electrons and positrons will annihilate. The photons will be heated by this process, while the neutrinos won't. Today the cosmic microwave background photons have a temperature of 2.73 K, while the cosmic microwave neutrinos have (according to theory) a temperature of 1.95 K. At around 100 keV most of the electrons and positrons have annihilated and essentially all the energy in the Universe is contained in the photons and neutrinos).

Photon era (100 s \rightarrow 380 000 y). As the photon era begins, the antimatter particles are all but extinct. The excess matter particles (electrons, protons, and neutrons) are outnumbered by the photons by roughly one to one billion. As we enter the photon era, the protons and neutrons start to clump together to form elements such as deuterium, helium, beryllium, and lithium. This happens gradually, but a well-used definition is 3 minutes after the Big Bang [17]. At this time the amount of helium-4 and deuterium was about one ten-thousandth that of the proton [8]. This is the Big Bang nucleosynthesis (BBN) (sub)era, and last until about 20 minutes after the Big Bang (see Figure B.1.) For thousands of years the Universe continued to dilute and accol. Eventually, after being radiation dominated since its formation the Universe became matter dominated, 47 000 years after the Big Bang [18].

During the photon era, the Universe is in a plasma phase, with free electrons and nuclei. Since photons interact strongly with the ionized particles the Universe was opaque. Eventually, the temperature becomes low enough for electrons and nuclei to form atoms. This period is called recombination, which is kind of a bad expression, as this suggests that they have previous been combined. The recombination happened quite rapidly, first with most ionized isotopes of beryllium, lithium, and helium,

and then most importantly with hydrogen at around 380 000 years after the Big Bang. Photons could now no longer interact with the neutral atoms, causing them to decouple from matter. Light would then travel unhindered and is what we today observe as the cosmic microwave background (CMB).

1.1.3 Structure formation

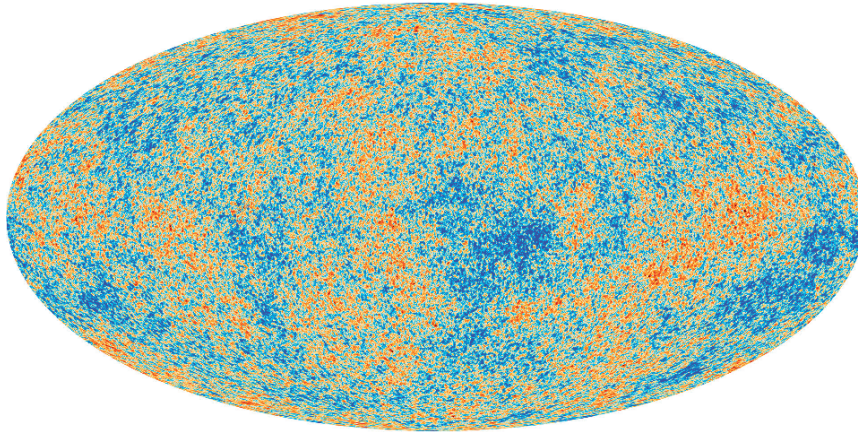


Figure 1.2: The cosmic microwave background gives an imprint of the Universe at the time of photon decoupling at around 380 000 years after the Big Bang (redshift $z = 1090$ [19]). The fluctuations of around 1 part per 100 000 is the start of structure formations. Photo: ESA.

Dark ages (380 000 y \rightarrow 400 million y). After recombination and photon decoupling, matter is quite evenly distributed with only small fluctuations in density. These small fluctuations will eventually grow to form clusters and galaxies, and voids. There are few new sources of light, hence the name *the dark ages*. Future studies of the 21 cm hydrogen line might shed some more light on this relatively unknown era.

Reionization (400 million y \rightarrow 1 billion y). As the matter clumps together they will form stars and quasars. These events will emit large amounts of radiation, which will reionize the Universe. The exact time when reionization starts is still a bit unclear, but the oldest galaxies we have observed dates back to roughly 400 million years after the Big Bang. Hopefully, future telescopes like the James Webb Space Telescope, scheduled to be launched in 2018 will give us more answers. The whole Universe is thought to be reionized at about 1 billion years after the Big Bang [20]. Because of the low density of the electrons and baryons, the interaction rate between them and the photons are so low that the opaqueness just barely increased and Universe remains transparent.

Current era (1 billion y \rightarrow 13.799 billion y). What happens after reionization is quite well understood. The Universe will continue to clump together and expand, leading to decreasing matter and radiation densities. The discovery of dark energy in 1998 [21, 22] gave us a new ingredient to include. Assuming this is a cosmological constant, its energy density is constant. This means that the Universe became dark energy dominated at around 9.8 billion years after the Big Bang [18].

1.2 Cosmological parameters

Today the Λ CDM (Lambda Cold Dark Matter) model is referred to as the Standard Model of Big Bang cosmology, as is the simplest model which reasonably describes the cosmos (e.g. the existence and structure of the CMB, the large-scale structure and distribution of galaxies, and the abundances of light elements through primordial nucleosynthesis). It can also be extended to include inflation. The Λ CDM is based on six independent (primary) parameters as shown in Table 1.1. Together with a few fixed parameters we also get some of the more famous calculated parameters shown in the same table.

Table 1.1: Cosmological parameters according to the Planck 2015 results with the **TT,TE,EE+lowP+lensing+ext** parameters with 68% confidence limits [19]. Ω is the density compared to critical density, h is the reduced Hubble constant, defined as $H_0/(100 \text{ kms}^{-1} \text{ Mpc}^{-1})$. What is listed as the *sound horizon at last scattering* is actually the Monte-Carlo calculated angular size of the sound horizon (of BAO) multiplied by a hundred. The reionization optical depth tells us about the opacity at the time of reionization. Perturbation amplitude tells us about the fluctuations in density in the early universe. The scalar spectral index tells us how the density fluctuations vary with scale.

	Description:	Symbol:	Value:
Primary	Physical baryon density	$\Omega_b h^2$	$0.022\,30 \pm 0.000\,14$
	Physical cold dark matter density	$\Omega_c h^2$	0.1188 ± 0.0010
	Sound horizon at last scattering	$100\theta_{\text{MC}}$	$1.040\,93 \pm 0.000\,30$
	Reionization optical depth	τ	0.066 ± 0.012
	Perturbation amplitude	$\ln(10^{10} A_s)$	3.064 ± 0.023
	Scalar spectral index	n_s	0.9667 ± 0.0040
Calculated	Hubble constant	H_0	67.74 ± 0.46
	Cosmological constant density	Ω_Λ	0.6911 ± 0.0062
	Matter density	Ω_m	0.3089 ± 0.0062
	Age of the Universe / Gyr	t_0	13.799 ± 0.021
	Redshift at decoupling	z_*	$1\,089.90 \pm 0.23$

¹ **TT**: temperature power spectrum, **TE**: temperature-polarization cross spectrum, **EE**: polarization power spectrum, **lowP**: Planck polarization data in the low- ℓ likelihood, **lensing**: CMB lensing reconstruction, **ext**: External data from Baryon acoustic oscillations (BAO), Joint Light-curve Analysis (JLA), and the Hubble constant.

2 Particle Physics Summary

2.1 Standard Model of elementary particles

The Standard Model of particle physics is one of the most successful theories in physics and explains the existence and composition of all the known particles. Figure 2.1 shows the most familiar representation of the Standard Model of elementary particles, where the particles are divided into four categories: the quarks, the leptons, the force-carrying gauge bosons, and finally the Higgs boson. The spin of elementary particles comes in units of the reduced Planck constant, \hbar . Particles with half-integer spin ($1/2, 3/2, \dots$) are called fermions, while bosons have an integer spin number ($0, 1, 2, \dots$). All matter particles (quarks and leptons) have spin- $1/2$, the gauge bosons have spin-1 and the Higgs boson has spin-0. Gravitation is not part of the Standard Model. However, most physicists believe that gravity is mediated by a massless particle called the graviton. This graviton should connect to what is called the stress-energy tensor. This is a second order tensor, i.e. a 4×4 matrix, and therefore the graviton must have spin-2. Fermions with the same quantum numbers can not occupy the space and follow Fermi-Dirac statistics. Bosons, on the other hand, can occupy the same state. They follow Bose-Einstein statistics.

Quarks come in six flavors. We can further divide these into three generations, with each next generation being more massive, but otherwise possessing the same properties. Only the first generation particles are stable. The six quarks (q) are: up (u) and down (down), charm (c) and strange (s), and finally top (t) and bottom (b). The quarks also have their own antiparticle (\bar{q}) with opposite electric charge ($\bar{u}, \bar{d}, \bar{c}, \bar{s}, \bar{t}, \bar{b}$). Quarks have charge $+2/3$ and $-1/3$ (particles) and $-2/3$ and $+1/3$ (antiparticles). Quarks interact through all the four forces: the strong, electromagnetic, weak, and gravitational. Similar to electric charge, the strongly interacting quarks have color charge. There are three colors for particles and three colors for antiparticles, namely: red, green, and blue; and antired, antigreen and antiblue. Quarks are bounded by color confinement and can never be directly observed in isolation. They need to form color-neutral particles. These can be combinations of three colored quarks (rgb), or three anticolored quarks ($\bar{r}\bar{g}\bar{b}$). We call these particles baryons. The most common baryons are the proton and the neutron. A quark can also combine with an antiquark in a color-anticolor combination ($r\bar{r}, g\bar{g}, b\bar{b}$, or some superposition of these) to form mesons (e.g. pions). Current research also suggests the existence of more exotic quark compositions like tetraquarks [23, 24] and pentaquarks [25]. All particles made up of quarks are called hadrons.

2 Particle Physics Summary

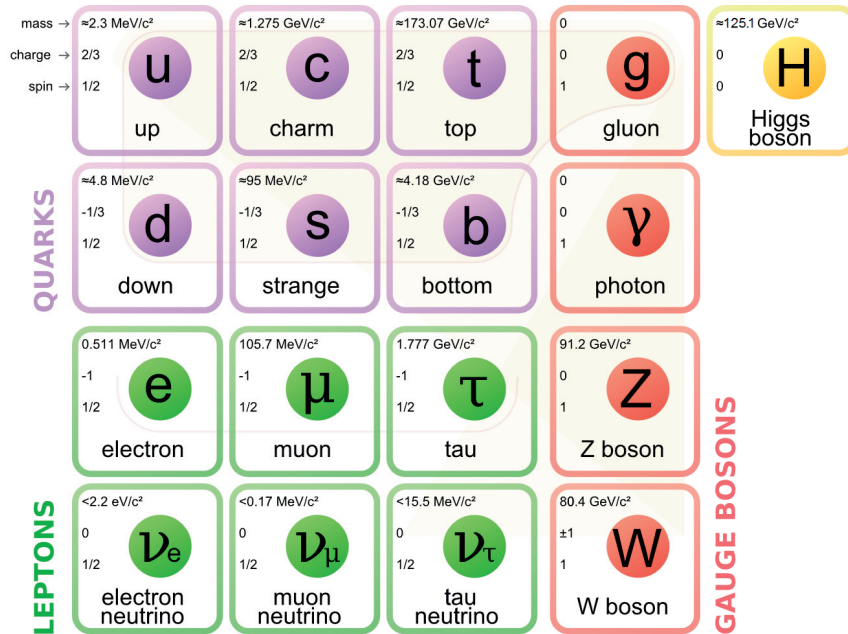


Figure 2.1: The Standard Model of elementary particles. (Figure is taken from Wikipedia.)

Leptons are organized in much the same way as the quarks: they are fermions and come in three generations. We have the charged leptons: the electron (e^-), the muon (μ^-), and the tau (τ^-). Then we have their accompanying neutrinos, the electron neutrino (ν_e), the muon neutrino (ν_μ), and the tau neutrino (ν_τ). The antiparticles of the charged leptons are normally expressed with a “+” superscript (e^+ , μ^+ , τ^+), while the antineutrinos use a bar-notation ($\bar{\nu}_e$, $\bar{\nu}_\mu$, $\bar{\nu}_\tau$). While it is clear that the charged leptons are Dirac fermions, that is, they are not their own antiparticles, this is unclear for the neutrinos. If they are their own antiparticles, they would be Majorana fermions.

The fundamental forces are carried by the so-called gauge bosons: The photon (γ), the eight gluons (g), and the W^+ , W^- and Z^0 , are all mediators for the electromagnetic, strong and weak forces. All these bosons are spin 1 particles. In addition, there is the hypothetical graviton (G), which, as mentioned, should be a massless spin-2 particle mediating the gravitational force. The latest addition to the Standard Model is the Higgs boson (H^0), which is responsible for giving fundamental particles their mass.

The total number of elementary particles depend on how we count. Disregarding the graviton which is not part of the Standard Model (and might not even exist), the common practice is to categorize the elementary particles by 17 different entries, as is done in Figure 2.1. If we count antiparticles as separate particles the number increases to 30. Further differentiating between colors gives us 61. By including

Table 2.1: The elementary particles and their degeneracy (internal degrees of freedom).

		Anti- Flavors:	particles:	Spins:	Colors:	Total:
Quarks	(u, d, c, s, t, b)	6	2	2	3	72
Charged leptons	(e, μ , τ)	3	2	2	1	12
Neutrinos	(ν_e , ν_μ , ν_τ)	3	2	1	1	6
Gluons	(g)	1	1	2	8	16
Photon	(γ)	1	1	2	1	2
Massive gauge bosons	(W^\pm , Z^0)	2	2+1	3	1	9
Higgs bosons	(H^0)	1	1	1	1	1
All elementary particles		17				118

possible spin states as well, we end up with 118 distinct intrinsic degrees of freedom, as listed in Table 2.1.

2.2 Baryon-to-photon-ratio

Just after the Big Bang when the temperature was high, the Universe was filled with photons, particles, and antiparticles. Because of constant annihilations and pair-productions, all particles were more or less in equilibrium and as abundant as the other. As the temperature fell, and no pair production ceased, the observable Universe was left with an asymmetry between matter and antimatter. For some reason which neither the Standard Model of particle physics nor general relativity can give, there is more of the former than the latter. This is normally expressed through the baryon asymmetry problem, which is one of the big unanswered questions in physics. The asymmetry parameter is expressed as

$$\eta = \frac{n_B - n_{\bar{B}}}{n_\gamma} \simeq \frac{n_B}{n_\gamma} . \quad (2.1)$$

Counting up the baryons and CMB-photons gives us η equal to roughly 6×10^{-10} . It is sometimes preferred to base the baryon asymmetry on entropy density instead of the photon density as entropy has, to a good approximation, stayed constant since at least the electroweak era¹. In such case, the asymmetry parameter may be expressed as

$$\eta_s = \frac{n_B - n_{\bar{B}}}{s} , \quad (2.2)$$

¹A reasonable assumption is that entropy has stayed fairly constant since the end of inflation. In Standard Cosmology, entropy per comoving volume is roughly constant, only increasing by a small amount [8].

where $s = 7.04n_\gamma$ at the present era, giving η_s a value of roughly 10^{-10} . This asymmetry led us to a Universe where we could have primordial nucleosynthesis (see appendix B).

2.3 Chemical potential

The chemical potential, μ , is related to the willingness for a certain reaction to occur, and we can associate a chemical potential to every particle. First a few observations:

1. The sum of the chemical potentials μ_i , is conserved in chemical equilibrium, and thus, also in thermodynamic equilibrium.
2. Since photons can be absorbed or emitted arbitrary in a reaction, the chemical potential for photons, μ_γ , is zero [26].
3. A particle-antiparticle pair can annihilate into photons, the chemical potential of a particle and its associated antiparticle is equal to zero and opposite [26].

The chemical potential is derived from the fundamental thermodynamic relation

$$dU = T dS - P dV + \sum_{j=1}^n \mu_j dN_j , \quad (2.3)$$

and give the following definition

$$\mu_j = \left(\frac{\partial U}{\partial N_j} \right)_{S, V, N_{i \neq j}} . \quad (2.4)$$

The chemical potential is thus the change in internal energy by adding or removing one particle to or from the system, keeping the volume and entropy constant. We can introduce a chemical potential μ_j for each conserved charge Q_j . This is done by replacing the Hamiltonian H of the system with $H - \mu_j N_{Q_j}$, where N_{Q_j} is the number operator of particles with charge Q_j . In the Standard Model, there are five independent conserved charges. These are the electric charge, baryon number, electron-lepton number, muon-lepton number, and tau-lepton number. This means there are also five independent chemical potentials [26]. The chemical potentials are determined by the number densities. The electric charge density is very close to zero. The baryon density is estimated to be less than a billionth of the photon density [27, 28]. Lepton density is also thought to be very small, on the same order as the baryon number. According to Weinberg [26], for an early universe scenario, we can put all these numbers equal to zero to a good approximation. For a correct representation of the Universe, the chemical potentials cannot all cancel out—otherwise, there would be no matter present today.

3 Statistical Mechanics

Statistical mechanics looks at the behavior of quantum systems on larger scales, and is so a bridge from the microscopic quantum world to the macroscopic world. Using probability theory, statistical mechanics studies the average behavior of mechanical systems where the state of the system is uncertain. In this chapter I will give a brief introduction to the topic. Most importantly to the distribution function which is the basis for paper one: “On the Effective Degrees of Freedom in the Early Universe” [1].

3.1 Distribution function

There is a fundamental assumption in statistical mechanics, namely that “in thermal equilibrium every distinct state with the same total energy are equally probable” [29]. Statistical mechanics is all about counting these states. However, things behave very differently in the quantum world, so before we can start counting states we need to know a few things about how particles occupy these states. Namely if the particles are distinguishable? And if more than one particle occupy the same state? With these two properties in mind we can categorize particles into three groups. First we have *classical particles*, which are distinguishable and can occupy the same state. Particles following this behavior obey the classical Maxwell-Boltzmann probability distribution. Next we have *bosons* (e.g. photons), which as classical particles can occupy the same state, but are indistinguishable. Bosons follow the Bose-Einstein distribution. Finally we have *fermions* (e.g. electrons and protons). These particles are also indistinguishable, but only one fermion can occupy one state. We have summarized the properties in Table 3.1. On the fundamental level, particles can only be fermions or bosons.

Table 3.1: Particles and their distributions.

Particles:	Probability distribution:	Distinguishable?	Can occupy same state?
Classical particles	Maxwell-Boltzmann	Yes	Yes
Bosons	Bose-Einstein	No	Yes
Fermions	Fermi-Dirac	No	No

The difference in these three probability distributions lies in how we count the microstates. A microstate describes the properties of the individual particles, like

position, velocity, spin, etc. A macrostate, on the other hand, describes the systems macroscopic properties (like pressure, volume, temperature, etc.). Interchanging two microstates do not change the macrostate of the system.

The *occupation number* N_i tells us how many particles are in each state, ψ_i , but does not care about which particles are in which states. The collection of all occupation numbers is called a *configuration*. The configuration which can be achieved in most different ways is the most probable configuration. When we are working with very large numbers we get one remarkable feature — it turns out that the distribution of individual particle energies, when they are in equilibrium, is just the most probable configuration [29, 30] (a simple example for a two-state system showing these feature given in Figure 3.1). The probability that a state is occupied depends on the energy of the system and if we are dealing with fermion or bosons, and can be approximated to

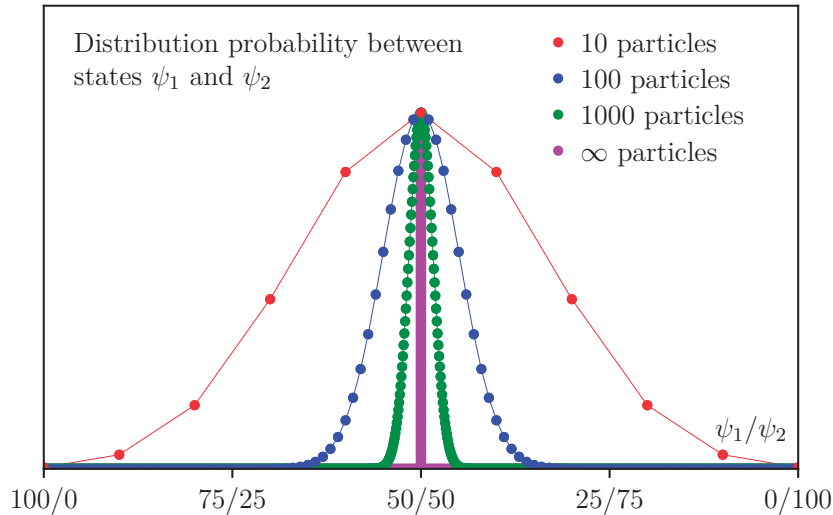


Figure 3.1: Example given a two-state classical system (particles are distinguishable and can occupy the same state). The probability that the particles will distribute themselves evenly between the two states increases with the number of particles in the system. For a large number of particles (e.g. Boltzmann's constant) this distribution is simply the most probable configuration.

$$N_i \simeq \begin{cases} \frac{g_i}{e^{(\alpha+\beta E_i)}} & \text{Maxwell-Boltzmann ,} \\ \frac{g_i}{e^{(\alpha+\beta E_i)} + 1} & \text{Fermi-Dirac ,} \\ \frac{g_i}{e^{(\alpha+\beta E_i)} - 1} & \text{Bose-Einstein ,} \end{cases} \quad (3.1)$$

where g_i is the degeneracy of state i and E_i is the energy of single particle in that

state. α and β are Lagrange multipliers, which can be identified as [29]

$$\beta = \frac{1}{k_B T}, \quad (3.2)$$

$$\alpha = -\frac{\mu(T)}{k_B T} = -\mu(T)\beta, \quad (3.3)$$

β is called the thermodynamic beta — a systems reciprocal thermodynamic temperature, and μ is the chemical potential. We can introduce ε_i as the energy associated with state i , such that for a one-particle state, $E_i = 0$ when it is unoccupied, and $E_i = \varepsilon_i$ when it is occupied by one particle. By dividing Eq. (3.1) by the degeneracy of its energy states, we find the most probable number of particles in a single “one-particle” state with energy ε , that is number density per state n :

$$n(\varepsilon) = \begin{cases} \frac{1}{e^{(\varepsilon-\mu)/k_B T}} & \text{Maxwell-Boltzmann,} \\ \frac{1}{e^{(\varepsilon-\mu)/k_B T} + 1} & \text{Fermi-Dirac,} \\ \frac{1}{e^{(\varepsilon-\mu)/k_B T} - 1} & \text{Bose-Einstein.} \end{cases} \quad (3.4)$$

For fermions this number will always be between zero and one, while it can be any positive number for bosons. Using this we can set up the distribution functions as functions of momenta for classical particles, fermions, and bosons:

$$f(\mathbf{p}) = \frac{1}{e^{(E(\mathbf{p})-\mu)/(k_B T)}} \quad (\text{Classical}), \quad (3.5a)$$

$$f(\mathbf{p}) = \frac{1}{e^{(E(\mathbf{p})-\mu)/(k_B T)} + 1} \quad (\text{Fermions}), \quad (3.5b)$$

$$f(\mathbf{p}) = \frac{1}{e^{(E(\mathbf{p})-\mu)/(k_B T)} - 1} \quad (\text{Bosons}). \quad (3.5c)$$

3.2 Particle velocities in Maxwell-Boltzmann and Maxwell-Jüttner distributions

We can distinguish between ultra-relativistic, semi-relativistic, and non-relativistic velocities, according to the value of the Lorentz factor, γ . Another way to look at it, is which energy-term is dominant — the kinetic term, the rest mass term, or both. The ratio of semi- and non-relativistic particles plays a central role in the production of viscous effects. We will here go through the distribution functions for particle velocities.

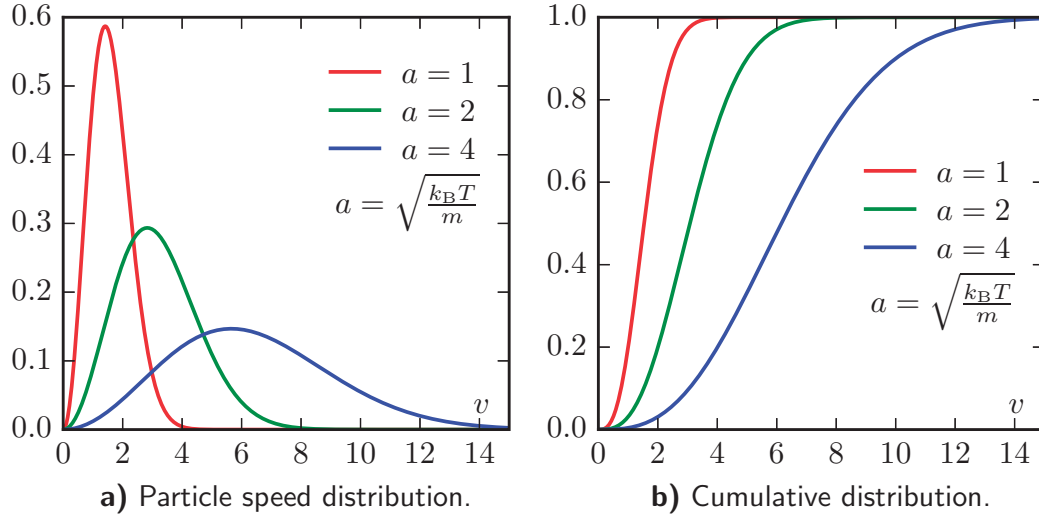


Figure 3.2: Particle distribution function (PDF) and cumulative distribution function (CDF) of a variable speed v and distribution parameter $a = k_B T / m$ (a large a gives a wider spread).

For a classical case the particle speed distribution, or probability density function (PDF), for particles with mass m at a temperature T is given by the Maxwell-Boltzmann distribution:

$$\begin{aligned} f(v) &= \left(\frac{m}{2\pi kT} \right)^{3/2} 4\pi v^2 e^{-\frac{mv^2}{2k_B T}}, \\ &= \sqrt{\frac{2}{\pi}} \frac{v^2 e^{-v^2/(2a^2)}}{a^3}, \end{aligned} \quad (3.6)$$

with $a = \sqrt{(k_B T / m)}$ being the distribution parameter.

For a relativistic gas the equivalent is the Jüttner distribution function [31].

$$f(\gamma) = \frac{\beta \gamma^2 z}{K_2(z) e^{\gamma z}}, \quad (3.7)$$

where $\beta = v/c$, $\gamma = (1 - (v/c)^2)^{-1/2}$ is the Lorentz factor, $z = (mc^2)/(k_B T)$ is the reciprocal dimensionless temperature, and $K_2(z)$ is the modified Bessel function of the second kind.

3.3 Ideal quantum gases in thermodynamic equilibrium

Calculating the macrostates for systems in thermodynamic equilibrium is quite straightforward. In this section I will derive the functions for number density (n), energy density (ε), pressure (P), and entropy density (s). This follows closely the theory described in the paper [1].

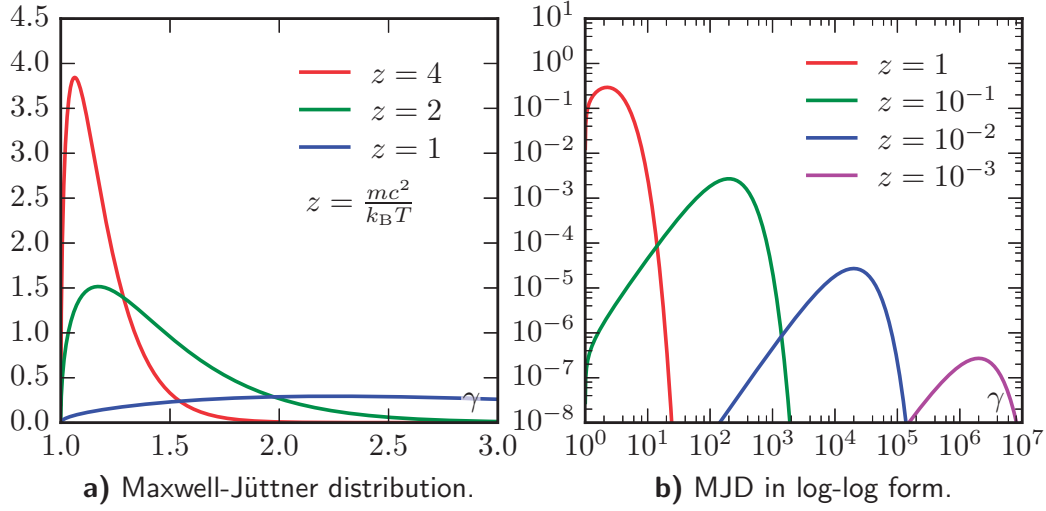


Figure 3.3: Maxwell Jüttner distributions (MJD) of speeds in the γ -representation as functions of z , the dimensionless temperature. This is really just the ratio of mass over temperature. Log-log plot for large γ 's on the right.

3.3.1 Thermodynamic functions

When we are dealing with a large (ideally infinite) system we can approximate the conditions by using small unit cells — or cubic boxes with periodic boundary conditions. For boxes of volume $V = L^3$, solving the Schrödinger equation for a particle, we find the possible momentum eigenvalues

$$\mathbf{p} = \vec{p} = \frac{h}{L}(n_1\vec{e}_x + n_2\vec{e}_y + n_3\vec{e}_z), \quad (3.8)$$

where h is the Planck constant, $n_i = 0, \pm 1, \pm 2, \pm 3, \dots$, and $\vec{e}_x, \vec{e}_y, \vec{e}_z$ are the standard units vectors in three-dimensional Euclidean space. The number of states in momentum space is thus:

$$\frac{n_1\vec{e}_x}{\Delta p_x} \frac{n_2\vec{e}_y}{\Delta p_y} \frac{n_3\vec{e}_z}{\Delta p_z} = \frac{L^3}{h^3}, \quad (3.9)$$

By adding the internal degrees of freedom (g) and dividing Eq. (3.9) with the volume (L^3) we find the density of states:

$$\text{dos} = \frac{g}{h^3} = \frac{g}{(2\pi\hbar)^3} \quad (3.10)$$

The energy of a particle with mass m and momentum \mathbf{p} is $E(\mathbf{p}) = \sqrt{m^2c^4 + \mathbf{p}^2c^2}$.

In thermal equilibrium, the probability that a single-particle state with momentum \mathbf{p} and energy $E(\mathbf{p})$ is occupied is given by the Bose-Einstein or Fermi-Dirac distribution functions given in Eqs. (3.5b) and (3.5c). In order to find the total number of

particles occupying a state with energy E , we must find the density of states in phase space. We see from Eq. (3.8) that the number of possible states in momentum space is L^3/h^3 . By dividing by the volume, L^3 , as well, we are left with the factor $(1/h)^3$. If there is an additional degeneracy g (for example, spin), we can write the density of states (dos) as

$$\text{dos} = \frac{g}{h^3} = \frac{g}{(2\pi)^3 \hbar^3} . \quad (3.11)$$

The density of particles with momentum \mathbf{p} is then given by

$$n(\mathbf{p}) = \frac{g}{(2\pi)^3 \hbar^3} \times f(\mathbf{p}) . \quad (3.12)$$

The total density of particles, n , can then be written as an integral over three-momentum involving the distribution function as

$$n = \frac{g}{(2\pi)^3 \hbar^3} \int f(\mathbf{p}) d^3\mathbf{p} . \quad (3.13)$$

By multiplying the distribution functions with the energy and integrating over three-momentum, we obtain the energy density ϵ of the system. The pressure, P , can be found in a similar manner by multiplying the distribution function with $|\mathbf{p}|^2/(3E/c^2)$ (a nice derivation of this is shown by Baumann [32]). This yields the integrals

$$\epsilon = \frac{g}{(2\pi)^3 \hbar^3} \int E(\mathbf{p}) f(\mathbf{p}) d^3\mathbf{p} , \quad (3.14)$$

$$P = \frac{g}{(2\pi)^3 \hbar^3} \int \frac{|\mathbf{p}|^2}{3(E/c^2)} f(\mathbf{p}) d^3\mathbf{p} . \quad (3.15)$$

The entropy density s can be calculated from the thermodynamic relation

$$s = \frac{\epsilon + P - \mu_T}{T} , \quad (3.16)$$

where the index μ_T is the total chemical potential.

3.3.2 From momentum to energy integrals

It is sometimes more convenient to use energy, E , instead of the momentum, \mathbf{p} , as the integration variable. By integrating over all angles, we can replace $d^3\mathbf{p}$ by $4\pi|\mathbf{p}|^2 d\mathbf{p}$. Using the energy momentum relation, we find $|\mathbf{p}| = \sqrt{E^2 - m^2c^2}/c$ and $c\mathbf{p} d\mathbf{p} = E dE$. The integrals will then go from mc^2 to infinity instead of $p = 0$ to infinity. We can simplify these formulas further by introducing the dimensionless variables u , z , and $\hat{\mu}$.

$$u = \frac{E}{k_B T} , \quad z = \frac{mc^2}{k_B T} , \quad \hat{\mu} = \frac{\mu}{k_B T} . \quad (3.17)$$

3.3 Ideal quantum gases in thermodynamic equilibrium

This yields the following expressions for the number density, energy density, and pressure for a species j , and for all species (as this is simply the sum of all particle species).

$$n_j(T) = \frac{g_j}{2\pi^2\hbar^3} \int_{m_j c^2}^{\infty} \frac{E \sqrt{E^2 - m_j^2 c^4}}{e^{(E-\mu_j)/k_B T} \pm 1} dE \quad (3.18a)$$

$$= \frac{g_j}{2\pi^2} \left(\frac{k_B T}{\hbar c} \right)^3 \int_{z_j}^{\infty} \frac{u \sqrt{u^2 - z_j^2}}{e^{u-\hat{\mu}_j} \pm 1} du , \quad (3.18b)$$

$$n(T) = \sum_j n_j = \sum_j \frac{g_j}{2\pi^2} \left(\frac{k_B T}{\hbar c} \right)^3 \int_{z_j}^{\infty} \frac{u \sqrt{u^2 - z_j^2}}{e^{u-\hat{\mu}_j} \pm 1} du , \quad (3.18c)$$

$$\epsilon_j(T) = \frac{g_j}{2\pi^2\hbar^3} \int_{m_j c^2}^{\infty} \frac{E^2 \sqrt{E^2 - m_j^2 c^4}}{e^{(E-\mu_j)/k_B T} \pm 1} dE \quad (3.19a)$$

$$= \frac{g_j}{2\pi^2} \frac{(k_B T)^4}{(\hbar c)^3} \int_{z_j}^{\infty} \frac{u^2 \sqrt{u^2 - z_j^2}}{e^{u-\hat{\mu}_j} \pm 1} du , \quad (3.19b)$$

$$\epsilon(T) = \sum_j \epsilon_j = \sum_j \frac{g_j}{2\pi^2} \frac{(k_B T)^4}{(\hbar c)^3} \int_{z_j}^{\infty} \frac{u^2 \sqrt{u^2 - z_j^2}}{e^{u-\hat{\mu}_j} \pm 1} du , \quad (3.19c)$$

$$P_j(T) = \frac{g_j}{6\pi^2\hbar^3} \int_{m_j c^2}^{\infty} \frac{(E^2 - m_j^2 c^4)^{3/2}}{e^{(E-\mu_j)/k_B T} \pm 1} dE \quad (3.20a)$$

$$= \frac{g_j}{6\pi^2} \frac{(k_B T)^4}{(\hbar c)^3} \int_{z_j}^{\infty} \frac{(u^2 - z_j^2)^{3/2}}{e^{u-\hat{\mu}_j} \pm 1} du , \quad (3.20b)$$

$$P(T) = \sum_j P_j = \sum_j \frac{g_j}{6\pi^2} \frac{(k_B T)^4}{(\hbar c)^3} \int_{z_j}^{\infty} \frac{(u^2 - z_j^2)^{3/2}}{e^{u-\hat{\mu}_j} \pm 1} du . \quad (3.20c)$$

As shown in Eq. (3.16) we can find the entropy density for a single species j and the total entropy as:

$$s_j(T) = \frac{\epsilon_j + P_j - \mu_j n_j}{T} , \quad (3.21a)$$

$$s(T) = \sum_j s_j = \sum_j \frac{\epsilon_j + P_j - \mu_j n_j}{T} = \frac{\epsilon + P - \sum_j \mu_j n_j}{T} . \quad (3.21b)$$

3.3.3 Massless particle contributions

In Eqs. (3.18)–(3.20), we see how dimensionless units, u , z , and $\hat{\mu}$, simplifies the integrals. In the ultrarelativistic limit, we can ignore the particle masses. Moreover, as we have set the chemical potentials to zero, we can easily solve the dimensionless integrals appearing in Eqs. (3.18b), (3.19b), and (3.20b) analytically. Since the integrals for energy density and pressure in the massless cases are the same, we find:

$$\int_0^\infty \frac{u^2}{e^u \pm 1} du = \begin{cases} \frac{3}{2}\zeta(3) \simeq 1.803 & \text{(Fermions)}, \\ 2\zeta(3) \simeq 2.404 & \text{(Bosons)}, \end{cases} \quad (3.22)$$

$$\int_0^\infty \frac{u^3}{e^u \pm 1} du = \begin{cases} \frac{7}{8}\frac{\pi^4}{15} \simeq 5.682 & \text{(Fermions)}, \\ \frac{\pi^4}{15} \simeq 6.494 & \text{(Bosons)}, \end{cases} \quad (3.23)$$

where $\zeta(3)$ is the Riemann zeta function of argument 3. Using these results, we find the values for n , ϵ , P , and indirectly s for massless bosons and fermions:

$$n_b(T) = g \frac{\zeta(3) (k_B T)^3}{\pi^2 (\hbar c)^3}, \quad n_f(T) = \frac{3}{4} g \frac{\zeta(3) (k_B T)^3}{\pi^2 (\hbar c)^3}, \quad (3.24)$$

$$\epsilon_b(T) = g \frac{\pi^2 (k_B T)^4}{30 (\hbar c)^3}, \quad \epsilon_f(T) = \frac{7}{8} g \frac{\pi^2 (k_B T)^4}{30 (\hbar c)^3}, \quad (3.25)$$

$$P_b(T) = g \frac{\pi^2 (k_B T)^4}{90 (\hbar c)^3}, \quad P_f(T) = \frac{7}{8} g \frac{\pi^2 (k_B T)^4}{90 (\hbar c)^3}, \quad (3.26)$$

$$s_b(T) = g \frac{2\pi^2 k_B^4 T^3}{45 (\hbar c)^3}, \quad s_f(T) = \frac{7}{8} g \frac{2\pi^2 k_B^4 T^3}{45 (\hbar c)^3}. \quad (3.27)$$

Here the subscript b is for bosons, and f is for fermions. We see that solving the integrals gives a difference between fermions and bosons, namely a factor $\frac{3}{4}$ for the number density and $\frac{7}{8}$ for energy density and pressure. We will call these two factors the “fermion prefactors”. We also see that the pressure is simply one third that of the energy density, while the entropy density can be found by multiplying the energy density by $4/(3T)$.

3.3.4 Effective degrees of freedom

In most cases we cannot ignore the particle masses. In these cases, we must solve the integrals in Eqs. (3.18b), (3.19b), and (3.20b) numerically. The integrals are decreasing functions of the temperature, and they vanish in the limit $k_B T/mc^2 \rightarrow 0$. We can normalize these by dividing their values by the case of the photon (but with g equal to one). As we recall, the photon has a bosonic nature with $m = 0$ and $\mu = 0$. This means that for massive particles at high temperature ($k_B T \gg mc^2$), one actual degree of freedom for bosons contributes as much as one degree of freedom for photons, and the fermions a little less. As the temperature drops, and less particles

are created, the effective contributions will be smaller. By including the intrinsic degrees of freedom (g), we find each particle species' *effective degree of freedom*, $g_{\star j}$:

$$g_{\star n_j}(T) = \frac{\frac{g_j}{2\pi^2} \left(\frac{k_B T}{\hbar c}\right)^3 \int_{z_j}^{\infty} \frac{u \sqrt{u^2 - z_j^2}}{e^u \pm 1} du}{\frac{1}{2\pi^2} \left(\frac{k_B T}{\hbar c}\right)^3 \int_0^{\infty} \frac{u^2}{e^u - 1} du} = \frac{g_j}{2\zeta(3)} \int_{z_j}^{\infty} \frac{u \sqrt{u^2 - z_j^2}}{e^u \pm 1} du, \quad (3.28)$$

$$g_{\star \epsilon_j}(T) = \frac{\frac{g_j}{2\pi^2} \left(\frac{k_B T}{\hbar c}\right)^4 \int_{z_j}^{\infty} \frac{u^2 \sqrt{u^2 - z_j^2}}{e^u \pm 1} du}{\frac{1}{2\pi^2} \left(\frac{k_B T}{\hbar c}\right)^4 \int_0^{\infty} \frac{u^3}{e^u - 1} du} = \frac{15g_j}{\pi^4} \int_{z_j}^{\infty} \frac{u^2 \sqrt{u^2 - z_j^2}}{e^u \pm 1} du, \quad (3.29)$$

$$g_{\star p_j}(T) = \frac{\frac{g_j}{6\pi^2} \left(\frac{k_B T}{\hbar c}\right)^4 \int_{z_j}^{\infty} \frac{(u^2 - z_j^2)^{3/2}}{e^u \pm 1} du}{\frac{1}{6\pi^2} \left(\frac{k_B T}{\hbar c}\right)^4 \int_0^{\infty} \frac{u^3}{e^u - 1} du} = \frac{15g_j}{\pi^4} \int_{z_j}^{\infty} \frac{(u^2 - z_j^2)^{3/2}}{e^u \pm 1} du, \quad (3.30)$$

$$g_{\star s_j}(T) = \frac{3g_{\star \epsilon_j}(T) + g_{\star p_j}(T)}{4}. \quad (3.31)$$

In Figure 3.4, we have plotted the effective degrees of freedom for massive bosons (panel **a**) and fermions (panel **b**) with $g = 1$ (and $\mu = 0$) as functions of the temperature. When the temperature is equal to the mass ($k_B T = mc^2$), the effective degrees of freedom for energy density is approximately 0.9 for bosons and 0.8 for fermions, compared to that of the photon. For number density, pressure, and entropy density, they are a little lower.

The effective degrees of freedom are defined as functions of the corresponding variables and temperature. We find the total effective degrees of freedom for $g_{\star n}$, $g_{\star \epsilon}$, and $g_{\star p}$ by summing Eqs. (3.28)–(3.31) over all particle species j :

$$g_{\star n}(T) \equiv \frac{\pi^2}{\zeta(3)} \frac{n(T)}{T^3} \quad (3.32a)$$

$$= \sum_j \frac{g_j}{2\zeta(3)} \int_{z_j}^{\infty} \frac{u \sqrt{u^2 - z_j^2}}{e^u \pm 1} du, \quad (3.32b)$$

$$g_{\star \epsilon}(T) \equiv \frac{30}{\pi^2} \frac{\epsilon(T)}{T^4} \quad (3.33a)$$

$$= \sum_j \frac{15g_j}{\pi^4} \int_{z_j}^{\infty} \frac{u^2 \sqrt{u^2 - z_j^2}}{e^u \pm 1} du, \quad (3.33b)$$

$$g_{\star p}(T) \equiv \frac{90}{\pi^2} \frac{P(T)}{T^4} \quad (3.34a)$$

$$= \sum_j \frac{15g_j}{\pi^4} \int_{z_j}^{\infty} \frac{(u^2 - z_j^2)^{3/2}}{e^u \pm 1} du. \quad (3.34b)$$

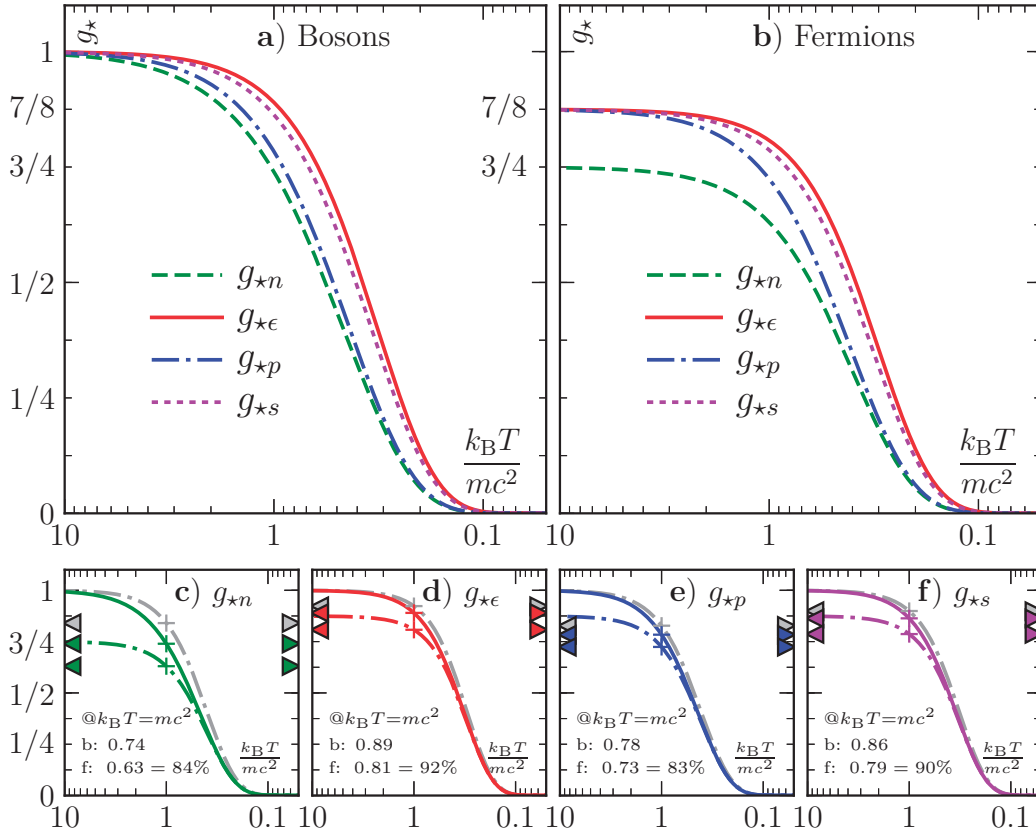


Figure 3.4: The effective degrees of freedom g_{*n} , $g_{*\epsilon}$, g_{*p} , and g_{*s} for bosons (a) and fermions (b) per intrinsic degree of freedom. A more detailed look at each of the four g_{*i} is given in the lower four panels (c–f). Here the solid colored curves are for the bosons, and the dash-dotted colored curves are for the fermions. The grey dash-dotted curves represent the fermions' contribution compared to its own relativistic value (such that it is 100% for $T \rightarrow \infty$). We have included the relative values at $k_B T = mc^2$ for the four cases (marked with “+” symbols). During particle annihilations, the energy density falls slower than the other quantities due to the impact of the rest mass energy. At temperatures close to the rest mass of some massive particle species, this rest mass is substantial to their total energy.

3.3 Ideal quantum gases in thermodynamic equilibrium

Finally, the effective degrees of freedom associated with entropy is then:

$$g_{*s}(T) \equiv \frac{45}{2\pi^2} \frac{s(T)}{T^3} \quad (3.35a)$$

$$= \frac{3g_{*\epsilon}(T) + g_{*p}(T)}{4} . \quad (3.35b)$$

4 The Friedmann Equations and Expansion of the Universe

The Friedmann equations describe the geometric expansion or contraction of homogeneous and isotropic universes. They are solutions to Einstein's field equations using the Friedmann-Lemaître-Robertson-Walker metric. They were derived by Alexander Friedmann in 1922 [33] and 1924 [34], and are valid for flat, positive, and negative spatial curvatures.

4.1 Newtonian gravity

In many cases, Newtonian gravity is a good approximation to describe gravity. From there, we remember that the force exerted on an object with mass m by an object of mass M is given by

$$F = \frac{GMm}{r^2}, \quad (4.1)$$

where Newton's gravitational constant, G , is roughly $6.67 \times 10^{-11} \text{ Nm}^2 \text{ kg}^{-2}$. The gravitational potential energy is

$$V = -\frac{GMm}{r}. \quad (4.2)$$

4.1.1 Deriving the Friedmann equations classically

One can partly derive Friedmann's (first) equation from Newtonian gravity [7]. First, we start off with a proof given by Newton in his *Philosophiæ Naturalis Principia Mathematica* [35]. Consider a spherical distribution of matter, with a particle of mass m at a distance r from the center of mass. The particle only feel the gravitational attraction from the mass inside this r -radial sphere, and as if all of that were a single point at the center of mass. The gravitational attractions from outside the radius of the sphere cancel out (just as an object inside a hollow sphere will feel no gravity at all). The mass inside the sphere is given by

$$M = \frac{4\pi}{3}r^3\rho, \quad (4.3)$$

where ρ is the mass density. The total energy for the particle is then the sum of kinetic and potential energy, respectively:

$$\begin{aligned} E_T &= \frac{1}{2}m\dot{r}^2 - \frac{GMm}{r} \\ &= \frac{1}{2}m\dot{r}^2 - \frac{4\pi r^2 \rho Gm}{3} . \end{aligned} \quad (4.4)$$

Using the cosmological principle as a basis, that the Universe is homogeneous and isotropic, every location may be considered to be the center, so we may choose one arbitrarily. For a uniform expansion (or contraction) of space we can use comoving coordinates. These comoving distances (x) between objects carried along the expansion remain the same. The relation between the actual distance r and x is given by the scale factor, a , and is a function of time alone ($r = a(t)x$). The comoving distances do not change, such that $\dot{x} = 0$, this gives us:

$$E_T = \frac{m\dot{a}^2 x^2}{2} - \frac{4\pi G \rho a^2 x^2 m}{3} . \quad (4.5)$$

Multiplying everything with $-2/(mx^2a^2)$ and rearranging gives us

$$\left(\frac{\dot{a}}{a}\right)^2 + \frac{2E_T}{mx^2a^2} = \frac{8\pi G}{3}\rho . \quad (4.6)$$

Setting $k = 2E_T/(mc^2x^2)$ we get

$$H^2 \equiv \left(\frac{\dot{a}}{a}\right)^2 = \frac{8\pi G}{3}\rho - \frac{kc^2}{a^2} , \quad (4.7)$$

which is the Friedmann equation without the cosmological constant. The unit of k is inverse comoving length squared — the curvature of space.

4.1.2 The fluid equation

The fluid equation can be derived from the first law of thermodynamics for a reversible process (for which the heat transfer, δQ , is zero)

$$dU + P dV = 0 , \quad (4.8)$$

where $U = \rho c^2$ is the internal energy, P is the pressure, and $V = 4\pi a^3/3$ is the volume. If the change happens over a period of dt we get

$$\begin{aligned} \frac{d}{dt} \left(\frac{4\pi}{3} a^3 \rho c^2 \right) + P \frac{d}{dt} \left(\frac{4\pi}{3} a^3 \right) &= 0 \\ 3 \frac{\dot{a}}{a} \rho c^2 + \dot{\rho} c^2 + 3 \frac{\dot{a}}{a} P &= 0 \\ \dot{\rho} &= -3 \frac{\dot{a}}{a} \left(\rho + \frac{P}{c^2} \right) . \end{aligned} \quad (4.9)$$

From this we can see that the mass density decreases both due to an increased volume and because of pressure work done by the material on the Universe. The pressure is material dependent and can be both positive, zero, or negative, as we will get back to in Section 4.3.

4.1.3 The acceleration equation

The rate of change of the expansion is given by the acceleration equation. It can be derived by first differentiating Eq. (4.7) with respect to time to get

$$2\frac{\dot{a}}{a}\frac{\ddot{a}a - \dot{a}^2}{a^2} - 2\frac{kc^2}{a^2}\frac{\dot{a}}{a} = -\frac{8\pi G}{3}\dot{\rho}, \quad (4.10)$$

Substituting $\dot{\rho}$ with Eq. (4.9) we get

$$2\frac{\dot{a}}{a}\frac{\ddot{a}a - \dot{a}^2}{a^2} - 2\frac{kc^2}{a^2}\frac{\dot{a}}{a} = -8\pi G\frac{\dot{a}}{a}\left(\rho + \frac{P}{c^2}\right), \quad (4.11)$$

and dividing everything with $2\dot{a}/a$

$$\frac{\ddot{a}}{a} - \left(\frac{\dot{a}}{a} + \frac{kc^2}{a^2}\right) = -4\pi G\left(\rho + \frac{P}{c^2}\right). \quad (4.12)$$

Putting Eq. (4.7) in we get

$$\begin{aligned} \frac{\ddot{a}}{a} - \frac{8\pi G}{3}\rho &= -\frac{12\pi G}{3}\left(\rho + \frac{P}{c^2}\right) \\ \frac{\ddot{a}}{a} &= -\frac{4\pi G}{3}G\left(\rho + \frac{3P}{c^2}\right), \end{aligned} \quad (4.13)$$

which is the acceleration equation.

4.2 Friedmann equations from general relativity

The three equations, Eqs. (4.7), (4.9), (4.13), which we just derived classically should be derived from Einstein's field equations if we want the full picture. Friedmann did this back in the early twenties, using what is now called the Friedmann-Lemaître-Robertson-Walker metric [33, 34]. This gives the Friedmann equation and the acceleration equation in the general form which also include the cosmological constant (the fluid equation remains unchanged). In many cases it is more convenient to express the Friedmann equations using energy density, $\varepsilon = \rho c^2$. We then end up with

$$\text{Friedmann Eq.} \quad \left(\frac{\dot{a}}{a}\right)^2 + \frac{kc^2}{a^2} = \frac{8\pi G}{3c^2}\varepsilon + \frac{\Lambda c^2}{3}, \quad (4.14)$$

$$\text{Acceleration Eq.} \quad \left(\frac{\ddot{a}}{a}\right) = -\frac{4\pi G}{3c^2}(\varepsilon + 3P) + \frac{\Lambda c^2}{3}, \quad (4.15)$$

$$\text{Fluid Eq.} \quad \dot{\varepsilon} = -3\frac{\dot{a}}{a}(\varepsilon + 3P). \quad (4.16)$$

If we are using $c = 1$, which is common, the Friedmann equations look the same using ρ or ε .

4.3 Equations of state and the evolution of our Universe

In cosmology, we have four main states in the sense of how its energy density evolves when space expands. These are the two trivial states of radiation (relativistic particles) and cold matter (non-relativistic particles), and the two less trivial: curvature and vacuum energy (cosmological constant). How these states evolve depends on how their pressures are related to their energy densities. This relation is expressed by the equation of state by the dimensionless number w , which is the ratio of pressure over energy density given by

$$w_i = \frac{P_i}{\rho_i c^2} = \frac{P_i}{\varepsilon_i}, \quad (4.17)$$

where w_i has the following values:

$$\text{Cold matter} \quad P = 0 \quad \rightarrow \quad w = 0. \quad (4.18a)$$

$$\text{Radiation} \quad P = 1/3\varepsilon \quad \rightarrow \quad w = 1/3. \quad (4.18b)$$

$$\text{Curvature} \quad P = -1/3\varepsilon \quad \rightarrow \quad w = -1/3. \quad (4.18c)$$

$$\text{Vacuum energy} \quad P = -\varepsilon \quad \rightarrow \quad w = -1. \quad (4.18d)$$

We can use this to get the equations of state for our cases. From the thermodynamic relation we have $dU = T dS - P dV$, with no increase in the entropy, such that

$$\begin{aligned} \varepsilon da^3 + a^3 d\varepsilon + P da^3 &= 0 \\ \varepsilon da^3 + a^3 d\varepsilon + w\varepsilon a^3 &= 0 \\ \varepsilon(1 + w) da^3 + a^3 d\varepsilon &= 0 \\ \frac{d\varepsilon}{\varepsilon} &= -(1 + w) \frac{da^3}{a^3} \\ \ln(\varepsilon) &= -(1 + w) \ln(a^3) + C \\ \ln(\varepsilon) &= \ln\left(a^{-3(1+w)}\right) + C \\ \varepsilon &= C a^{-3(1+w)}, \end{aligned} \quad (4.19)$$

where C is a constant to be defined shortly.

The curvature of our Universe depends on the Hubble parameter and the energy density. A high density leads to a positive curvature and a low density to a negative curvature. The critical density is the density which gives the Universe a flat curvature, that is k equal to zero. We can find the conditions for this by rearranging Eq. (4.14):

$$\frac{k}{a^2} = \frac{8\pi G\varepsilon}{3c^2} - H^2 = 0. \quad (4.20)$$

4.3 Equations of state and the evolution of our Universe

Solving this for ε gives us the critical density ε_c :

$$\varepsilon_c = \frac{3H^2c^2}{8\pi G} . \quad (4.21)$$

The critical density is crucial for the evolution of the Universe, and the actual densities can be expressed as a ratio in comparison to this density. We call the ratio the density parameter, and define it as:

$$\Omega_i \equiv \frac{\varepsilon_i}{\varepsilon_c} = \frac{8\pi G}{3H^2c^2}\varepsilon_i , \quad (4.22)$$

where the index i can be the one of the states from Eq. (4.18). We can then express the energy densities as

$$\varepsilon_i = \varepsilon_c\Omega_i . \quad (4.23)$$

We now have two different equations for ε in Eqs. (4.19, 4.23). By defining the scale factor at a given time, t_0 (e.g. present time) to be $a = 1$, we get a value for the constant C in Eq. (4.19) for that time to be $\varepsilon_c\Omega_0$. Or as expressed by its components:

$$C_i = \varepsilon_c\Omega_{i,0} . \quad (4.24)$$

The time-varying energy density will thus be

$$\varepsilon_i = \varepsilon_c\Omega_{i,0}a^{-3(1+w_i)} . \quad (4.25)$$

The current value of Ω , that is the sum over all Ω_i looks like it is very close to one. This is a peculiar thing, since if Ω were ever slightly different from one, it would rapidly move away from this ratio. This is known as the flatness problem. One of the most popular theories which solves this conundrum is inflation theory. In this scenario the observable Universe is just a very small part of something much larger, so even though the whole Universe might be curved, it will appear flat to us. Assuming a flat non-curved Universe (or alternately put the curvature as part of the energy density) we can set up the first Friedmann equation (Eq. (4.14)) to account for the different states of matter.

$$\begin{aligned} \left(\frac{\dot{a}}{a}\right)^2 &= \frac{8\pi G}{3c^2}\varepsilon_c \sum_i \Omega_{i,0}a^{-3(1+w_i)} \\ &= H_0^2 \sum_i \Omega_{i,0}a^{-3(1+w_i)} . \end{aligned} \quad (4.26)$$

We can rewrite this as

$$\dot{a}^2 = H_0^2 \sum_i \Omega_{i,0}a^{-(1+3w_i)} . \quad (4.27)$$

Taking the time-derivative on the left hand side in two different ways gives us

$$\begin{aligned} \frac{d}{dt}\dot{a}^2 &= 2\dot{a}\ddot{a} \\ &= \frac{d\dot{a}^2}{da} \frac{da}{dt} = \dot{a} \frac{d\dot{a}^2}{da} \\ \rightarrow \ddot{a} &= \frac{1}{2} \frac{d\dot{a}^2}{da} . \end{aligned} \quad (4.28)$$

Taking the d/da -derivative on the right hand side of Eq. (4.27) gives us

$$H_0^2 \sum_i -(1 + 3w_i)\Omega_{i,0}a^{-(2+3w_i)} . \quad (4.29)$$

By further combining Eq. (4.28) and Eq. (4.29) we get the following equation for the acceleration of the Universe, telling us how the Universe evolved in the past, and will evolve in the future:

$$\ddot{a} = -\frac{H_0^2}{2} \sum_i \frac{1 + 3w_i}{a^{2+3w_i}} \Omega_{i,0} . \quad (4.30)$$

By using the latest estimates for the Hubble variable and the density parameters we can calculate that the radiation dominated era ended roughly 50,000 years after the Big Bang, and the following matter dominated era ended about 10 billion years later. These transitions happens gradually as is shown in Figure 4.1. The evolution of the scale factor is shown in Figure 4.1 together with scenarios using different energy densities.

4.4 Adding viscosity to the Friedmann equations

If the cosmic fluid has a bulk viscosity, the pressure will be reduced accordingly such that we get an effective pressure, $P_{\text{eff.}} = P - P_{\text{visc.}}$, where P is the thermodynamic equilibrium pressure and $P_{\text{visc.}}$ is the viscous pressure given as $3\eta_v H$, where η_v is the bulk viscosity [36]. We can then express the effective pressure as a function of the viscosity:

$$P_{\text{eff.}} = P - 3\eta_v H . \quad (4.31)$$

By simulating the early universe, where we can put both k and Λ equal to zero, we can incorporate the viscous pressure into the accelerating and fluid equation (the first Friedmann equation remains unchanged as it is independent of the pressure):

$$\text{Visc. acceleration Eq.} \quad \frac{\ddot{a}}{a} = -\frac{H^2}{2} - \frac{4\pi G}{c^2} (P - 3\eta_v H) , \quad (4.32)$$

$$\text{Visc. fluid Eq.} \quad \dot{\epsilon} = -3H(\epsilon + P) + 9\eta_v H^2 . \quad (4.33)$$

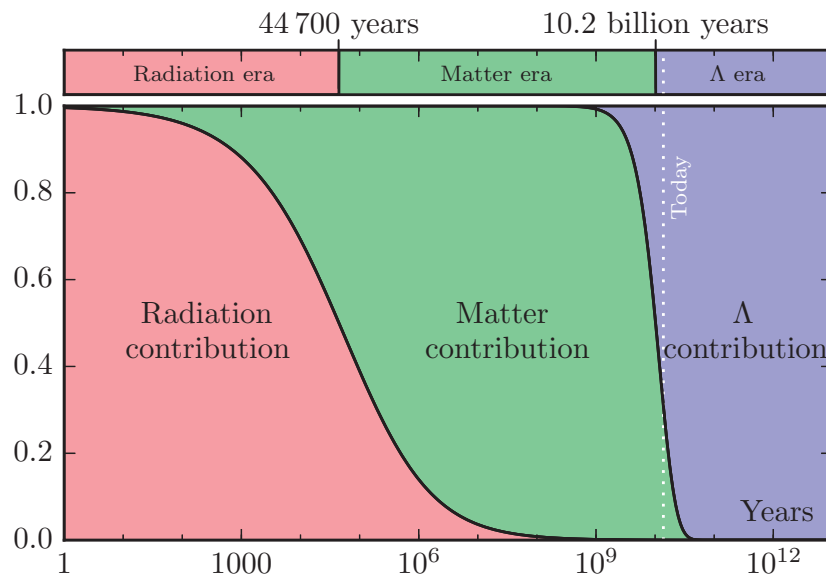


Figure 4.1: Energy contribution in the Universe by radiation, matter and a cosmological constant (Λ). The energy density for these three cases evolves differently during expansion ($\varepsilon_r \propto a^{-4}$, $\varepsilon_m \propto a^{-3}$, $\varepsilon_\Lambda \propto 1$). This lead to the Universe going through different eras. Radiation dominated for the first 44 700 years after the Big Bang, followed by matter. We are currently living in an era where dark energy (e.g. a cosmological constant) is the dominant energy contributor.

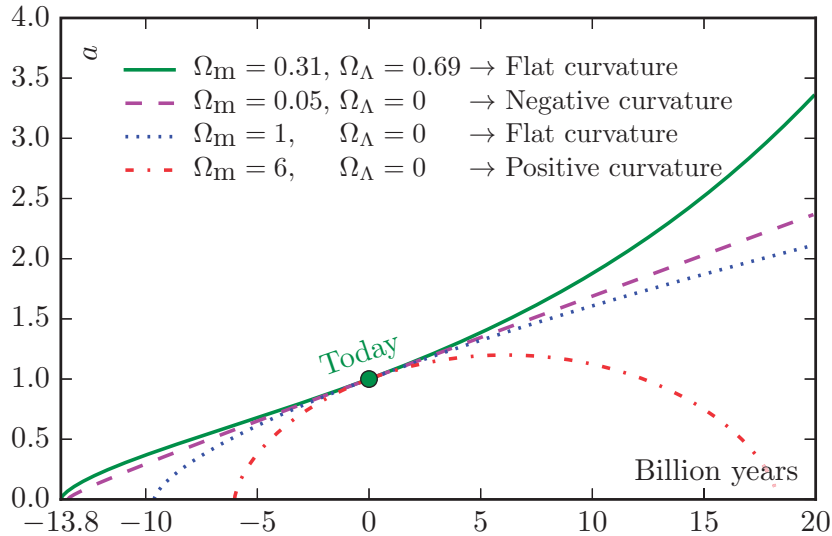


Figure 4.2: Mapping the evolution of the Universe by Ω contributions. In (hypothetical) scenarios with no dark energy, the curvature (and overall geometry) is determined by the matter contribution. Ω_m below, equal to, or above the critical density (here in magenta, blue and red colors) will give negative, flat and positive curvatures. Using the current Λ CDM parameters as of 2015 [19] gives us the green plot. Baryonic matter (5%) and dark matter (26%) make up the 31% matter contribution, while dark energy (here in the form of the cosmological constant) make up 69%.

4.5 Viscosity by numbers and illustrations

The concept of shear and bulk viscosity is discussed in my second paper “Viscosity in a lepton-photon universe” [2], and shown briefly here in Figure 4.3 and 4.4. The first numerical calculation of shear viscosity η_s was done by Misner in 1967, where he studied a mixture of massive particles interacting with massless photons and neutrinos. He got a result of [37]:

$$\eta_s = \frac{4}{15} \varepsilon \tau \approx 1.23 \times 10^{38} T^{-1}, \quad (4.34)$$

where τ is the mean free time of flight. In 1978, Caderni, Fabbri, Van den Horn, and Sisskens came of with a much smaller value of the η_s during the lepton era [38]:

$$\eta_s = 2.20 \times 10^{35} T^{-1}. \quad (4.35)$$

In the early eighties, a lot of progress were done on the topic of relativistic kinetic theory by, among others, Hoogeveen, et al. This group estimated the shear viscosity to [39]:

$$\eta_s = 9.81 \times 10^{35} T^{-1}. \quad (4.36)$$

The two latter papers also gave estimates to the bulk viscosity during the lepton era. These vary much more with temperature but for a temperature of 10^{12} K, Caderni’s

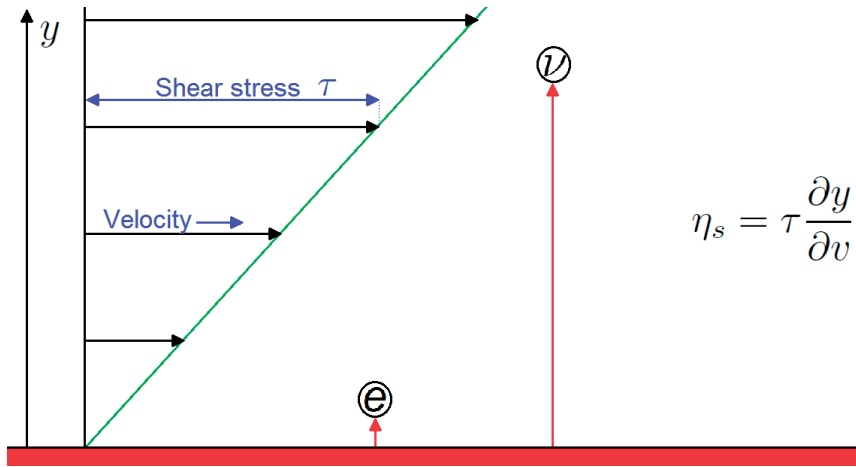


Figure 4.3: Concept drawing of shear viscosity for a flow. The shear stress increases as the particles travel farther in the perpendicular direction of the flow. Weakly interacting particles is thus the main contributor to shear viscosity.

group found

$$\eta_v = 5.85 \times 10^{12} \text{g cm}^2 \text{s}^{-1}, \quad (4.37)$$

while Hoogeveen's group came to a result of

$$\eta_v = 2.30 \times 10^{13} \text{g cm}^2 \text{s}^{-1}, \quad (4.38)$$

which is roughly 5 times larger.

4.6 The deceleration parameter

The deceleration parameter is used to make corrections when calculating the luminosity distance. It is actually just the acceleration equation divided by the Friedmann equation, and is defined as

$$q = -\frac{\ddot{a}a}{\dot{a}^2} = \frac{1}{2} \frac{\sum (1 + 3w_i)\Omega_i}{\sum \Omega_i}. \quad (4.39)$$

The sum of the density parameters is very close to one (in many models it is defined as one), so we can remove the denominator (otherwise $\sum \Omega_i$ varies over time). By inserting the values for w we can express Eq. (4.39) as

$$q = \frac{1}{2} \Omega_M + \Omega_r - \Omega_\Lambda. \quad (4.40)$$

It is worth noting that the deceleration parameter is independent of the curvature term (because $w_k = -1/3$ and hence the nominator becomes zero). We can easily

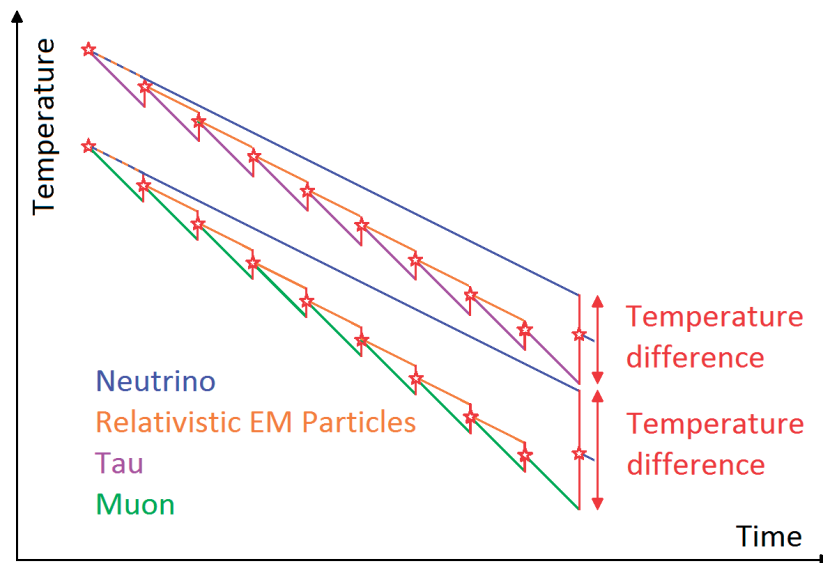


Figure 4.4: Concept drawing of bulk viscosity. If we have two types of particles, which wants to cool down at different rates we get a heat transfer from the hotter particles to the colder particles. In my papers [2, 3], a model universe consisting only of the known leptons and the photons have been used. In this scenario, the first particles which stops behaving purely relativistic are the tau-particles. As the rest mass becomes a significant contribution to the tau's total energy, it will start to cool down slightly faster, and then more so as the temperature drops further. We can divide the heat transfer into two events. First, we have the very-frequent-low-momentum-exchange heat transfer between the taus and the other electromagnetically charged particles. All these particles are thus cooled down slightly faster than before. The second event is the heat exchange between *all* the charged leptons and the neutrinos. The neutrinos, which only interact weakly and thus have kept their temperature for a longer time, will give rise to a much larger momentum transfer.

calculate today's value of q_0 using the latest data. The radiation contribution today is negligible, and we get:

$$q_0 = -0.54 , \tag{4.41}$$

which we see is a negative value, meaning that the expansion of the Universe is accelerating.

5 Kinetic Theory

5.1 Four-vectors, velocities and momenta

Four-vectors are important in relativistic kinetic theory, and a short primer is given here. The familiar spatial vectors from Euclidean geometry has to be replaced with new ones containing the time coordinate as well. We will use a metric signature of $(+ - - -)$, which in Minkowski space gives the following matrix

$$\begin{pmatrix} 1 & 0 & 0 & 0 \\ 0 & -1 & 0 & 0 \\ 0 & 0 & -1 & 0 \\ 0 & 0 & 0 & -1 \end{pmatrix} .$$

We will use the following notation for variables for positions, velocities, and momenta

$$x = x^\mu = (x^0, x^1, x^2, x^3) = (ct, x, y, z) = (ct, \mathbf{x}) , \quad (5.1)$$

$$u = u^\mu = (u^0, u^1, u^2, u^3) = \gamma(c, v_x, v_y, v_z) = \gamma(c, \mathbf{v}) , \quad (5.2)$$

$$p = p^\mu = (p^0, p^1, p^2, p^3) = (E/c, p_x, p_y, p_z) = (E/c, \mathbf{p}) , \quad (5.3)$$

where $\gamma = [1 - (v/c)^2]^{-1/2}$ is the Lorentz factor. The momentum four-vector is defined as $p^\mu = mu^\mu$. We have used bold parameters to represent the three spatial variables. Thus for a particle with mass m and momenta \mathbf{p} , the energy is given as

$$E = cp^0 = c\sqrt{\mathbf{p}^2 + m^2c^2} . \quad (5.4)$$

The magnitudes of the four-velocity and four-momentum is given as

$$u \cdot u = u^\mu u_\nu = g_{\mu\nu} u^\mu u^\nu = c^2 , \quad (5.5)$$

$$p \cdot p = p^\mu p_\nu = g_{\mu\nu} p^\mu p^\nu = (E/c)^2 - |\mathbf{p}|^2 = m^2c^2 , \quad (5.6)$$

where $g_{\mu\nu}$ is the metric. Finally we may write down the four-flow which is the relativistic equivalence of particle flow, $\mathbf{j}(\mathbf{x}, t)$:

$$N^\mu(x) = (cn(\mathbf{x}, t), \mathbf{j}(\mathbf{x}, t)) . \quad (5.7)$$

5.2 Cross sections and mean free paths

Charged leptons interact via the weak and electromagnetic forces, neutrinos only through the weak force, and photons only through the electromagnetic force. If we limit ourselves to the lepton era we can distinguish between four different collisions:

1. $\nu\nu$ and νe collisions \rightarrow governed by the weak force (wk),
2. ee and $e\gamma$ collisions \rightarrow governed by the electromagnetic force (em),
3. $\gamma\gamma$ collisions,
4. $\nu\gamma$ collisions.

As functions of the mean kinetic energy, $k_{\text{B}}T$, we have approximate expressions for these four cross sections [39, 40]:

$$\sigma_{\text{wk}} \approx \left(\frac{Gk_{\text{B}}T}{2\pi\hbar^2c^2} \right)^2, \quad (5.8)$$

$$\sigma_{\text{em}} \approx \left(\frac{\alpha\hbar c}{k_{\text{B}}T} \right)^2, \quad (5.9)$$

$$\sigma_{\gamma\gamma} \approx \left(\frac{\alpha^2\hbar c}{k_{\text{B}}T} \right)^2, \quad (5.10)$$

$$\sigma_{\nu\gamma} \approx 0. \quad (5.11)$$

The mean free path is the inverse of the number density and cross section:

$$l = \frac{1}{n\sigma}. \quad (5.12)$$

As we see from Eqs. (5.8)–(5.10), the weak and electromagnetic cross sections behave quite differently as functions of temperature. One gets smaller as the temperature drops, and the other one increases. The electromagnetic force and the weak force merge together to what we call the electroweak force at around 100 GeV (around the masses of the intermediate vector bosons — the W 's and Z). These simple approximated cross sections and mean free paths are shown in Fig. 5.1. For a more rigorous estimate we need to take the particle flavors into account.

5.3 Weinberg-Salam model for weak interactions

We can make a more precise estimate of the weak cross sections by using the Weinberg-Salam model for electroweak interactions. For the lepton era (at energies below the mass-equivalent of the intermediate vector bosons: W^+ , W^- , and Z^0) we can use a current-current coupling approximation [39]. The *charged current* is the exchange of either W^+ or W^- bosons, and the *neutral current* is the exchange of the Z^0 boson. This is equivalent to the photon exchange in the electromagnetic interaction. For elastic collisions we have:

$$k + l \rightarrow k + l. \quad (5.13)$$

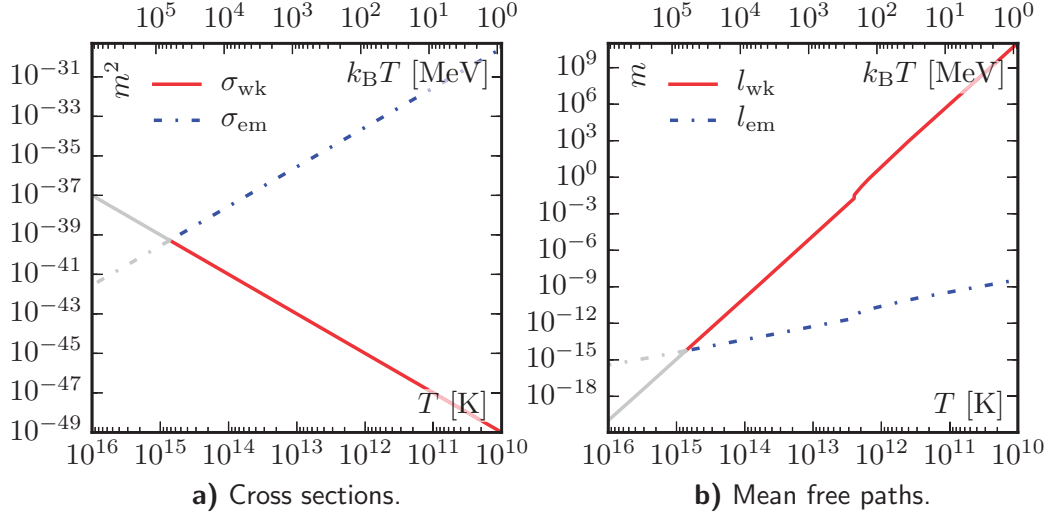


Figure 5.1: Simplified plots of cross sections (left plot) and mean free paths (right plot) for electromagnetically interacting and weakly interacting particles. At around 100 GeV the two forces merge together to the electroweak force.

The charged leptons will predominantly interact with each other (and the photon) through the electromagnetic force, while the interactions involving neutrinos can only happen through the weak force. For the interactions involving neutrinos we have:

$$k = \nu_e, \bar{\nu}_e, \nu_\mu, \bar{\nu}_\mu, \nu_\tau, \bar{\nu}_\tau, \quad (5.14)$$

$$l = \nu_e, \bar{\nu}_e, \nu_\mu, \bar{\nu}_\mu, \nu_\tau, \bar{\nu}_\tau, e, \bar{e}, \mu, \bar{\mu}, \tau, \bar{\tau}. \quad (5.15)$$

Before we go any further we should introduce what are called the Mandelstam variables.

5.3.1 Mandelstam variables

For scattering processes with two particles (k and l) going in and two particles going out, we can use the center-of-momentum frame as is done in Figure 5.2. The four-momentum of the ingoing particles are thus p_k and p_l , and the two particles going out have four-momentum p'_k and p'_l . This gives us three possible scenarios, or channels, which represent the different outcomes, namely the s , t , and u channel (shown in Figure 5.3). The associated variables are called the *Mandelstam variables* and are related to energy, momentum, and angles in the scattering process. They are defined as:

$$s = (p_k + p_l)^2 = (p'_k + p'_l)^2, \quad (5.16a)$$

$$t = (p_k - p'_k)^2 = (p_l - p'_l)^2, \quad (5.16b)$$

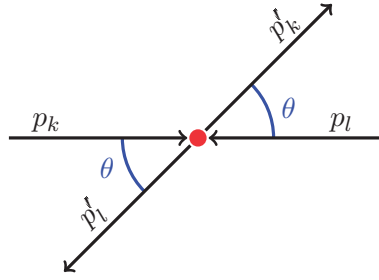


Figure 5.2: Two-particle (p_k and p_l) to two-particle (p'_k and p'_l) elastic scattering with corresponding angle in the center-of-momentum frame of the system.

$$u = (p_k - p'_l)^2 = (p_l - p'_k)^2 . \quad (5.16c)$$

Here s is the square of the center-of-mass energy (invariant mass) for the two incoming particles k and l . t is the square of the four-momentum transfer, and is related to the scattering angle in the center of momentum system, which is defined later in Eq. (5.23). p'_k is the four-momentum of particle k after the collision.

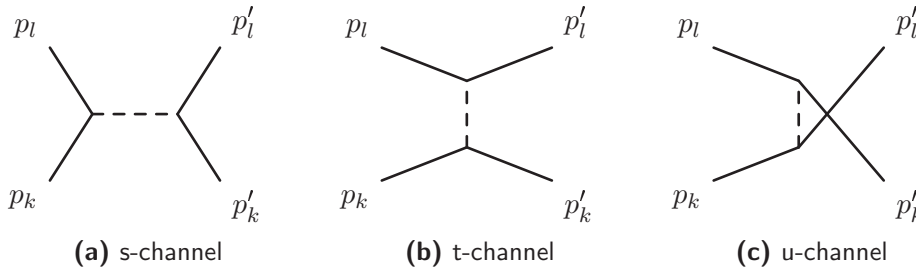


Figure 5.3: Feynman diagrams for s (space), t (time), and u channel. They represent the different possible scatterings with two incoming and two outgoing particles. The s -channel represents the two incoming particles, p_k and p_l , merging together to form an intermediate particle, which then splits into particles p'_k and p'_l . In the t -channel particle p emits a particle, becoming particle p'_k , and particle p_l absorbs the intermediate particle and becoming particle p'_l . For the u -channel the roles of the two outgoing particles are changed, such that p_k becomes p'_l and p_l becomes p'_k .

5.3.2 Weak currents

The effective interaction Lagrangian density for the currents are [39]:

$$\mathcal{L}_{\text{eff}} = \frac{G_F}{\sqrt{2}} \left(J^{c\lambda} J_\lambda^{c\dagger} + 2J^{n\lambda} J_\lambda^n \right) , \quad (5.17)$$

where $J^{c\lambda}$ and $J^{n\lambda}$ are the charged and neutral currents, and λ is the four-vector index (used instead of μ to avoid confusion with the symbol for the muon particle),

and the \dagger symbol is for the Hermitian conjugate. The three (six if we count anti particles) charged lepton contributions to these are:

$$J_e^{c\lambda} = \bar{\nu}_e \gamma^\lambda (1 - \gamma^5) e, \quad (5.18a)$$

$$J_\mu^{c\lambda} = \bar{\nu}_\mu \gamma^\lambda (1 - \gamma^5) \mu, \quad (5.18b)$$

$$J_\tau^{c\lambda} = \bar{\nu}_\tau \gamma^\lambda (1 - \gamma^5) \tau, \quad (5.18c)$$

$$J_e^{n\lambda} = \frac{1}{2} \bar{\nu}_e \gamma^\lambda (1 - \gamma^5) \nu_e - \frac{1}{2} \bar{e} \gamma^\lambda (1 - 4 \sin^2 \theta_W - \gamma^5) e, \quad (5.18d)$$

$$J_\mu^{n\lambda} = \frac{1}{2} \bar{\nu}_\mu \gamma^\lambda (1 - \gamma^5) \nu_\mu - \frac{1}{2} \bar{\mu} \gamma^\lambda (1 - 4 \sin^2 \theta_W - \gamma^5) \mu, \quad (5.18e)$$

$$J_\tau^{n\lambda} = \frac{1}{2} \bar{\nu}_\tau \gamma^\lambda (1 - \gamma^5) \nu_\tau - \frac{1}{2} \bar{\tau} \gamma^\lambda (1 - 4 \sin^2 \theta_W - \gamma^5) \tau. \quad (5.18f)$$

The γ^λ 's here are the four gamma matrices (also known as 4×4 Dirac matrices), and $\gamma^5 \equiv i\gamma^0\gamma^1\gamma^2\gamma^3$. They are given in Appendix C.

The amplitude for any $k + l \rightarrow k + l$ reaction is the sum of the aforementioned s -channel, t -channel, and u -channel contribution. According to Hoogeveen [39] we can write all these using the s and t channel only with the addition of two matrices: v and a (as given in Tables 5.1 and 5.2). This leads to the following equations for the weak cross sections:

$$\frac{d\sigma_{kl}}{d\Omega_{\text{CM}}} = \frac{G_F^2 s}{32\pi^2 \hbar^4 c^2} S f(s, t), \quad (5.19)$$

where G_F is the Fermi coupling constant. s is the square of center-of-mass collision energy, and was defined in Eq. (5.16a). S is a prefactor which compensates for the number of identical particles in the final state ($n_f!$), and contains a factor 2 for each neutrino in the initial state (incoming particles). This latter factor comes from the fact that neutrinos only have one polarization state, while the other particles have 2 (spin up and spin down), which gives us the following value:

$$S = \frac{2^{n_\nu}}{n_f!}. \quad (5.20)$$

The final variable in Eq. (5.19) is $f(s, t)$, which is a function of the Mandelstam variables, s and t and two prefactors, a and v . a and v relate the current couplings to flavors of the k and l particle. This gives us [39]:

$$f(s, t) = (v+a)^2 \left(\frac{s - m^2 c^2}{s} \right)^2 + (v-a)^2 \left(\frac{s + t - m^2 c^2}{s} \right)^2 + (v^2 - a^2) \frac{2m^2 c^2 t}{s^2}, \quad (5.21)$$

where m is the mass of the charged lepton¹. The a and v matrices are given in Tables 5.1 and 5.2.

Table 5.1: a matrix.

	ν_e	$\bar{\nu}_e$	ν_μ	$\bar{\nu}_\mu$	ν_τ	$\bar{\nu}_\tau$	e^-	e^+	μ^-	μ^+	τ^-	τ^+
ν_e :	1	-1	1/2	-1/2	1/2	-1/2	1/2	-1/2	-1/2	1/2	-1/2	1/2
$\bar{\nu}_e$:	-1	1	-1/2	1/2	-1/2	1/2	-1/2	1/2	1/2	-1/2	1/2	-1/2
ν_μ :	1/2	-1/2	1	-1	1/2	-1/2	-1/2	1/2	1/2	-1/2	-1/2	1/2
$\bar{\nu}_\mu$:	-1/2	1/2	-1	1	-1/2	1/2	1/2	-1/2	-1/2	1/2	1/2	-1/2
ν_τ :	1/2	-1/2	1/2	-1/2	1	-1	-1/2	1/2	-1/2	1/2	1/2	-1/2
$\bar{\nu}_\tau$:	-1/2	1/2	-1/2	1/2	-1	1	1/2	-1/2	1/2	-1/2	-1/2	1/2

Table 5.2: v matrix. w^+ and w^- are abbreviations for $\sin^2 \theta_W \pm 1/2$, which are equal to 0.7223 and -0.2777 , respectively.

	ν_e	$\bar{\nu}_e$	ν_μ	$\bar{\nu}_\mu$	ν_τ	$\bar{\nu}_\tau$	e^-	e^+	μ^-	μ^+	τ^-	τ^+
ν_e :	1	1	1/2	1/2	1/2	1/2	w^+	w^+	w^-	w^-	w^-	w^-
$\bar{\nu}_e$:	1	1	1/2	1/2	1/2	1/2	w^+	w^+	w^-	w^-	w^-	w^-
ν_μ :	1/2	1/2	1	1	1/2	1/2	w^-	w^-	w^+	w^+	w^-	w^-
$\bar{\nu}_\mu$:	1/2	1/2	1	1	1/2	1/2	w^-	w^-	w^+	w^+	w^-	w^-
ν_τ :	1/2	1/2	1/2	1/2	1	1	w^-	w^-	w^-	w^-	w^+	w^+
$\bar{\nu}_\tau$:	1/2	1/2	1/2	1/2	1	1	w^-	w^-	w^-	w^-	w^+	w^+

We may rewrite Eq. (5.16a) as

$$P_{kl}^2 \equiv s = (p_k + p_l)^2, \quad (5.22)$$

and then Eq. (5.16b) as

$$t = m_k^2 c^2 + m_l^2 c^2 - P_{kl}^2 + \frac{(P_{kl}^2 + m_k^2 c^2 - m_l^2 c^2)(P_{kl}^2 - m_k^2 c^2 + m_l^2 c^2)}{2P_{kl}^2} + \frac{[P_{kl}^2 - (m_k c + m_l c)^2][P_{kl}^2 - (m_k c - m_l c)^2]}{2P_{kl}^2} \cos \theta_{kl}, \quad (5.23)$$

where θ_{kl} is the scattering angle in the center-of-momentum of the system, as is shown if Figure 5.2. We can define the angle θ as [40]

$$\cos \theta = \left[\frac{\mathbf{p}_k \cdot \mathbf{p}'_k}{|\mathbf{p}_k| |\mathbf{p}'_k|} \right]_{\text{CM}} = \frac{(p_k^\mu + p_l^\mu)(p'_{k\mu} + p'_{l\mu})}{(p_k - p_l)^2}, \quad (5.24)$$

and relate it to the parameter, t , through the relation

$$\cos \theta - 1 = \frac{2t}{s - 4m^2 c^2}. \quad (5.25)$$

¹We don't include interactions involving two charged leptons, as they interact mainly through the electromagnetic force.

For pure neutrino-neutrino interactions (here we treat them as massless, which is very close to reality), Eq. (5.23) and Eq. (5.21) simplifies significantly to

$$t_{m=0} = \frac{P_{kl}^2}{2} (\cos \theta - 1) , \quad (5.26)$$

$$f(s, t)_{m=0} = (v + a)^2 + \frac{(v - a)^2}{4} (1 + \cos \theta)^2 . \quad (5.27)$$

For the interaction between neutrinos and the massive leptons, we need to do the full calculation.

5.4 Relativistic kinetic equation

The classical Boltzmann transport equation, or kinetic equation, was derived by Ludwig Boltzmann in 1872. It describes macroscopic quantities in non-equilibrium systems, such as energy and number of particles, in terms of statistical behavior. The relativistic version of the kinetic equation was developed gradually during the last century. We will here give a short version following the theory developed by de Groot, van Leeuwen, and van Weert in the book “Relativistic kinetic theory” [40]. To quote them: “The kinetic equation is a closed equation (meaning it can be calculated in a finite number of operations, and usually do not contain any limits) for the space-time behavior of the distribution function”. In relativistic kinetic theory, all the macroscopic quantities are defined with help from the distribution functions. In Section 3.1, Eqs. (3.5), we defined those in the cases of thermodynamic equilibrium. For non-equilibrium states, we need to include the positions as well such that we get $f(x, p)$. The relativistic kinetic equation requires, first of all, that the number of particles in the system is large enough that a statistical approach is justified. A second requirement is that the equations are covariant². The kinetic equation also assumes three properties (both in the classical and relativistic case):

1. Only two particle interactions are considered.
2. The hypothesis of molecular chaos. By that, we assume that the velocities of the colliding particles are uncorrelated and independent of position. The number of (binary) collisions is proportional to the product of the distributions functions of the two colliding particles. It is also proportional to a transition rate, which is a measure of the probability of the collision process.
3. The change in the distribution function is negligible in spacetime. That is: the characteristic lengths and times are negligibly small.

²An equation is Lorentz covariant if all its key properties are valid in all inertial reference frames

5.4.1 Kinetic equation without collisions

Consider a small volume $\Delta^3\sigma$ located at position x . The changes in its three-surface element changes is given by the four vector $d^3\sigma_\mu$. In the Lorentz frame this vector is purely time-like $(d^3x, 0, 0, 0)$. The number of particle world lines crossing the segment $\Delta^3\sigma$ with momentum in the range Δp around \vec{p} is given by:

$$\Delta N(x, p) = \int_{\Delta^3\sigma} \int_{\Delta^3p} d^3\sigma_\mu \frac{d^3p}{p^0} p^\mu f(x, p) . \quad (5.28)$$

In the Minkowski space element Δ^4x the net flow through the surface $\Delta^3\sigma$ vanishes such that Eq. (5.28) becomes zero. By using the divergence theorem we can rewrite this as

$$\int_{\Delta^4x} \int_{\Delta^3p} d^4x \frac{d^3p}{p^0} p^\mu \partial_\mu f(x, p) , \quad (5.29)$$

where $\partial_\mu = \partial/\partial x^\mu = (c^{-1}\partial_t, \nabla)$ is the differential with respect to the space-time coordinates. However, since the intervals Δ^4x and Δ^3p are arbitrary, we get:

$$p^\mu \partial_\mu f(x, p) = 0 \quad \text{4-vector notation} \quad (5.30a)$$

$$(\partial_\mu + \vec{u} \cdot \nabla) f(x, p) = 0 \quad \text{3-vector notation} , \quad (5.30b)$$

which is the *collisionless relativistic transport equation*.

5.4.2 Kinetic equation with collisions

If we have collisions between particles within the range of Δ^4x and a given momentum, changes. For a particle k , with momenta in the range Δ^3p_k the change is equal to

$$\Delta^4x \frac{\Delta^3p}{p^0} C(x, p) , \quad (5.31)$$

where $C(x, p)$ is an invariant function. Using the theory of molecular chaos, the average number of collisions in a volume element Δ^3x during a time interval Δt is proportional to

1. The average number of particles per unit volume with three momentum in the range $(\mathbf{p}_k, \mathbf{p}_k + \Delta\mathbf{p}_k) = \Delta^3p_k f(x, p_k)$.
2. The average number of particles per unit volume with three momentum in the range $(\mathbf{p}_l, \mathbf{p}_l + \Delta\mathbf{p}_l) = \Delta^3p_l f(x, p_l)$.
3. The intervals $\Delta^3p'_k$, $\Delta^3p'_l$, and Δ^4x .

The proportionality factor is denoted as:

$$\frac{W(p_k, p_l | p'_k, p'_l)}{p_k^0 p_l^0 p_k'^0 p_l'^0} , \quad (5.32)$$

where the nominator $W(p_k, p_l | p'_k, p'_l)$ is called the transition rate. It is Lorentz scalar (a scalar which is invariant under a Lorentz transformation), and depends only on the four-momenta before and after collision. We can rewrite Eq. (5.32) using three vectors as:

$$w(\mathbf{p}_k, \mathbf{p}_l | \mathbf{p}'_k, \mathbf{p}'_l) \equiv \frac{cW(p_k, p_l | p'_k, p'_l)}{p_k^0 p_l^0 p'_k{}^0 p'_l{}^0}. \quad (5.33)$$

The quantity $w(\mathbf{p}_k, \mathbf{p}_l | \mathbf{p}'_k, \mathbf{p}'_l) \Delta^3 p'_k \Delta^3 p'_l$ is the transition probability per unit volume and per unit time that two particles having momenta \mathbf{p}_k and \mathbf{p}_l are scattered with an outgoing momenta of $(\mathbf{p}_k \pm \Delta \mathbf{p}_k)$ and $(\mathbf{p}_l \pm \Delta \mathbf{p}_l)$.

According to the theory of molecular chaos the total number of particles lost to collisions in the range $\Delta^4 x$ and $(\mathbf{p} + \Delta \mathbf{p})$ is found by integrating the proportionality factor over all values of \mathbf{p}_l , \mathbf{p}'_k , and \mathbf{p}'_l . We also gain particles due to collisions, that is particles with initial momenta $(\mathbf{p}'_k, \mathbf{p}'_l)$ ending up with momenta $(\mathbf{p}_k, \mathbf{p}_l)$. We also have to include a factor 1/2, since the two momenta states $(\mathbf{p}'_k, \mathbf{p}'_l)$ and $(\mathbf{p}'_l, \mathbf{p}'_k)$ can not be distinguished. The resulting net change of particles in the interval $\Delta^4 x$ and $\Delta^3 p$ is the collision function $C(x, p_k)$

$$C(x, p_k) = \frac{1}{2} \int \frac{d^3 p_l}{p_l^0} \frac{d^3 p'_k}{p'_k{}^0} \frac{d^3 p'_l}{p'_l{}^0} [f(x, p'_k) f(x, p'_l) W(p'_k, p'_l | p_k, p_l) - f(x, p_k) f(x, p_l) W(p_k, p_l | p'_k, p'_l)]. \quad (5.34)$$

We then get the following explicit equation for the *relativistic transport equation with elastic collision*:

$$p_k^\mu \partial_\mu f(x, p_k) = C(x, p_k) = \frac{1}{2} \int \frac{d^3 p_l}{p_l^0} \frac{d^3 p'_k}{p'_k{}^0} \frac{d^3 p'_l}{p'_l{}^0} [f(x, p'_k) f(x, p'_l) W(p'_k, p'_l | p_k, p_l) - f(x, p_k) f(x, p_l) W(p_k, p_l | p'_k, p'_l)]. \quad (5.35)$$

In non-relativistic theory, $p^\mu \partial_\mu f(x, p_k)$ is called the *streaming term*, while $C(x, p_k)$ is also called the *collision term*.

If k and l are different particles (mixture) we need to sum over all particle species

$$p_k^\mu \partial_\mu f(x, p_k) = \sum_{l=1}^N C_{kl}(x, p_k), \quad (5.36)$$

with the collision matrix given by

$$C_{kl} = \gamma_{kl} \int \frac{d^3 p_l}{p_l^0} \frac{d^3 p'_k}{p'_k{}^0} \frac{d^3 p'_l}{p'_l{}^0} [f(x, p'_k) f(x, p'_l) W_{kl}(p'_k, p'_l | p_k, p_l) - f(x, p_k) f(x, p_l) W_{kl}(p_k, p_l | p'_k, p'_l)] \quad (5.37)$$

$$k, l = 1, 2, 3, \dots, N, \quad (5.38)$$

5 Kinetic Theory

where $\gamma_{kl} = 1 - 1/2\delta_{kl}$, δ_{kl} being the Kronecker delta. Finally, if we have inelastic scattering, we get $k + l \rightarrow i + j$, and a transition rate given as

$$W_{kl|ij} \equiv W_{kl|ij}(p_k, p_l | p_i, p_j) \quad (5.39)$$

and a collision matrix

$$C_{kl} = \frac{1}{2} \sum_{i,j=1}^N \int \frac{d^3 p_l}{p_l^0} \frac{d^3 p_i}{p_i^0} \frac{d^3 p_k}{p_j^0} [f(x, p_i) f(x, p_j) W_{ij|kl} - f(x, p_k) f(x, p_l) W_{kl|ij}] \quad (5.40)$$

$$k, l = 1, 2, 3, \dots, N. \quad (5.41)$$

For reactions $k + l \rightarrow i + j$ for the i and j particles are heavier, the transition rate $W_{kl|ij}$ should go zero at a certain treshold.

Appendices

A Short history of Modern Cosmology

We will start with a short history of modern cosmology. This section is based upon several sources. Among them are the books by Guth, Lederman, Randall and Panek [41, 42, 43, 44]. These are highly recommended introductory texts meant for the layman.

One could say that modern cosmology started with Albert Einstein. Not long after publishing his theory on special relativity in 1905 (which concerns space and time in inertial frames [45]), Einstein began thinking about incorporating gravity into his theory. The first step was his principle of equivalence, which roughly says that there is no difference between inertial mass and gravitational mass [46]. It would, however, take almost another decade before all the pieces fell into place. In 1915 he published his famous field equations which describe gravity as spacetime being curved by matter and energy [47]. The year after he published his final version of the general theory of relativity [48] Einstein quickly understood the implications his theory would have for cosmology, namely that the Universe could not be static. In order to fix this “problem”, he introduced the famous cosmological constant in his 1917 paper “Cosmological Considerations in the General Theory of Relativity” [49], an act which he supposedly would call the biggest blunder of his life [50, 51]. Also, his fix was not a stable solution.

Karl Schwarzschild was the first to find an exact solution to Einstein’s field equations, for the limited case of a spherical non-rotating mass [52]. He also found the equation for the event horizon [53]. In 1917 Willem de Sitter found another solution — one for a massless universe with a positive cosmological constant [54]. Arguably the most important solution was first found by Alexander Friedmann in 1922 [33] and 1924 [34] and describes a homogeneous and isotropic expanding or contracting universe.

In 1915 V.M. Slipher was the first to measure the radial velocity of galaxies [58]. In 1927 the Belgium priest and physicist, Georges Lemaître proposed a theory of an expanding Universe [59]. Combining his own measurements with Sliphers, Edwin Hubble published his paper about the relation between distance and radial velocity of galaxies in 1929 [56] (see Figure A.1).

After the discovery of the cosmic expansion, two competing models arose: the Big Bang theory and the Steady State theory. The Big Bang theory is often credited to Lemaître who in 1931 wrote a short article [60] suggesting that the Universe began as a dense “primeval atom”. The most important implication of this theory is that as we go back in time, the Universe gets denser and hotter — and thus

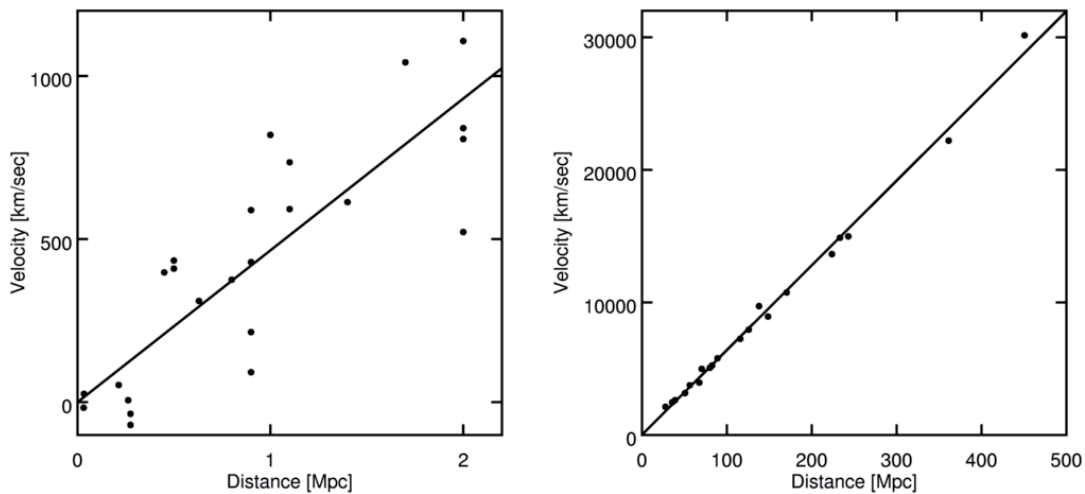


Figure A.1: Two Hubble diagrams, showing radial velocity vs. distance (as replotted in [55]). Hubble's original data plotted from 1929 on the left [56]. By looking at much larger scales (and using newer data [57]) the straight line representing the Hubble constant fits much better.

both have a beginning and a finite size. The Steady State theory was proposed by Fred Hoyle, among others, in 1948 [61]. This theory suggests that the Universe continuously creates new matter as it expands. This would happen at a pace which would perfectly balance the dilution caused by expansion. In the Steady State model, the Universe on a large scale will always have the same density and always look the same. This theory is truthful to the *Perfect Cosmological Principle*, which says that the Universe is homogeneous and isotropic both in space and time. A steady state expanding universe does not run into Olbers' paradox (If the Universe is infinite, how can the night be dark?) as the light gets redshifted. The total energy flux from the sky thus remains finite.

The same year as Hoyle's Steady State paper; Alpher, Bethe, and Gamow published their famous paper on Big Bang nucleosynthesis [62], predicting the proportion of heavier elements in the Universe. Bethe was actually only added by his friend Gamow to make a wordplay on α, β, γ . This undoubtedly brought a lot of extra attention to the paper as describes in Figure A.2. The same Alpher, together with Herman predicted that a Big Bang model would cause a cosmic microwave background [63].

The death of the Steady State theory came in 1964 when the two astronomers Arno Penzias and Robert Wilson at Bell Labs discovered the 2.7 K microwave background more or less by accident [65]. The noise was interpreted as black body radiation from the Big Bang by Robert Dicke, James Peebles, Peter Roll, and David T. Wilkinson [66].

A few years later, in 1967, Andrei Sakharov wrote a famous paper about the requirements for a baryon-antibaryon asymmetry [67], which is one of the main unanswered questions in physics: why is there more matter than antimatter?

The Origin of Chemical Elements

R. A. ALPHER*

*Applied Physics Laboratory, The Johns Hopkins University,
Silver Spring, Maryland*

AND

H. BETHE

Cornell University, Ithaca, New York

AND

G. GAMOW

The George Washington University, Washington, D. C.

February 18, 1948

"The results of these calculations were first announced in a letter to The Physical Review, April 1, 1948. This was signed Alpher, Bethe, and Gamow, and is often referred to as the 'alphabetical article.' It seemed unfair to the Greek alphabet to have the article signed by Alpher and Gamow only, and so the name of Dr. Hans A. Bethe (in absentia) was inserted in preparing the manuscript for print. Dr. Bethe, who received a copy of the manuscript, did not object, and, as a matter of fact, was quite helpful in subsequent discussions."

Figure A.2: Alpher, Bethe, and Gamow's 1948 paper. The story behind as quoted in Gamow's book "The Creation of the Universe" from 1952 [64].

In the late sixties, the Big Bang theory was presented with several problems. Charles Misner and Robert Dicke formally presented the horizon problem [68] and flatness problem [69]. The first being that distant regions in the Universe, according to the standard Big Bang theory, have never been in contact with each other, and hence it is peculiar why they would have the same temperature. The flatness problem is about the overall curvature of the observable universe and why it appears to be so close to flat. The curvature is related to the overall energy-density in the Universe, and it can be shown that if this is slightly off the critical density, it will quickly diverge. This means that if the Universe is flat now, it must have been incredibly flat in its very early stages. It can be shown that if the observable universe had just a single gram of extra matter it would tip off balance [70]).

In 1970 Vera Rubin and Kent Ford found evidence for dark matter by measuring galaxy rotation curves at large radii [71], although it was already postulated by both Jan Oort and Fritz Zwicky in 1932 and 1933 [72].

In 1980 Alan Guth, among others, came up with the inflationary theory [11], proposing that the Universe went through a period of extremely rapid exponential expansion from when it was around 10^{-36} to 10^{-32} seconds old. This theory solves the magnetic monopole problem, which was one of the original motivations for his theory, as well as the flatness and horizon problem.

The last 25 years have been a golden age for experimental cosmology and astronomy. There has been a boost in new telescopes and technologies. The COBE (COsmic Background Explorer) satellite was launched in 1989 to measure the cosmic microwave background radiation (CMB). When adjusted to the cosmic frame the results matched that of a blackbody spectrum to a precision of 1 to 100 000. It also gave the first (and very famous) picture of the full-sky anisotropy of the CMB. A year later, the Hubble Space Telescope was launched, giving us some of the most spectacular pictures of our universe. As of 2015, on its 25th year, the Hubble telescope is still operational. By observing distant Type Ia supernovae in the late 90s, two teams (the High-Z Supernova Search Team and Supernova Cosmology Project) found evidence that the Universe is expanding at an accelerating rate [21, 22]. The most accepted

hypothesis to explain these observations is dark energy, an unknown form of energy which permeates all space. If this energy is constant in space and time it will act as the cosmological constant, Λ , which Einstein introduced in 1917. There can, however, be different solutions, such as quintessence which is a dynamic quantity which can vary in space and/or time.

The COBE mission had two successors: WMAP (Wilkinson Microwave Anisotropy Probe), launched in 2001 and then the Planck satellite which was launched in 2009. Data from these two missions [73, 27] have been the main contributions for estimating several important cosmological parameters, like the age of the universe, the energy constituents, and the Hubble parameter. The Λ CDM (cosmological constant with cold dark matter) model is considered the Standard Model of cosmology. The 2015 result from the Planck mission suggests a universe consisting of roughly 5% baryonic matter, 26% dark matter, and 69% dark energy [19]. The results from the Planck mission are discussed a bit further in Section 1.2.

It seems almost poetic that this section which started with Einstein will also end with him. On February 11, 2016, one of the biggest scientific discoveries was announced — namely the first direct detection of gravitational waves [74]. These waves were predicted by Einstein in 1916 [75, 76] and was indirectly discovered in 1974 by measuring the orbits of the HulseTaylor binary system [77]. The measured changes in the orbit of this system and others due to the radiation of gravitational waves are in very good agreement with the theory. The first direct detection of gravitational waves, however, came almost a hundred years after Einstein's prediction. This happened on September 14, 2015, when the gravitational waves from two merging black holes were detected here on Earth. Gravitational waves open up a completely new field of astronomy as we will be able to observe the Universe not only through the electromagnetic spectrum but through the ripples of spacetime itself.

B Big Bang Nucleosynthesis

At temperatures above a few MeV, the neutrons and protons were essentially in the same abundance, being kept in equilibrium by the reactions

$$n + \nu_e \rightleftharpoons p + e^- , \quad (\text{B.1})$$

$$n + e^+ \rightleftharpoons p + \nu_e . \quad (\text{B.2})$$

The neutron is slightly heavier than the proton, and this will significantly affect the ratio of neutrons to protons when the temperature ($k_B T$) is in the same order as the mass difference between the two particles. This neutron-to-proton-ratio given as [18]

$$\frac{n_n}{n_p} = \exp\left(-\frac{m_n c^2 - m_p c^2}{k_B T}\right) = \exp\left(-\frac{1.29 \text{ MeV}}{k_B T}\right) . \quad (\text{B.3})$$

Luckily for us, at $k_B T \sim 1 \text{ MeV}$, the cross-sections for the reactions given in Eqs. (B.1, B.2) are very small. The reaction involve weak force, which effectively the reactions stop and the neutrons freeze out at around 0.8 MeV [18]. This happens at $t = 1 \text{ s}$, and the neutron-to-proton-ratio is down to 1/6. As we know, free neutrons have a mean life of about 15 minutes, resulting in a slighter lower number of neutron-to-proton-ratio after nucleosynthesis is complete. Around 10 seconds after the Big Bang, the production of nuclei with more that one nucleon start, what we call primordial nuclear synthesis. The majority of nucleosynthesis happens between three and twenty minutes, as is shown in the left panel of Figure B.1. Only light elements are created during this period, the most important one being helium-4, and a smaller amount of deuterium (hydrogen-2), helium-3, lithium-7, and the two radioactive elements tritium (hydrogen-3) and beryllium-7. The latter two would decay into helium-3 and lithium-7. A reaction chain is given in the right panel in Figure B.1. All other elements are believed to have been created much later. The main source being evolving and exploding stars (stellar and supernova nucleosynthesis). Some of the lighter elements are also created by cosmic rays spallation. After the primordial nuclear synthesis ended the Universe consisted (by mass) of roughly 75% of hydrogen-1, about 25% helium-4, a few times 10^{-5} of deuterium and helium-3, and just trace amounts (in the order of 10^{-10}) of lithium [81].

B Big Bang Nucleosynthesis

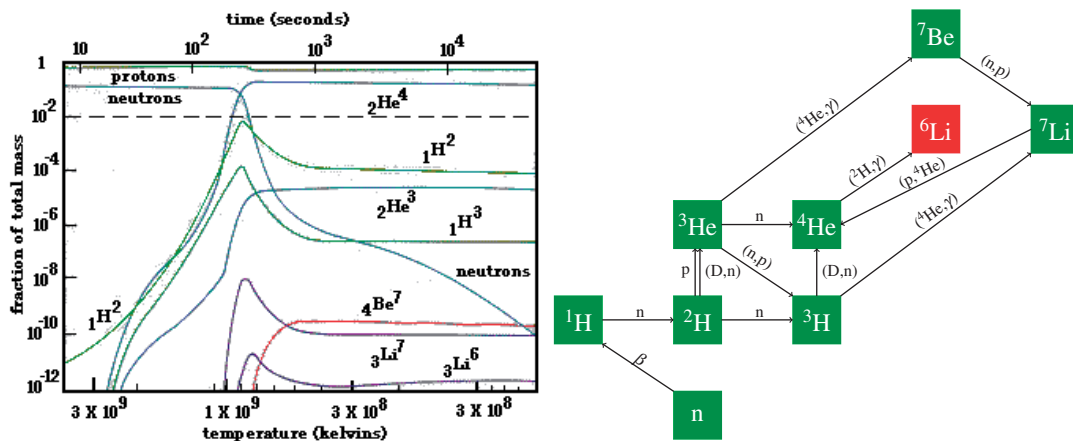


Figure B.1: Model for elements created during Big Bang nucleosynthesis (BBN). Timeline on right and main reactions on left. Timeline from [78]. Recent studies suggests that the BBN is not the source of Lithium-6 [79, 80].

C Gamma matrices

The γ -matrices, also known as the 4×4 Dirac matrices being used in Section 5.3 are defined using contravariant representation and metric signature of $(+ - - -)$ as:

$$\gamma^0 = \begin{pmatrix} 1 & 0 & 0 & 0 \\ 0 & 1 & 0 & 0 \\ 0 & 0 & -1 & 0 \\ 0 & 0 & 0 & -1 \end{pmatrix}, \quad (\text{C.1})$$

$$\gamma^1 = \begin{pmatrix} 0 & 0 & 0 & 1 \\ 0 & 0 & 1 & 0 \\ 0 & -1 & 0 & 0 \\ -1 & 0 & 0 & 0 \end{pmatrix}, \quad (\text{C.2})$$

$$\gamma^2 = \begin{pmatrix} 0 & 0 & 0 & -i \\ 0 & 0 & i & 0 \\ 0 & i & 0 & 0 \\ -i & 0 & 0 & 0 \end{pmatrix}, \quad (\text{C.3})$$

$$\gamma^3 = \begin{pmatrix} 0 & 0 & 1 & 0 \\ 0 & 0 & 0 & -1 \\ -1 & 0 & 0 & 0 \\ 0 & 1 & 0 & 0 \end{pmatrix}. \quad (\text{C.4})$$

The product of the four gives us $\gamma^5 \equiv i\gamma^0\gamma^1\gamma^2\gamma^3$ which we can represent as

$$\gamma^5 = \begin{pmatrix} 0 & 0 & 1 & 0 \\ 0 & 0 & 0 & 1 \\ 1 & 0 & 0 & 0 \\ 0 & 1 & 0 & 0 \end{pmatrix}. \quad (\text{C.5})$$

Bibliography

- [1] L. Husdal, *On Effective Degrees of Freedom in the Early Universe*, *Galaxies* **4** (2016), no. 78.
- [2] L. Husdal, *Viscosity in a Lepton-Photon Universe*, *Astrophys. Space Sci.* **361** (2016), no. 8 p. 263.
- [3] L. Husdal and I. Brevik, *Entropy Production in a Lepton-Photon Universe*, *Astrophys. Space Sci.* **362** (2017), no. 2 p. 39.
- [4] **Planck** collaboration, P. A. R. Ade et. al., *Planck 2013 results. XVI. Cosmological Parameters*, *Astron.Astrophys.* **571** (2014) p. A16, [arXiv:1303.5076].
- [5] R. Wald, *General Relativity*. University of Chicago Press, Chicago, IL, 1984.
- [6] H. Georgi and S. L. Glashow, *Unity of All Elementary-Particle Forces*, *Phys. Rev. Lett.* **32** (Feb., 1974) p. 438–441.
- [7] A. R. Liddle, *An Introduction to Modern Cosmology*. Wiley, Chichester, 2003.
- [8] E. W. Kolb and M. S. Turner, *The Early Universe*. Westview Press, Boulder, CO, 1990.
- [9] A. A. Starobinsky, *Spectrum of relict gravitational radiation and the early state of the universe*, *JETP Lett.* **30** (1979) p. 682–685. [Pisma Zh. Eksp. Teor. Fiz.30,719(1979)].
- [10] A. A. Starobinsky, *A New Type of Isotropic Cosmological Models Without Singularity*, *Phys. Lett.* **B91** (1980) p. 99–102.
- [11] A. H. Guth, *The Inflationary Universe: A Possible Solution to the Horizon and Flatness Problems*, *Phys. Rev. D* **D23** (1981) p. 347–356.
- [12] A. D. Linde, *A New Inflationary Universe Scenario: A Possible Solution of the Horizon, Flatness, Homogeneity, Isotropy and Primordial Monopole Problems*, *Phys. Lett.* **B108** (1982) p. 389–393.
- [13] S. Weinberg, *Cosmology*. Oxford University Press, Oxford, 2008.
- [14] V. F. Mukhanov and G. V. Chibisov, *Quantum fluctuations and a nonsingular universe*, *ZhETF Pisma Redaktsiiu* **33** (May, 1981) p. 549–553.

Bibliography

- [15] V. F. Mukhanov and G. V. Chibisov, *Energy of vacuum and the large-scale structure of the universe*, Zhurnal Eksperimentalnoi i Teoreticheskoi Fiziki **83** (Aug., 1982) p. 475–487.
- [16] S. Hawking, *The development of irregularities in a single bubble inflationary universe*, Physics Letters B **115** (1982), no. 4 p. 295 – 297.
- [17] S. Weinberg, *The First Three Minutes: A Modern View of the Origin of the Universe*. Basic Books, New York, NY, second ed., 1993.
- [18] B. Ryden, *Introduction to Cosmology*. Addison-Wesley, San Francisco, CA, 2003.
- [19] **Planck** collaboration, P. A. R. Ade et. al., *Planck 2015 Results. XIII. Cosmological Parameters*, Astron. Astrophys. **594** (2016) p. A13.
- [20] NASA, “The end of the dark ages: First stars and reionization.” http://imagine.gsfc.nasa.gov/features/satellites/archive/jwst_darkages.html, 2007.
- [21] **Supernova Cosmology Project** collaboration, S. Perlmutter et. al., *Measurements of Ω and Λ from 42 High Redshift supernovae*, Astrophys. J. **517** (1999) p. 565–586. The Supernova Cosmology Project.
- [22] **Supernova Search Team** collaboration, A. G. Riess et. al., *Observational evidence from supernovae for an accelerating universe and a cosmological constant*, Astron. J. **116** (1998) p. 1009–1038, [astro-ph/9805201].
- [23] C. O’Luanaigh, “LHCb confirms existence of exotic hadrons.” <http://home.web.cern.ch/about/updates/2014/04/lhcb-confirms-existence-exotic-hadrons/>, 2014.
- [24] **LHCb** collaboration, R. Aaij et. al., *Observation of the Resonant Character of the $Z(4430)^-$ State*, Phys. Rev. Lett. **112** (June, 2014) p. 222002.
- [25] G. Amit, “Pentaquark discovery at LHC shows long-sought new form of matter.” <https://www.newscientist.com/article/dn27892-pentaquark-discovery-at-lhc-shows-long-sought-new-form-of-matter/>, 2015.
- [26] S. Weinberg, *Gravitation and Cosmology*. John Wiley & Sons, New York, NY, 1972.
- [27] **WMAP** collaboration, C. Bennett et. al., *Nine-Year Wilkinson Microwave Anisotropy Probe (WMAP) Observations: Final Maps and Results*, Astrophys. J. Suppl. **208** (2013) p. 20.

-
- [28] **Particle Data Group** collaboration, K. Olive et. al., *Review of Particle Physics*, Chin. Phys. C **38** (2014) p. 090001.
- [29] D. J. Griffiths, *Introduction to Quantum Mechanics*. Pearson Prentice Hall, Upper Saddle River, NJ, 2 ed., 2005.
- [30] R. Baierlein, *Thermal Physics*. Cambridge University Press, Cambridge, 1999.
- [31] F. Jüttner, *Das Maxwellsche Gesetz der Geschwindigkeitsverteilung in der Relativtheorie*, Annalen der Physik **339** (1911), no. 5 p. 856–882.
- [32] D. Baumann, “Cosmology lectures.”
www.damtp.cam.ac.uk/user/db275/Cosmology.pdf.
- [33] A. Friedmann, *Über die Krümmung des Raumes*, Zeitschrift für Physik **10** (1922) p. 377–386.
- [34] A. Friedmann, *Über die Möglichkeit einer Welt mit konstanter negativer Krümmung des Raumes*, Zeitschrift für Physik **21** (1924) p. 326–332.
- [35] I. Newton, *Philosophiae Naturalis Principia Mathematica*. J. Societatis Regiae ac Typis J. Streater, 1687.
- [36] I. Brevik and O. Gorbunova, *Dark Energy and Viscous Cosmology*, Gen. Rel. Grav. **37** (2005) p. 2039–2045, [gr-qc/0504001].
- [37] C. W. Misner, *The Isotropy of the universe*, Astrophys. J. **151** (1968) p. 431–457.
- [38] N. Caderni, R. Fabbri, L. van der Horn, and T. Siskens, *The weak interaction and the isotropy of the universe*, Physics Letters A **66** (1978), no. 3 p. 251 – 254.
- [39] F. Hoogeveen, W. A. Van Leeuwen, G. A. Q. Salvati, and S. E. E., *Viscous Phenomena in Cosmology: I. Lepton era*, Physica A **134** (1986), no. 2 p. 458–473.
- [40] S. R. de Groot, W. A. van Leeuwen, and C. G. van Weert, *Relativistic kinetic theory: principles and applications*. North-Holland Publishing Company, Amsterdam, 1980.
- [41] A. H. Guth, *The Inflationary Universe*. Vintage, 1998.
- [42] L. Lederman and D. Teresi, *The God Particle*. Houghton Mifflin Harcourt, Boston, MA, 2006.
- [43] L. Randall, *Warped Passages: Unravelling the Universe’s Hidden Dimensions*. Harper and Collins, New York, NY, 2005.
- [44] R. Panek, *The 4% Universe: Dark Matter, Dark Energy, and the Race to Discover the Rest of Reality*. Houghton Mifflin Harcourt, 2011.

Bibliography

- [45] A. Einstein, *On the Electrodynamics of Moving Bodies*, *Annalen der Physik* **17** (1905) p. 891–921.
- [46] A. Einstein, *Relativitätsprinzip und die aus demselben gezogenen Folgerungen*, *Jahrbuch der Radioaktivität* **4** (1907) p. 411–462.
- [47] A. Einstein, *The Field Equations of Gravitation*, *Preussische Akademie der Wissenschaften, Sitzungsberichte* **2** (1915) p. 844–847.
- [48] A. Einstein, *The Foundations of the Theory of General Relativity*, *Annalen der Physik* **354** (1916), no. 7 p. 769–822.
- [49] A. Einstein, *Cosmological Considerations in the General Theory of Relativity*, *Sitzungsber Preuss Akad Wiss Berlin (Math.Phys.)* **1917** (1917) p. 142–152.
- [50] G. Gamow, *My World Line*. Viking Press, New York, NY, 1970.
- [51] R. J. Rosen, “Einstein likely never said one of his most oft-quoted phrases.” <http://www.theatlantic.com/technology/archive/2013/08/einstein-likely-never-said-one-of-his-most-oft-quoted-phrases/278508/>, 2013.
- [52] K. Schwarzschild, *On the gravitational field of a mass point according to Einstein’s theory*, *Preussische Akademie der Wissenschaften, Sitzungsberichte* (1916) p. 189–196.
- [53] K. Schwarzschild, *On the gravitational field of a sphere of incompressible fluid according to Einstein’s theory*, *Preussische Akademie der Wissenschaften, Sitzungsberichte* (1916) p. 424–434.
- [54] W. de Sitter, *On Einstein’s theory of gravitation and its astronomical consequences. Third paper*, *Monthly Notices of the Royal Astronomical Society* **78** (Nov., 1917) p. 3–28.
- [55] N. Wright, “Hubble diagrams.” http://www.astro.ucla.edu/~wright/cosmo_01.htm.
- [56] E. Hubble, *A relation between distance and radial velocity among extra-galactic nebulae*, *Proc. Nat. Acad. Sci.* **15** (1929) p. 168–173.
- [57] A. G. Riess, W. H. Press, and R. P. Kirshner, *A Precise Distance Indicator: Type IA Supernova Multicolor Light-Curve Shapes*, *Astrophys. J.* **473** (Dec., 1996) p. 88.
- [58] V. M. Slipher, *Spectrographic Observations of Nebulae*, *Popular Astronomy* **23** (Jan., 1915) p. 21–24.

-
- [59] G. Lemaitre, *A homogeneous Universe of constant mass and growing radius accounting for the radial velocity of extragalactic nebulae*, Annales Soc. Sci. Brux. Ser. I Sci. Math. Astron. Phys. **A47** (1927) p. 49–59.
- [60] G. Lemaitre, *Republication of: The beginning of the world from the point of view of quantum theory*, Nature **127** (1931) p. 706.
- [61] F. Hoyle, *A New Model for the Expanding Universe*, Mon.Not.Roy.Astron.Soc. **108** (1948) p. 372–382.
- [62] R. A. Alpher, H. Bethe, and G. Gamow, *The Origin of Chemical Elements*, Phys. Rev. **73** (Apr., 1948) p. 803–804.
- [63] R. A. Alpher and R. C. Herman, *On the Relative Abundance of the Elements*, Phys. Rev. **74** (Dec., 1948) p. 1737–1742.
- [64] G. Gamow, *The Creation of the Universe*. Viking Press, New York, NY, 1952.
- [65] A. A. Penzias and R. W. Wilson, *A Measurement of Excess Antenna Temperature at 4080 Mc/s*, Astrophys. J. **142** (1965) p. 419–421.
- [66] R. H. Dicke, P. J. E. Peebles, P. G. Roll, and D. T. Wilkinson, *Cosmic Black-Body Radiation*, Astrophys. J. **142** (July, 1965) p. 414–419.
- [67] A. Sakharov, *Violation of CP Invariance, P Asymmetry and Baryon Asymmetry of the Universe*, Pisma Zh.Eksp.Teor.Fiz. **5** (1967) p. 32–35.
- [68] C. W. Misner, *Mixmaster Universe*, Phys. Rev. Lett. **22** (1969) p. 1071–1074.
- [69] A. Lightman, *Ancient Light: Our Changing View of the Universe*. Harvard University Press, Cambridge, MA, 1993.
- [70] M. Trodden and S. M. Carroll, *TASI lectures: Introduction to cosmology*, Progress in string theory. Proceedings, Summer School, TASI 2003, Boulder, USA, June 2-27, 2003 (2004) p. 703–793, [astro-ph/0401547].
- [71] V. C. Rubin and J. Ford, W. Kent, *Rotation of the Andromeda Nebula from a Spectroscopic Survey of Emission Regions*, Astrophys. J. **159** (1970) p. 379–403.
- [72] F. Zwicky, *Die Rotverschiebung von extragalaktischen Nebeln*, Helv. Phys. Acta **6** (1933) p. 110–127.
- [73] **Planck** collaboration, P. A. R. Ade et. al., *Planck 2013 results. XVI. Cosmological parameters*, arXiv:1303.5076.
- [74] **LIGO and Virgo** collaboration, B. P. Abbott et. al., *Observation of Gravitational Waves from a Binary Black Hole Merger*, Phys. Rev. Lett. **116** (Feb., 2016) p. 061102.

Bibliography

- [75] A. Einstein, *Approximative Integration of the Field Equations of Gravitation*, Preussische Akademie der Wissenschaften, Sitzungsberichte **1** (1916) p. 688–696.
- [76] A. Einstein, *On Gravitational Waves*, Preussische Akademie der Wissenschaften, Sitzungsberichte **1** (1918) p. 154–167.
- [77] R. A. Hulse and J. H. Taylor, *Discovery of a pulsar in a binary system*, Astrophysical Journal Letters **195** (Jan., 1975) p. L51–L53.
- [78] N. Wright, “Big bang nuclear synthesis vs. time.”
http://www.astro.ucla.edu/~wright/BBNS_vs_t.gif.
- [79] **LUNA** collaboration, M. Anders et. al., *First Direct Measurement of the ${}^2\text{H}(\alpha, \gamma){}^6\text{Li}$ Cross Section at Big Bang Energies and the Primordial Lithium Problem*, Phys. Rev. Lett. **113** (July, 2014) p. 042501.
- [80] H. Johnston, “Big Bang ruled out as origin of lithium-6.”
<http://physicsworld.com/cws/article/news/2014/sep/02/big-bang-ruled-out-as-origin-of-lithium-6>, Sept., 2014.
- [81] **Particle Data Group** collaboration, C. Patrignani et. al., *Review of Particle Physics*, Chin. Phys. **C40** (2016), no. 10 p. 100001.

Part II
Papers

Paper I

On Effective Degrees of Freedom in the Early Universe

Galaxies 4 (2016) no. 78

Article

On Effective Degrees of Freedom in the Early Universe

Lars Husdal

Department of Physics, Norwegian University of Science and Technology, N-7491 Trondheim, Norway;
lars.husdal@ntnu.no

Academic Editor: Emilio Elizalde

Received: 20 October 2016; Accepted: 8 December 2016; Published: 17 December 2016

Abstract: We explore the effective degrees of freedom in the early Universe, from before the electroweak scale at a few femtoseconds after the Big Bang until the last positrons disappeared a few minutes later. We look at the established concepts of effective degrees of freedom for energy density, pressure, and entropy density, and introduce effective degrees of freedom for number density as well. We discuss what happens with particle species as their temperature cools down from relativistic to semi- and non-relativistic temperatures, and then annihilates completely. This will affect the pressure and the entropy per particle. We also look at the transition from a quark-gluon plasma to a hadron gas. Using a list of known hadrons, we use a “cross-over” temperature of 214 MeV, where the effective degrees of freedom for a quark-gluon plasma equals that of a hadron gas.

Keywords: viscous cosmology; shear viscosity; bulk viscosity; lepton era; relativistic kinetic theory

1. Introduction

The early Universe was filled with different particles. A tiny fraction of a second after the Big Bang, when the temperature was 10^{16} K \approx 1 TeV, all the particles in the Standard Model were present, and roughly in the same abundance. Moreover, the early Universe was in thermal equilibrium. At this time, essentially all the particles moved at velocities close to the speed of light. The average distance travelled and lifetime of these ultra-relativistic particles were very short. The frequent interactions led to the constant production and annihilation of particles, and as long as the creation rate equalled that of the annihilation rate for a particle species, their abundance remained the same. The production of massive particles requires high energies, so when the Universe expanded and the temperature dropped, the production rate of massive particles could not keep up with their annihilation rate. The heaviest particle we know about, the top quark and its antiparticle, started to disappear just one picosecond (10^{-12} s) after the Big Bang. During the next minutes, essentially all the particle species except for photons and neutrinos vanished one by one. Only a very tiny fraction of protons, neutrons, and electrons, what makes up all the matter in the Universe today, survived due to baryon asymmetry (the imbalance between matter and antimatter in the Universe). The fraction of matter compared to photons and neutrinos is less than one in a billion, small enough to be disregarded in the grand scheme for the first stages of the Universe.

We know that the early Universe was close to thermal equilibrium from studying the Cosmic Microwave Background (CMB) radiation. Since its discovery in 1964 [1], the CMB has been thoroughly measured, most recently by the Planck satellite [2]. After compensating for foreground effects, the CMB almost perfectly fits that of a black body spectrum, deviating by about one part in a hundred thousand [3]. It remained so until the neutrinos decoupled. For a system in thermal equilibrium, we can use statistical mechanics to calculate quantities such as energy density, pressure, and entropy density. These quantities all depend on the number density of particles present at any given time. How the different particles contribute to these quantities depends of their nature—most important

being their mass and degeneracy. The complete contribution from all particles is a result of the sum of all the particle species' effective degrees of freedom. We call these temperature-dependent functions g_* , and we have one for each quantity, such as g_{*n} related to number density, and $g_{*\epsilon}$, g_{*p} , and g_{*s} , related to energy density, pressure, and entropy density, respectively.

In this paper, we will show how to calculate these four quantities (n, ϵ, P, s), as well their associated effective degrees of freedom ($g_{*n}, g_{*\epsilon}, g_{*p}, g_{*s}$). These latter functions describe how the number of different particles evolve, and we have plotted these values in Figure 1. Throughout this paper, we will look more closely at five topics. After first having a quick look at the elementary particles of the Standard Model and their degeneracy (Section 3), we address the standard approach when everything is in thermal equilibrium in Section 4. Next, we take a closer look at the behavior during the QCD phase transition; i.e., the transition from a quark-gluon plasma (QGP) to a hot hadron gas (HG) in Section 5. We then look at the behavior during neutrino decoupling (Section 6). For the fifth topic, we study how the temperature decreases as function of time (Section 8). In Appendix A, we have also included a table with the values for all four g_{*s} , as well as time, from temperatures of 10 TeV to 10 keV. The table includes three different transition temperatures as we go from a QGP to a HG. This article was inspired by the lecture notes by Baumann [4] and Kurki-Suonio [5]. Other important books on the subject are written by Weinberg [6,7], Kolb and Turner [8], Dodelson [9], Ryden [10], and Lesgourgues, Mangano, Miele, and Pastor [11].

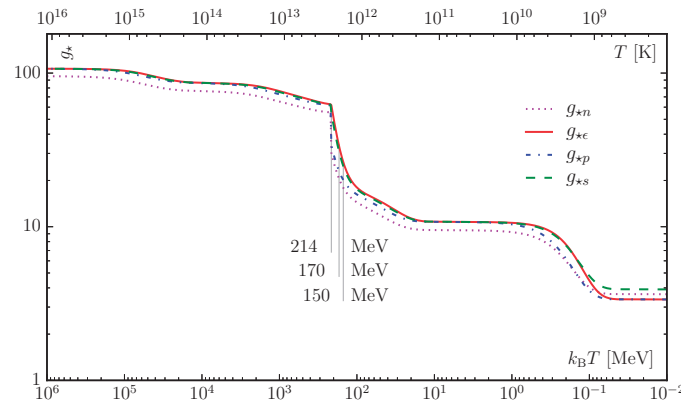


Figure 1. The evolution of the number density (g_{*n}), energy density ($g_{*\epsilon}$), pressure (g_{*p}), and entropy density (g_{*s}) as functions of temperature.

2. Notations and Conventions

The effective degrees of freedom of a particle species is defined relative to the photon. This is not just an arbitrary choice, but chosen since the photon is massless, and whose density history is best known. The most important source of information about the early Universe comes from the CMB photons. Even though the photon is the natural choice as a reference particle, technically any particle could be used. Additionally, when talking about effective degrees of freedom, we most often do so in the context of energy density $g_{*\epsilon}$, which in most textbooks is just called “ g_* ”. Here, we use the notation $g_{*\epsilon}$ for that matter, and g_* as a collective term for all four quantities.

The term “particle annihilations” frequently appears in this paper. Strictly speaking, we have particle creations and annihilations all the time, but in this context, “particle annihilations” refers to periods where the annihilation rate is (noticeable) faster than the production rate for a particle species.

In many textbooks, the value of the speed of light (c), the Boltzmann constant (k_B), and the Planck reduced constant (\hbar) are set to unity. We have chosen to keep these units in our equations to avoid any problems with dimensional analysis during actual calculations. One of the advantages of using

$\hbar = c = k_B = 1$ is that we can use temperature, energy, and mass interchangeably. For our equations, we use $k_B T$ and mc^2 when we want to express temperature and mass in units of MeV, but in the main text, when we talk about temperature and mass, it is implied that these are $k_B T$ and mc^2 .

Simplifications are important when we first want to approach a new subject. One of our assumptions in this paper is that the early Universe was in total thermal equilibrium. There were, however, periods where this was not so. In those cases, viscous effects drove the system (the Universe) towards equilibrium. This increased the entropy. For our purposes, all viscous effects have been neglected. Some relevant papers address this issue [12–14].

3. The Standard Model Particles and Their Degeneracy

Let us start by looking at the degeneracy of the different particle species—their intrinsic degrees of freedom, g . The Standard Model of elementary particles are often displayed as in Figure 2. The quarks, leptons, and neutrinos are grouped into three families, shown as the first three columns. These are all fermions. The two last columns are the bosons. The fourth column consists of force mediator particles, also called gauge bosons. These are the eight gluons, the photon, and the three massive gauge bosons. The Higgs boson that was discovered at CERN in 2012 [15,16] comprises the fifth and last column.

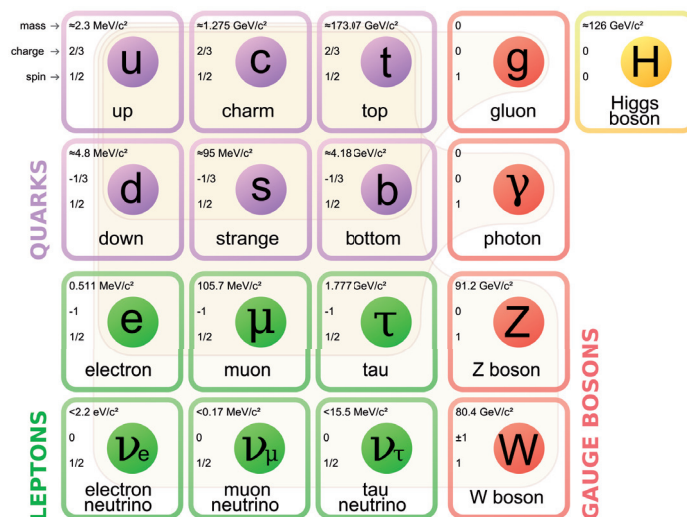


Figure 2. All particle species of the Standard Model of elementary particles.

A particle's degeneracy depends on its nature and which properties it possesses. We have listed these as four different columns in Table 1. They are: (1) Number of different flavors. These are different types of particles with similar properties, but different masses. These are listed as separate entries in Figure 2; (2) Existence of antiparticles. Antiparticles have different charge, chirality, and color than their particle companion. Not all particles have anti-partners (e.g., the photon); (3) Number of color states. Strongly interacting particles have color charge. For quarks and their anti-partners, there are three possibilities (red, green, blue, or antired, antiblue). Gluons have eight possible color states. These are superpositions of combined states of the three plus three colors; (4) Number of possible spin states. We remember from quantum mechanics that all bosons have integer spins, while fermions have half integer spins, both in units of \hbar . The spin alignment of a particle in some direction is called its polarization. Quarks and the charged leptons have two possible polarizations: $+\frac{1}{2}$ or $-\frac{1}{2}$. Another way of saying this is that they can be either left-handed or right-handed. Neutrinos, on the other hand, can only be left-handed (and antineutrinos only right-handed), so they only have one spin state. Actually,

whether neutrinos are Dirac or Majorana fermions is still an open question. Majorana fermions are their own antiparticles, while Dirac fermions have distinct particles and antiparticles. In the latter case, we expect there to be additional right-handed neutrinos and left-handed antineutrinos, whose weak interaction is suppressed. These “new” neutrinos are expected to have negligible density compared to the left-handed neutrinos and right-handed antineutrinos [17]. The book by Lesgourgues, Mangano, Miele, and Pastor [11] also discusses this topic in detail. The massive spin-1 bosons (W^\pm and Z^0) have three possible polarizations $(-1, 0, 1)$: one longitudinal and two transverse. The massless spin-1 bosons (photons and gluons) have only two possible polarizations, namely the transverse ones. The Higgs particle is a scalar particle and has spin-0. Finally, we should say that hadrons can have multiple possible spin states, depending on their composition.

Table 1. The Standard Model of elementary particles and their degeneracies.

	Flavors	Particle + Antiparticle	Colors	Spins	Total
Quarks (u, d, c, s, t, b)	6	2	3	2	72
Charged leptons (e, μ , τ)	3	2	1	2	12
Neutrinos (ν_e, ν_μ, ν_τ)	3	2	1	1	6
Gluons (g)	1	1	8	2	16
Photon (γ)	1	1	1	2	2
Massive gauge bosons (W^\pm, Z^0)	2	2, 1	1	3	9
Higgs bosons (H^0)	1	1	1	1	1
All elementary particles	17				118

At high temperatures where all the particles of the Standard Model are present, we have 28 bosonic and 90 fermionic degrees of freedom. It turns out that fermions do not contribute as much as bosons, since they can not occupy the same state. We will get back to this in the next section, and just say that fermions have $28 + \frac{7}{8} \times 90 = 106.75$ effective degrees of freedom for energy density, pressure, and entropy density. For the number density, the effective degrees of freedom is $28 + \frac{3}{4} \times 90 = 95.5$.

4. Statistical Mechanics of Ideal Quantum Gases in Thermodynamic Equilibrium

In this section, we briefly review the statistical mechanics of ideal quantum gases in thermal equilibrium. We also introduce the concept of effective number of degrees of freedom for a particle species, and how to count these as functions of the temperature.

4.1. Thermodynamic Functions

In order to calculate the thermodynamic functions, we need to know the single-particle energies of the system. We consider a cubic box with periodic boundary conditions, and with sides of length L and volume $V = L^3$. Solving the Schrödinger equation for a particle, we find the possible momentum eigenvalues

$$\vec{p} = \frac{h}{L}(n_1\vec{e}_x + n_2\vec{e}_y + n_3\vec{e}_z), \quad (1)$$

where h is the Planck constant, $n_i = 0, \pm 1, \pm 2, \pm 3, \dots$, and $\vec{e}_x, \vec{e}_y, \vec{e}_z$ are the standard units vectors in three-dimensional Euclidean space. The energy of a particle with mass m and momentum \vec{p} is $E(\vec{p}) = \sqrt{m^2c^4 + \vec{p}^2c^2}$.

In thermal equilibrium, the probability that a single-particle state with momentum \vec{p} and energy $E(\vec{p})$ is occupied is given by the Bose–Einstein or Fermi–Dirac distribution functions

$$f(\vec{p}) = \frac{1}{e^{(E(\vec{p})-\mu)/(k_B T)} \pm 1}, \quad (2)$$

where the upper sign is for fermions and the lower sign for bosons. Moreover, k_B is the Boltzmann constant and μ is the chemical potential. In order to find the total number of particles occupying a state

with energy E , we must find the density of states in phase space. We see from Equation (1) that the number of possible states in momentum space is L^3/h^3 . By dividing by the volume, L^3 , as well, we are left with the factor $(1/h)^3$. If there is an additional degeneracy g (for example, spin), we can write the density of states (dos) as

$$\text{dos} = \frac{g}{h^3} = \frac{g}{(2\pi)^3 h^3} . \quad (3)$$

The density of particles with momentum \vec{p} is then given by

$$n(\vec{p}) = \frac{g}{(2\pi)^3 h^3} \times f(\vec{p}) . \quad (4)$$

The total density of particles, n , can then be written as an integral over three-momentum involving the distribution function as

$$n = \frac{g}{(2\pi)^3 h^3} \int f(\vec{p}) d^3 \vec{p} . \quad (5)$$

By multiplying the distribution function (2) with the energy and integrating over three-momentum, we obtain the energy density ϵ of the system. The pressure, P , can be found in a similar manner by multiplying the distribution function with $|\vec{p}|^2/(3E/c^2)$ (a nice derivation of this is shown by Baumann [4]). This yields the integrals

$$\epsilon = \frac{g}{(2\pi)^3 h^3} \int E(\vec{p}) f(\vec{p}) d^3 \vec{p} , \quad (6)$$

$$P = \frac{g}{(2\pi)^3 h^3} \int \frac{|\vec{p}|^2}{3(E/c^2)} f(\vec{p}) d^3 \vec{p} . \quad (7)$$

Finally, let us mention the entropy density s . It can be calculated from the thermodynamic relation

$$s = \frac{\epsilon + P - \mu_T}{T} , \quad (8)$$

where the index μ_T is the total chemical potential. We will get back to chemical potentials in Section 4.3.

4.2. From Momentum to Energy Integrals

It is sometimes more convenient to use energy, E , instead of the momentum, \vec{p} , as the integration variable. By integrating over all angles, we can replace $d^3 \vec{p}$ by $4\pi |\vec{p}|^2 d\vec{p}$. Using the energy momentum relation, we find $|\vec{p}| = \sqrt{E^2 - m^2 c^2}/c$ and $c\vec{p} d\vec{p} = E dE$. We can simplify these formulas further by introducing the dimensionless variables u , z , and $\hat{\mu}$.

$$u = \frac{E}{k_B T} , \quad z = \frac{mc^2}{k_B T} , \quad \hat{\mu} = \frac{\mu}{k_B T} . \quad (9)$$

This yields the following expressions for the number density, energy density, and pressure for a species j , and for all species (as this is simply the sum of all particle species).

$$n_j(T) = \frac{g_j}{2\pi^2 h^3} \int_{m_j c^2}^{\infty} \frac{E \sqrt{E^2 - m_j^2 c^4}}{e^{(E - \mu_j)/k_B T} \pm 1} dE \quad (10a)$$

$$= \frac{g_j}{2\pi^2} \left(\frac{k_B T}{hc} \right)^3 \int_{z_j}^{\infty} \frac{u \sqrt{u^2 - z_j^2}}{e^{u - \hat{\mu}_j} \pm 1} du , \quad (10b)$$

$$n(T) = \sum_j n_j = \sum_j \frac{g_j}{2\pi^2} \left(\frac{k_B T}{hc} \right)^3 \int_{z_j}^{\infty} \frac{u \sqrt{u^2 - z_j^2}}{e^{u - \hat{\mu}_j} \pm 1} du , \quad (10c)$$

$$\epsilon_j(T) = \frac{g_j}{2\pi^2\hbar^3} \int_{m_j c^2}^{\infty} \frac{E^2 \sqrt{E^2 - m_j^2 c^4}}{e^{(E-\mu_j)/k_B T} \pm 1} dE \quad (11a)$$

$$= \frac{g_j}{2\pi^2} \frac{(k_B T)^4}{(\hbar c)^3} \int_{z_j}^{\infty} \frac{u^2 \sqrt{u^2 - z_j^2}}{e^{u-\beta_j} \pm 1} du, \quad (11b)$$

$$\epsilon(T) = \sum_j \epsilon_j = \sum_j \frac{g_j}{2\pi^2} \frac{(k_B T)^4}{(\hbar c)^3} \int_{z_j}^{\infty} \frac{u^2 \sqrt{u^2 - z_j^2}}{e^{u-\beta_j} \pm 1} du, \quad (11c)$$

$$P_j(T) = \frac{g_j}{6\pi^2\hbar^3} \int_{m_j c^2}^{\infty} \frac{(E^2 - m_j^2 c^4)^{3/2}}{e^{(E-\mu_j)/k_B T} \pm 1} dE \quad (12a)$$

$$= \frac{g_j}{6\pi^2} \frac{(k_B T)^4}{(\hbar c)^3} \int_{z_j}^{\infty} \frac{(u^2 - z_j^2)^{3/2}}{e^{u-\beta_j} \pm 1} du, \quad (12b)$$

$$P(T) = \sum_j P_j = \sum_j \frac{g_j}{6\pi^2} \frac{(k_B T)^4}{(\hbar c)^3} \int_{z_j}^{\infty} \frac{(u^2 - z_j^2)^{3/2}}{e^{u-\beta_j} \pm 1} du. \quad (12c)$$

As shown in Equation (8) we can find the entropy density for a single species j and the total entropy as:

$$s_j(T) = \frac{\epsilon_j + P_j - \mu_j n_j}{T}, \quad (13a)$$

$$s(T) = \sum_j s_j = \sum_j \frac{\epsilon_j + P_j - \mu_j n_j}{T} = \frac{\epsilon + P - \sum_j \mu_j n_j}{T}. \quad (13b)$$

4.3. Chemical Potentials

Before we proceed, we briefly discuss the chemical potentials. We recall from statistical mechanics that we can introduce a chemical potential μ_j for each conserved charge Q_j . This is done by replacing the Hamiltonian H of the system with $H - \mu_j N_{Q_j}$, where N_{Q_j} is the number operator of particles with charge Q_j .

In the Standard Model, there are five independent conserved charges. These are electric charge, baryon number, electron-lepton number, muon-lepton number, and tau-lepton number. This means there are also five independent chemical potentials [7]. The chemical potentials are determined by the number densities. The electric charge density is very close to zero. The baryon density is estimated to be less than a billionth of the photon density [18,19]. Lepton density is also thought to be very small, on the same order as the baryon number. According to Weinberg [7], for an early Universe scenario, we can put all these numbers equal to zero to a good approximation. For a correct representation of the Universe, the chemical potentials cannot all cancel out—otherwise, there would be no matter present today. For more general calculations including chemical potentials, the book by Weinberg is recommended [6]. The implications of a large neutrino chemical potential is discussed by Pastor and Lesgourgues [20]. Mangano, Miele, Pastor, Pisanti, and Sarikasa discuss the chemical potentials and their influence on the effective number of neutrino species [21] (we will briefly mention effective neutrino species in Section 6.2).

4.4. Massless Particle Contributions

In Equations (10)–(12), we see how dimensionless units, u , z , and $\hat{\mu}$, simplifies the integrals. In the ultrarelativistic limit, we can ignore the particle masses. Moreover, as we have set the chemical potentials to zero, we can easily solve the dimensionless integrals appearing in Equations (10b), (11b), and (12b) analytically. Since the integrals for energy density and pressure in the massless cases are the same, we find:

$$\int_0^\infty \frac{u^2}{e^u \pm 1} du = \begin{cases} \frac{3}{2} \zeta(3) \simeq 1.803 & \text{(Fermions),} \\ 2 \zeta(3) \simeq 2.404 & \text{(Bosons),} \end{cases} \quad (14)$$

$$\int_0^\infty \frac{u^3}{e^u \pm 1} du = \begin{cases} \frac{7}{8} \frac{\pi^4}{15} \simeq 5.682 & \text{(Fermions),} \\ \frac{\pi^4}{15} \simeq 6.494 & \text{(Bosons),} \end{cases} \quad (15)$$

where $\zeta(3)$ is the Riemann zeta function of argument 3. Using these results, we find the values for n , ϵ , P , and indirectly s for massless bosons and fermions:

$$n_b(T) = g \frac{\zeta(3) (k_B T)^3}{\pi^2 (hc)^3}, \quad n_f(T) = \frac{3}{4} g \frac{\zeta(3) (k_B T)^3}{\pi^2 (hc)^3}, \quad (16)$$

$$\epsilon_b(T) = g \frac{\pi^2 (k_B T)^4}{30 (hc)^3}, \quad \epsilon_f(T) = \frac{7}{8} g \frac{\pi^2 (k_B T)^4}{30 (hc)^3}, \quad (17)$$

$$P_b(T) = g \frac{\pi^2 (k_B T)^4}{90 (hc)^3}, \quad P_f(T) = \frac{7}{8} g \frac{\pi^2 (k_B T)^4}{90 (hc)^3}, \quad (18)$$

$$s_b(T) = g \frac{2\pi^2 k_B^4 T^3}{45 (hc)^3}, \quad s_f(T) = \frac{7}{8} g \frac{2\pi^2 k_B^4 T^3}{45 (hc)^3}. \quad (19)$$

Here the subscript b is for bosons, and f is for fermions. We see that solving the integrals gives a difference between fermions and bosons, namely a factor $\frac{3}{4}$ for the number density and $\frac{7}{8}$ for energy density and pressure. We will call these two factors the “fermion prefactors”. We also see that the pressure is simply one third that of the energy density, while the entropy density can be found by multiplying the energy density by $4/(3T)$.

4.5. Effective Degrees of Freedom

In most cases we cannot ignore the particle masses. In these cases, we must solve the integrals in Equations (10b), (11b), and (12b) numerically. The integrals are decreasing functions of the temperature, and they vanish in the limit $k_B T/mc^2 \rightarrow 0$. We can normalize these by dividing their values by the case of the photon (but with g equal to one). As we recall, the photon has a bosonic nature with $m = 0$ and $\mu = 0$. This means that for massive particles at high temperature ($k_B T \gg mc^2$), one actual degree of freedom for bosons contributes as much as one degree of freedom for photons, and the fermions a little less. As the temperature drops, and less particles are created, the effective contributions will be smaller. By including the intrinsic degrees of freedom (g), we find each particle species’ *effective degree of freedom*, g_{*j} :

$$g_{*n_j}(T) = \frac{g_j \left(\frac{k_B T}{hc}\right)^3 \int_{z_j}^\infty \frac{u \sqrt{u^2 - z_j^2}}{e^u \pm 1} du}{\frac{1}{2\pi^2} \left(\frac{k_B T}{hc}\right)^3 \int_0^\infty \frac{u^2}{e^u \pm 1} du} = \frac{g_j}{2\zeta(3)} \int_{z_j}^\infty \frac{u \sqrt{u^2 - z_j^2}}{e^u \pm 1} du, \quad (20)$$

$$g_{*\epsilon_j}(T) = \frac{g_j}{2\pi^2} \frac{(k_B T)^4}{(\hbar c)^3} \int_{z_j}^{\infty} \frac{u^2 \sqrt{u^2 - z_j^2}}{e^{u \pm 1}} du = \frac{15g_j}{\pi^4} \int_{z_j}^{\infty} \frac{u^2 \sqrt{u^2 - z_j^2}}{e^{u \pm 1}} du, \quad (21)$$

$$g_{*p_j}(T) = \frac{g_j}{6\pi^2} \frac{(k_B T)^4}{(\hbar c)^3} \int_{z_j}^{\infty} \frac{(u^2 - z_j^2)^{3/2}}{e^{u \pm 1}} du = \frac{15g_j}{\pi^4} \int_{z_j}^{\infty} \frac{(u^2 - z_j^2)^{3/2}}{e^{u \pm 1}} du, \quad (22)$$

$$g_{*s_j}(T) = \frac{3g_{*\epsilon_j}(T) + g_{*p_j}(T)}{4}. \quad (23)$$

In Figure 3, we have plotted the effective degrees of freedom for massive bosons (panel a) and fermions (panel b) with $g = 1$ (and $\mu = 0$) as functions of the temperature. We have also listed the results in Table B1 in Appendix B. When the temperature is equal to the mass ($k_B T = mc^2$), the effective degrees of freedom for energy density is approximately 0.9 for bosons and 0.8 for fermions, compared to that of the photon. For number density, pressure, and entropy density, they are a little lower.

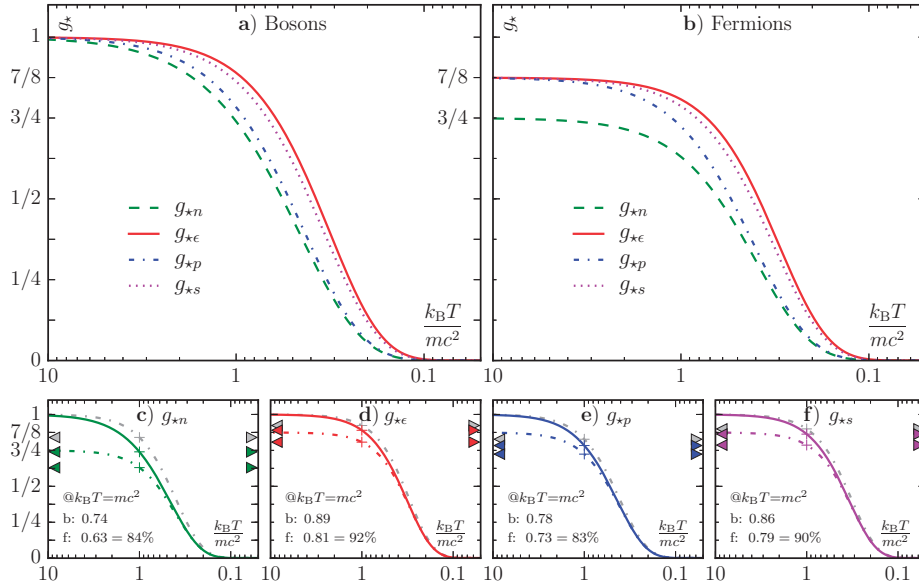


Figure 3. The effective degrees of freedom g_{*n} , $g_{*\epsilon}$, g_{*p} , and g_{*s} for bosons (a) and fermions (b) per intrinsic degree of freedom. A more detailed look at each of the four g_{*s} is given in the lower four panels (c–f). Here the solid colored curves are for the bosons, and the dash-dotted colored curves are for the fermions. The grey dash-dotted curves represent the fermions' contribution compared to its own relativistic value (such that it is 100% for $T \rightarrow \infty$). We have included the relative values at $k_B T = mc^2$ for the four cases (marked with “+” symbols). During particle annihilations, the energy density falls slower than the other quantities due to the impact of the rest mass energy. At temperatures close to the rest mass of some massive particle species, this rest mass is substantial to their total energy.

The effective degrees of freedom are defined as functions of the corresponding variables and temperature. We find the total effective degrees of freedom for g_{*n} , $g_{*\epsilon}$, and g_{*p} by summing Equations (20)–(23) over all particle species j :

$$g_{*n}(T) \equiv \frac{\pi^2}{\zeta(3)} \frac{n(T)}{T^3} \quad (24a)$$

$$= \sum_j \frac{g_j}{2\zeta(3)} \int_{z_j}^{\infty} \frac{u \sqrt{u^2 - z_j^2}}{e^u \pm 1} du, \quad (24b)$$

$$g_{*\epsilon}(T) \equiv \frac{30}{\pi^2} \frac{\epsilon(T)}{T^4} \quad (25a)$$

$$= \sum_j \frac{15g_j}{\pi^4} \int_{z_j}^{\infty} \frac{u^2 \sqrt{u^2 - z_j^2}}{e^u \pm 1} du, \quad (25b)$$

$$g_{*p}(T) \equiv \frac{90}{\pi^2} \frac{P(T)}{T^4} \quad (26a)$$

$$= \sum_j \frac{15g_j}{\pi^4} \int_{z_j}^{\infty} \frac{(u^2 - z_j^2)^{3/2}}{e^u \pm 1} du. \quad (26b)$$

Finally, the effective degrees of freedom associated with entropy is then:

$$g_{*s}(T) \equiv \frac{45}{2\pi^2} \frac{s(T)}{T^3} \quad (27a)$$

$$= \frac{3g_{*\epsilon}(T) + g_{*p}(T)}{4}. \quad (27b)$$

We again emphasize that Equations (24b), (25b), (26b), and (27b) are only valid for a system in thermal equilibrium (i.e., all the particles have the same temperature). It turns out that after the neutrinos decouple from the electromagnetically interacting particles (i.e., photons, electrons, and positrons) and the electrons and positrons annihilate, we cannot calculate the four g_{*s} s that straightforwardly. We will return to neutrino decoupling in Section 6.1.

5. Particle Evolution During the Cooling of the Universe

Our analysis starts with all the particles of the Standard Model present. As the Universe expands and cools, the annihilation rate of the more massive particles will become smaller and smaller compared to their creation rate. As the heavier particles disappear, this again will lead to a relatively larger creation rate for all the remaining lighter particle species. The overall number of particles in a comoving volume will thus remain (almost) constant. A few minutes after the Big Bang, when the temperature was down to 10 keV (corresponding to 100 million Kelvin), the Universe was mainly filled with photons and neutrinos. As we mentioned in Sections 1 and 4.3, a small—and at this stage, negligible—portion of matter survived due to the baryon asymmetry. Without the presence of antiparticles, the matter particles (i.e., nucleons and electrons) thus survived and “froze out” when their reaction rate (i.e., annihilation and creation rate) became slower than the expansion rate of the Universe (or equivalently, when the time scale of the weak interaction became longer than the age of the Universe) [8]. This process has some similarities with the decoupling of the neutrinos (which we will discuss in more detail in Section 6). These relic matter particles still interact with the photons and remain in thermal equilibrium until after the photon decoupling at around 380,000 years after the Big Bang [2]. Although negligible in the early stages of the Universe, matter eventually became the dominant energy contributor around 47,000 years after the Big Bang [10]. This is because non-relativistic (cold) matter receive their energy mainly from their rest mass. The energy density for cold matter goes as T^{-3} . This is solely due to the dilution of the particles. The kinetic contribution to the energy is negligible. Radiation (massless particles) goes as T^{-4} , because it is also subject to redshift as the Universe expands. A simple overview of events which affects the four g_{*s} s is given in Table 2.

Table 2. List of events which impacts g_{*n} , $g_{*\epsilon}$, g_{*p} , and g_{*s} . For the particle annihilation events, we have here used the particle masses as a reference. By combining this Table with Table B1 in Appendix B, we get a more precise picture.

Event	Temperature	g_{*n}	$g_{*\epsilon}$	g_{*p}	g_{*s}
Annihilation of $t\bar{t}$ quarks	<173.3 GeV	95.5	106.75	106.75	106.75
Annihilation of Higgs boson	<125.6 GeV	86.5	96.25	96.25	96.25
Annihilation of Z^0 boson	<91.2 GeV	85.5	95.25	95.25	95.25
Annihilation of W^+W^- bosons	<80.4 GeV	82.5	92.25	92.25	92.25
Annihilation of $b\bar{b}$ quarks	<4190 MeV	76.5	86.25	86.25	86.25
Annihilation of $\tau^+\tau^-$ leptons	<1777 MeV	67.5	75.75	75.75	75.75
Annihilation of $c\bar{c}$ quarks	<1290 MeV	64.5	72.25	72.25	72.25
QCD transition [†]	150–214 MeV	55.5	61.75	61.75	61.75
Annihilation of $\pi^+\pi^-$ mesons	<139.6 MeV	15.5	17.25	17.25	17.25
Annihilation of π^0 mesons	<135.0 MeV	13.5	15.25	15.25	15.25
Annihilation of $\mu^+\mu^-$ leptons	<105.7 MeV	13.5	14.25	14.25	14.25
Neutrino decoupling	<800 keV	9.5	10.75	10.75	10.75
Annihilation of e^+e^- leptons	<511.0 keV	6.636	6.863	6.863	7.409
		3.636	3.363	3.363	3.909

[†] Using lattice QCD, this transition is normally calculated to 150–170 MeV.

5.1. Quark-Gluon Plasma vs. Hadron Gas

In the early Universe, quarks and gluons moved freely around. A gas consisting of quarks and gluons at high temperature is referred to as a quark-gluon plasma, in analogy with an ordinary electromagnetic plasma. This is in contrast to today, where we do not observe free quarks, but only hadrons (e.g., pions and nucleons) that are bound states of either three quarks, three antiquarks, or a quark-antiquark pair. These different combinations are called baryons and mesons, and are both bound together by the gluons. While quarks and gluons carry color charge, the hadrons we observe are color neutral. At some critical temperature of the Universe T_c , a phase transition from a quark-gluon plasma to a hadronic phase took place. We call the gas formed immediately after the phase transition a hadron gas. This is similar to the formation of atoms, where the nucleus and electrons are bound together by electric forces. The aforementioned phase transition took place when the temperature of the Universe was approximately 150–170 MeV [22,23]. The transition temperature can be calculated by so-called lattice Monte Carlo simulations. Although the study of the phase transition from a quark-gluon plasma to a hadron gas is rather difficult, we can get an estimate of the critical temperature by evaluating the effective degrees of freedom for the energy density. This estimate could be thought of as an upper limit bound, as we cannot have an increase in $g_{*\epsilon}$ (i.e., the energy density) as the universe expands

5.2. Effective Degrees of Freedom in the QGP and HG Phases

Let us start an analysis at very high temperature, where all the elementary particles are present and effectively massless. $g_{*\epsilon}$ is therefore at a maximum. As the temperature decreases, the various

particles annihilate, and g_{*e} falls accordingly. We trace the number of effective degrees of freedom as a function of the temperature in Figure 4a. Here, the yellow dotted curve shows the effective degrees of freedom in the quark-gluon plasma phase (if it would exist for all temperatures). Without a phase transition, the quarks disappear only when the temperatures drop below their rest mass value. At the far right (colder) part of the scale, the gluons are still present together with the photons and neutrinos. In a similar manner, we can trace the effective degrees of freedom in a hadronic phase (if it would exist for all temperatures), as shown in the purple dash-dotted curve. As in the real world, relatively speaking we only have photons and neutrinos present at low temperatures. As we go left to higher temperatures, the first increase in g_{*e} is caused by the presence of electron-positron pairs. The muons and the lightest mesons (namely, the pions), are the next particles to appear. We then get a very steep increase in g_{*e} , starting at around 100 MeV. This is due to the appearance of many heavier hadrons, whose numbers grow almost exponentially as the temperature increases.

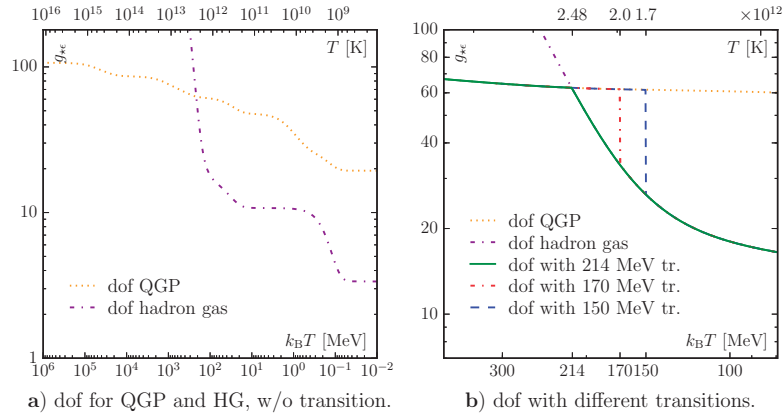


Figure 4. Panel (a) shows the effective degrees of freedom (dof) for g_{*e} in the quark-gluon and hadronic phases as functions of temperature. The yellow dotted curve represents the quark-gluon degrees of freedom and the purple dash-dotted curve is for the hadronic equivalent. In panel (b), we have zoomed in around the phase transition and plotted g_{*e} for three different transition temperatures: $k_B T_c = 214$ MeV in solid green, $k_B T_c = 170$ MeV in dash-dotted red, and $k_B T_c = 150$ MeV in dashed blue.

We can now define a “cross-over” temperature T_* , which is the temperature at which the two curves intersect. Hence, the phase with the lower number of effective degrees of freedom for energy density wins (in QCD theory, one normally compares the pressure of the two phases, and the phase with the higher pressure wins). Using the particles listed by the Particle Data Group [19] (and listed in Appendices C and D), this yields $k_B T_* = 214$ MeV. However, if there are more possible baryonic states (which there most likely are), this temperature will be lower. This cross-over temperature could be thought of as the QCD transition temperature. To get a more accurate estimate for the transition temperature, one can use the numerical method called lattice simulations. Using this latter method, one obtains a transition temperature $k_B T_c$ in the 150–170 MeV range. The value depends on the number of quarks and their mass used for the calculation. Thus, our simple estimate gives us the correct order of magnitude, but a bit too high. Speculatively, however, it is possible that it can be thought of as an upper bound.

In Figure 4b, we zoom in around the transition temperature. We recognize the partly covered yellow and purple curves from panel-a, representing the QGP and HG scenarios. The green curve represents a transition temperature of the aforementioned 214 MeV. If we insist on a critical temperature of 170 MeV, we follow the yellow curve for the QGP to the right, and as we hit this temperature, we jump down to the HG curve. This discontinuous curve for g_{*e} is shown in dash-dotted red color.

We will later see (Section 8) that this can be interpreted as the temperature remaining constant over a time while the degrees of freedom are reduced. The same remarks apply to the blue curve, which represents a 150 MeV transition.

5.3. A Closer Look at Each Particle Group

Let us have a closer look at how each group of particle species contributes to g_{*e} . Figure 5a shows how the different particle groups contribute to the energy density as the temperature of the Universe drops. Let us look at the simplest case first—the photon (shown as the black dashed line). It always has two degrees of freedom, and thus a constant contribution, $g_{*e\gamma}$, equal to two. The charged leptons (l) consist of the taus, muons, electrons, and their antiparticles. They are fermions, with two possible spin states. Each generation has a degeneracy of 3.5, which adds up to 10.5 at high temperatures. The magenta dash-dotted curve in Figure 5a shows how the charged lepton contribution drops around the time when the temperature ($k_B T$) goes below that of the particle masses (mc^2). The tau and antitau have a mass of 1777 MeV, so when the temperature drops below this value, their abundance will drop, and at a few hundred MeV they are all but gone, and g_{*el} will have dropped to about 7. The same process happens for the muons and electrons from $k_B T \sim 100$ MeV and $k_B T \sim 0.5$ MeV, when the value of g_{*el} drops to 3.5, and finally zero. The case is more or less the same for the massive bosons (W^\pm , Z^0 , and H^0). They have a total degeneracy of 10, and all have masses of around 100 GeV, which means that their annihilations will overlap as seen in the red dotted curve. For neutrinos (solid blue curve), we see a fall in $g_{*e\nu}$ after they have decoupled, and the electron–positrons start to annihilate. We look closer at this in Section 6.1.

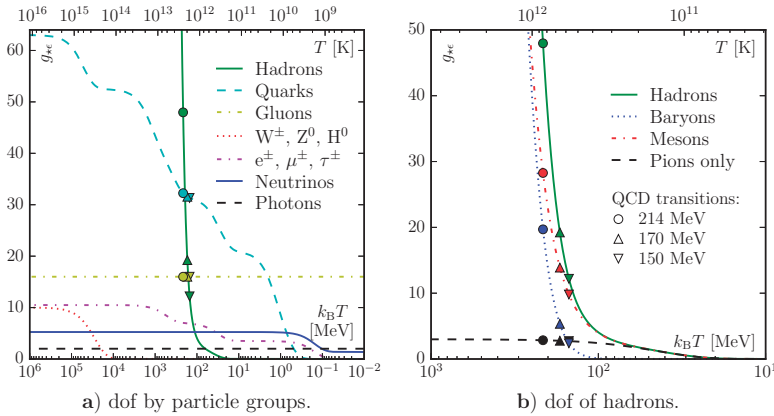


Figure 5. Panel (a) shows the contribution to the effective degrees of freedom (dof) for energy density from all particle groups. The drop in each group's g_{*e} value corresponds to ongoing annihilations of particles at that temperature. Panel (b) shows the total hadron contribution (green solid curve) to g_{*e} around the QCD phase transition temperature. We have further divided this into a baryon part (blue dotted curve) and a meson part (red dash-dotted curve). We have also plotted the pions specifically (black dashed curve), as they are the main hadronic contributor to g_{*e} at low temperatures. The two plots clearly show how fast the hadronic contribution increases at temperatures beyond 100 MeV. In both panels, we have marked the contribution to g_{*e} from hadrons, baryons, and mesons, at the three transition values of 214 MeV (\circ symbols), 170 MeV (\triangle symbols), and 150 MeV (∇ symbols), respectively.

For the color-charged particles (gluons and quarks), things are a bit more complicated due to the differences before and after the QCD phase transition. In Figure 5a, we have plotted both the quark-gluon plasma and hadron gas without any transition. Instead, we have marked their value at three different transition values: $k_B T_c = 214$ MeV (marked with \circ), $k_B T_c = 170$ MeV (marked with \triangle),

and $k_B T_c = 150$ MeV (marked with ∇). The case for the gluons is straightforward—they have 16 degrees of freedom for $T > T_c$, and zero after. Quarks—being massive—begin with 63 effective degrees of freedom, which will gradually decrease as the top, bottom, and charm particles disappear. At the time of the phase transition, this value is down to about ~ 32 , depending on T_c .

After the phase transition, we need to count the hadronic degrees of freedom. We can distinguish these by baryons and mesons, as is done in Figure 5b. The only hadrons with masses less than $k_B T_c$ are the three pions, which for $T = T_c$ have roughly three degrees of freedom. There are, however, many heavier hadrons, which single-handedly do not contribute much at low temperatures, but the sheer number of different hadronic states results in a collective significant contribution. Going from low to high temperatures in Figure 5b, the effective degrees of freedom from mesons (red dash-dotted curve) and baryons (blue dotted curve) increase almost exponentially. This value is quite different at different T_c . Following the hadrons (green curve) from right to left, we see that at $k_B T = 150$ MeV, the hadrons make up roughly 12 effective degrees of freedom. At $k_B T = 170$ MeV, this number is approximately 19, and at $k_B T = 214$ MeV, we have roughly 48—which is the same as the $16 + 32$ degrees of freedom from the free quarks and gluons.

6. Decoupling

As we mentioned in Section 1, particles are kept in thermal equilibrium by constantly colliding (interacting) with each other. The collision rate depends on two factors—the cross section σ and the particle density n . The cross section depends on several factors, but the most important one is by which forces the particles interact. Those which feel the strong and electromagnetic force interact strongly, while those which only feel the weak force interact much weaker. The cross sections related to the different forces depend on the temperature, or more correctly on the energy involved in the reaction. How these interaction strengths change are different for the four forces. In general, they become closer in strength for higher temperatures.

When the Universe expands, dilutes, and cools, particles travel farther and farther before interacting. That is, their mean free path and lifetime increases. As mentioned in Section 5, at some time the interaction rate for some particles can become slower than the expansion rate of the Universe, and (on average) those particles will never interact again. The time at which this happens is defined as the time of decoupling. For neutrinos, this happened about one second after the Big Bang (and we will get back to this in the next section), and for photons this happened about 380,000 years later (due to recombination and forming of neutral atoms). Let us look at the general case. First we need to introduce the concept of comoving coordinates and volumes. Comoving coordinates move with the rest frame of the Universe; i.e., they do not change as the Universe expands. An analogy of this would be to draw dots on a balloon. The actual distance between the dots increases as the balloon is inflated, but their comoving distance remains the same. For a comoving volume with constant entropy S , we can write

$$S = s(T)a^3 = g_{*s}(T) \frac{2\pi^2}{45} T^3 a^3 = \text{constant}$$

$$\rightarrow g_{*s}(T) T^3 a^3 = \text{constant} . \quad (28)$$

One of the consequences of this is that the temperature will fall slower during particle annihilations (i.e., when the effective degrees of freedom decreases). To understand this, we need to look at what is going on during particle creations and annihilations, as well as rest mass energy vs. kinetic energy.

During reactions where we go from two massive particles to two lighter particles, the excess rest mass energy will be converted to kinetic energy. Thus, the lighter particles will on average have a higher kinetic energy than the other particles in the thermal “soup”. Normally, this is countered by the reversed reaction—namely, reactions where two lighter particles create two more massive ones with less kinetic energy. Throughout periods where we have particle annihilations, there will be a net

flow of massive particles to lighter particles plus kinetic energy. Hence, the temperature will fall slower in these periods.

In order to maintain thermal equilibrium, particles need to constantly interact. That is, there needs to be some coupling between them (directly or indirectly). If some particles decouple, it means that they on average will never interact again, so if a particle species has decoupled before an annihilation process starts, their temperature will decrease independently of those which are still coupled together. As a result, there will be two different temperatures: the photon-coupled temperature (T) (those particles that directly or indirectly interact with the photons), and the decoupled-particle temperature (T_{dc}). Solving Equation (28) before and after an annihilation process (indicated by subscripts "1" and "2") for the photon-coupled (γc) and decoupled (dc) particles gives us

$$g_{\gamma c1} T_1^3 a_1^3 = g_{\gamma c2} T_2^3 a_2^3, \quad (29)$$

$$g_{dc1} T_{dc1}^3 a_1^3 = g_{dc2} T_{dc2}^3 a_2^3. \quad (30)$$

After decoupling, but before an annihilation process, the two temperatures are the same. Well, close enough, as we will briefly discuss in Section 8. Once a photon-coupled particle species start to annihilate, the degrees of freedom for (all) the coupled particles will reduce, while it will remain the same for the decoupled ones. Solving for the decoupled temperature after annihilation gives us:

$$T_{dc2}^3 = \frac{g_{\gamma c2}}{g_{\gamma c1}} T_2^3, \quad (31)$$

which we normally write as

$$T_{dc} = \sqrt[3]{\frac{g_{\gamma c2}}{g_{\gamma c1}}} T. \quad (32)$$

In principle, we can do this for more than one decoupled particle species, and get two or more different temperatures for the decoupled particles.

6.1. Neutrino Decoupling

Before they are decoupled, neutrinos are kept in thermal equilibrium with the photon-coupled particles mainly via weak interactions with electrons and positrons. Around one second after the Big Bang, the rate of the neutrino–electron interactions becomes slower than the rate of expansion of the Universe, H . The collision rate between neutrinos and electrons (and its antiparticle), Γ_ν , is given by [6,17]:

$$\begin{aligned} \Gamma_\nu &= n_e \sigma_{wk} \approx \left(\frac{k_B T}{\hbar c} \right)^3 (\hbar c G_{wk} k_B T)^2 \\ &\approx \frac{G_{wk}^2 (k_B T)^5}{\hbar c}, \end{aligned} \quad (33)$$

where n_e is the number density of electrons and σ_{wk} is the neutrino–electron scattering cross section. $G_{wk} = G_F/(\hbar c)^3 \approx 1.166 \times 10^{-5} \text{ GeV}^{-2}$ is the weak coupling constant [24,25]. By using the equation for energy density, either from Equation (11c), or better, by fast-forwarding to Equation (48), the expansion rate at the same time is given by the first Friedmann equation:

$$\begin{aligned} H &= \sqrt{\frac{8\pi G}{3c^2} \epsilon} = \sqrt{\frac{8\pi G}{3c^2} g_{*\epsilon}(T) \frac{\pi^2 (k_B T)^4}{30 (\hbar c)^3}} \\ &\approx \sqrt{\frac{5G (k_B T)^4}{(\hbar c)^3}}. \end{aligned} \quad (34)$$

The prefactors in Γ_V and H roughly cancel each other, such that we end up with

$$\frac{\Gamma_V}{H} \approx G_{\text{wk}}^2 \sqrt{\frac{\hbar c}{5G}} (k_B T)^3 \approx \left(\frac{T}{10^{10} \text{ K}} \right)^3. \quad (35)$$

This is a rough estimate, but one that is most commonly used (e.g., by Weinberg [6]). Being relativistic, the neutrino temperature T_V scales as a^{-1} , while the energy density and number density scale as a^{-4} and a^{-3} , respectively.

6.2. Neutrino Temperature and Entropic Degrees of Freedom

Let us look more closely at the effective degrees of freedom at the time just after the neutrinos decouple. For the entropy density before the electrons and positrons annihilate, they have 10.75 degrees of freedom, divided as 5.25 for the neutrinos and $2 + 3.5 = 5.5$ for the photon plus the electron and positron. The latter one is reduced to just 2 once all the electrons and positrons have annihilated (i.e., $g_{\gamma c2}/g_{\gamma c1} = 2/5.5 = 4/11$). We now have a higher photon temperature and a lower neutrino temperature. Using Equation (32), we find the neutrino temperature after all electrons and positrons have annihilated to be

$$T_V = \sqrt[3]{\frac{4}{11}} T \approx 0.71 T. \quad (36)$$

Hence, after the electron–positron annihilation, the neutrino temperature is 71% that of the photon temperature. Measurements of the Cosmic Microwave Background (CMB) radiation is found to be 2.73 K. This means that the neutrino background temperature should be 1.95 K (it should be mentioned that no measurement of the cosmic neutrino background have been made, or is likely to be made in the near future that would confirm this prediction).

The colder neutrinos do not contribute as much as the hotter particles to the four different g_{*s} , and this has to be taken into account when we calculate the different effective degrees of freedom. In general, after a particle species decouples, we need to introduce a species-dependent temperature ratio into our equations; that is, $T \rightarrow T(T_j/T)$. Here T_j is the temperature of the decoupled particle species, while T is the photon-coupled (reference) temperature. We thus get the following g_{*n} , g_{*e} , g_{*p} , and g_{*s} after electron–positron annihilation is completed

$$g_{*n} = 2 + 6 \times \frac{3}{4} \left(\frac{T_V}{T} \right)^3 = 2 + 6 \times \frac{3}{4} \times \frac{4}{11} = \frac{40}{11} \approx 3.636. \quad (37)$$

$$g_{*e} = g_{*p} = 2 + 6 \times \frac{7}{8} \left(\frac{T_V}{T} \right)^4 = 2 + 6 \times \frac{7}{8} \left(\frac{4}{11} \right)^{4/3} \approx 3.363, \quad (38)$$

$$g_{*s} = 2 + 6 \times \frac{7}{8} \left(\frac{T_V}{T} \right)^3 = 2 + 6 \times \frac{7}{8} \times \frac{4}{11} = \frac{43}{11} \approx 3.909. \quad (39)$$

The neutrino contribution during electron–positron annihilation is found by subtracting the electron–positron contribution in the following way:

$$g_{*n_V} = \frac{6 \times 3}{4} \times \left[\frac{4}{11} + \left(1 - \frac{4}{11} \right) \frac{4}{4 \times 3} g_{*n_e} \right], \quad (40)$$

$$g_{*e_V} = \frac{6 \times 7}{8} \times \left[\left(\frac{4}{11} \right)^{4/3} + \left(1 - \left(\frac{4}{11} \right)^{4/3} \right) \frac{8}{4 \times 7} g_{*e_e} \right], \quad (41)$$

$$g_{*p_V} = \frac{6 \times 7}{8} \times \left[\left(\frac{4}{11} \right)^{4/3} + \left(1 - \left(\frac{4}{11} \right)^{4/3} \right) \frac{8}{4 \times 7} g_{*p_e} \right], \quad (42)$$

$$g_{*s\nu} = \frac{6 \times 7}{8} \times \left[\frac{4}{11} + \left(1 - \frac{4}{11} \right) \frac{8}{4 \times 7} g_{*se} \right], \quad (43)$$

where the four g_{*x_e} are the effective electron-positron contributions.

In reality, as can be seen in Figure 3 and Table B1, the first electron-positron annihilations began slightly before the neutrino decoupling was complete. Hence, some of the energy from the decaying electron-positron pairs heated up the neutrinos. This caused a small deviation from the above-mentioned values, which resulted in effective numbers of neutrino species slightly larger than three. This number is given to be 3.046 by Mangano [26] and 3.045 by de Salas and Pastor [27]. By using Mangano's result, a compensated result will be

$$g_{*n} = 2 + 2 \times 3.046 \times \frac{3}{4} \times \frac{4}{11} \approx 3.661, \quad (44)$$

$$g_{*\epsilon} = g_{*p} = 2 + 2 \times 3.046 \times \frac{7}{8} \left(\frac{4}{11} \right)^{4/3} \approx 3.384, \quad (45)$$

$$g_{*s} = 2 + 2 \times 3.046 \times \frac{7}{8} \times \frac{4}{11} \approx 3.938. \quad (46)$$

7. Functions for n , ϵ , P , and S , and Their Implications

We can now express the complete number density, energy density, pressure, and entropy density in terms of their effective degrees of freedom:

$$\text{Number density: } n(T) = \frac{\zeta(3)}{\pi^2} g_{*n}(T) \frac{(k_B T)^3}{(hc)^3}, \quad (47)$$

$$\text{Energy density: } \epsilon(T) = \frac{\pi^2}{30} g_{*\epsilon}(T) \frac{(k_B T)^4}{(hc)^3}, \quad (48)$$

$$\text{Pressure: } P(T) = \frac{\pi^2}{90} g_{*p}(T) \frac{(k_B T)^4}{(hc)^3}, \quad (49)$$

$$\text{Entropy density: } s(T) = \frac{2\pi^2}{45} g_{*s}(T) \frac{k_B^4 T^3}{(hc)^3}. \quad (50)$$

We have plotted these functions as well as the g_* values in Figure 6. The energy density and pressure have the same dimension, while the dimensions of entropy density and number density differ by the Boltzmann constant (unit: J K^{-1}).

When the prefactors are accounted for, the difference in s and n , and P and ϵ , lies in the deviations between g_{*s} and g_{*n} , and g_{*p} , and $g_{*\epsilon}$. So, let us discuss a bit more about what is actually happening. Both the increase in entropy per particle and the decrease in pressure (which we see as bumps and dips in panels (g) and (h) in Figure 6) are due to the presence of particles at semi- and non-relativistic temperatures. Before we go any farther, we should address the QCD phase transition. As not all four g_{*s} can be continuous (as we see in panels (b)–(d) in Figure 6), we get inconsistencies and some unphysical results. For most of our plots, we use $T_c = 214 \text{ MeV}$, keeping $g_{*\epsilon}$ continuous, leaving g_{*n} , g_{*p} , and g_{*s} discontinuous at this point.

We see from panel (a) in Figure 6 that both number density and entropy density decrease more rapidly during annihilation periods. However, this is a bit deceiving, since we are looking at their values as functions of temperature. In fact, the total entropy stays constant (it actually increases ever so slightly if we do not have perfect thermal equilibrium). Both s and n fall a bit as we cross the transition temperature. We thus get a jump in the entropy per particle at this time, as can be seen in panel (g) in Figure 6. The other bumps in entropy per particle are continuous. The entropy per particle will start to rise when the rest mass of some massive particles becomes more significant. s then flattens out and drops again as these particles gradually become less numerous. After all these massive particles have annihilated and disappeared, the value of s returns to its original value (before the annihilations

started). As mentioned in Figure 3 in Section 4.5, particles whose rest mass energy is significant have a higher total energy, and thus a higher entropy. This entropy is eventually transferred to the remaining particles after they annihilate. It is important to emphasize that it is not the total entropy that changes, but rather the (total) particle number that falls and rises again. The change in entropy density after the neutrino decoupling, as we can see at the lowest temperature in panel (b) in Figure 6, is due to the fact that the neutrinos have a lower temperature and thus contribute less.

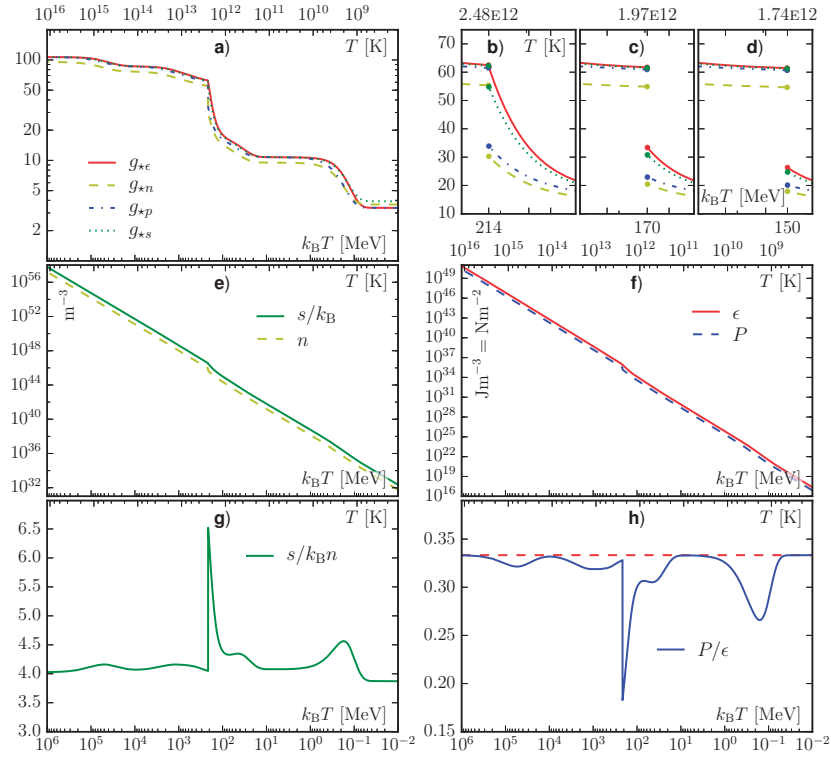


Figure 6. Panel (a) shows the four g_{*s} . At $k_B T = 214$ MeV, only g_{*q} is continuous, while g_{*l} , g_{*e} , $g_{*μ}$ drops in value by between 10 and 30. The three upper right panels show these jumps at transition values of 214 MeV (b), 170 MeV (c), and 150 MeV (d). Panels (e) and (f) show the evolution of n , ϵ , P , and s/k_B as a function of temperature. In the two lower panels, we look at the relation between entropy density and number density (g) and pressure and energy density (h). We see small fluctuations during periods with particle annihilations, especially right after the QCD phase transition. As we remember from Figure 3, this is because the pressure and number density drop quicker than energy density and entropy density at these times. The short physical explanation is that semi- and non-relativistic particles exert less pressure and have a higher entropy than relativistic particles (at the same temperature). One consequence of this is that particle numbers are not conserved, which is not a requirement for particles whose chemical potential is zero.

The same explanation goes for the fall in pressure, as seen in panel (h) in Figure 6. Non-relativistic particles exert (relatively) zero pressure. The pressure is thus at its lowest at times where the ratio of semi- and non-relativistic particles are at their highest. We see that the two most significant drops in pressure are just after the QCD phase transition and in the middle of the electron–positron annihilations. We have used a naive definition for our QCD phase transition—namely, that of the lowest energy density. In reality, this transition is quite complex, and we should interpret our result with a grain of

salt. With that in mind, we go from an almost pure relativistic gas (QGP) to a case where the majority of the particles are semi- or non-relativistic (HG)—which is the reason for the jump down in pressure at $T = 214$ MeV.

As we will get back to in the next section, the Universe expands faster when it is matter-dominated as compared to when it is radiation-dominated. So even though the early Universe was the latter, we know from our study that we have periods with a significant fraction of semi-relativistic particles. One can thus argue that a should grow slightly faster at these times.

8. Time–Temperature Relation

As mentioned in Section 1, the measurements of the CMB thermal spectrum is very close to that of a perfect black body [28]. The early Universe should be very homogeneous, with the same features everywhere. How fast the early Universe expands depends on which energy contributor is dominating—the relativistic particles (radiation), or non-relativistic particles (cold matter). By solving the Friedmann equations for a flat adiabatic Universe with no cosmological constant, we find the relation between the scale factor (a) and time (t) to be $a = t^{1/2}$ for a pure radiation case, and $a = t^{2/3}$ for a pure cold matter case. Simple derivations for this are given by Ryden [10] and Liddle [29]. Similarly, a relation between the scale factor and temperature for the two extreme cases is given as $T = a^{-1}$ and $T = a^{-2}$ for the two cases [8,30]. This gives us the following relation between the three quantities:

$$\begin{aligned} \text{Just radiation:} \quad T &\propto t^{-1/2} \propto a^{-1}, & (51) \\ \text{Just cold matter:} \quad T &\propto t^{-4/3} \propto a^{-2}. & (52) \end{aligned}$$

For a mixture of both types of particles, we should have something in between the two single-component cases. So, if radiation is the more dominant energy contributor, a grows almost proportional to $t^{1/2}$, or more proportional $t^{2/3}$ for the matter case. Regarding temperature, for a radiation-dominated scenario, the relation between temperature and time (after the Big Bang) can be calculated as a function of g_{*e} , as follows [19]:

$$\begin{aligned} t &= \sqrt{\frac{90\hbar^3 c^5}{32\pi^3 G g_{*e}(T)}} (k_B T)^{-2} \\ &= \frac{2.4}{\sqrt{g_{*e}(T)}} T_{\text{MeV}}^{-2}. \end{aligned} \quad (53)$$

The Universe becomes matter-dominated at roughly 10^5 years after the Big Bang, long after the scope of this article. However, it should be noted that the temperature of both photons and matter drop as the inverse of the scale factor, even long after this radiation–matter equality. This is because temperature is determined by the kinetic energy of the particles, while the definition of a radiation- or matter-dominated Universe is that of the total energy (where rest mass is included). Being outnumbered more than a billion to one, matter is unable to cool down the photons, and the temperature of the Universe drops as the inverse of the scale factor until matter decouples from the photons.

On the other hand, when massive particles die out, their annihilation energy is transferred to the remaining particles in the thermal bath. This should make the temperature drop slower as a function of time. If we assume that this latter argument is dominant, we will get a Universe which drops in temperature more slowly when g_{*e} is decreasing. Figure 7 shows the temperature as a function of time assuming a pure radiation-dominated Universe, as given by Equation (53). During particle annihilations, we have a smooth continuous function, but this is not the case for the QGP-to-HG transition using our models. Here we have to consider the three different transition temperatures separately. Using $k_B T_C = 214$ MeV, we have a scenario where the temperature will drop more slowly

right after T_c . Using $k_B T_c = 170$ MeV and $k_B T_c = 150$ MeV, the degrees of freedom (g_{*e}) will jump down at T_c . For $k_B T_c = 170$ MeV, the value of g_{*e} falls from around 62 to 33, while for $k_B T_c = 150$ MeV, this value falls from around 61 to 26. This would, however, take some time. Using our simple model, the temperature and energy density of the Universe would stay constant as the Universe expands until it reaches its pure hadron-gas state.

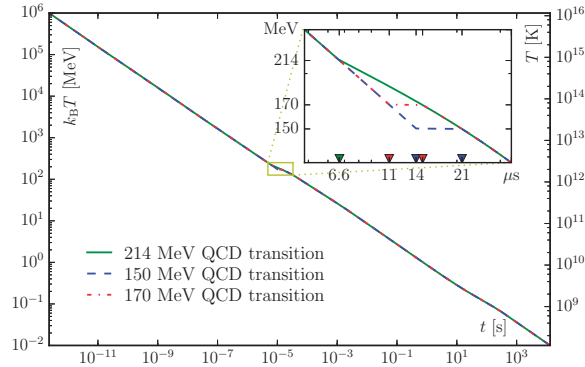


Figure 7. Energy and temperature as functions of time using the three different transition temperatures. For the $k_B T_c = 214$ MeV transition, the temperature will drop slower after T_c , but nonetheless always decrease over time. For $k_B T_c = 170$ MeV and $k_B T_c = 150$ MeV, there will be a period with constant temperature and energy density while g_{*e} decreases from its quark-gluon value to its hadron gas value.

The relation made here between time and temperature during the QCD transition is naive and simple, and the numerical values thereafter. Small deviations from our plot during the QCD transition (and for that matter, during regular particle annihilations) only affect the period on hand, and become negligible as time go on.

9. On the QCD Phase Transition and Cross-Over Temperature

Our method of using $k_B T_c = 214$ MeV is based on a calculation where we add all the g_{*e} from the quark-gluon state on one hand (easy), and all the g_{*e} from the hadrons on the other hand (not so easy). We have used the hadronic particles as listed in Appendices C and D. These are the particles listed by the *Particle Data Group* [19]. There are additional candidates to these lists—some good candidates, and some more speculative. There could also be more hadronic states which are hard to detect. For every new hadron we add to our model, the cross-over temperature decreases. Not so much for the most massive candidates, but more so for the lighter ones.

The phase transition we have used is of first order. Only g_{*e} is continuous at this point, and g_{*n} , g_{*p} , and g_{*s} are not. This will lead to some unphysical consequences—such as an instantaneous increase of the scale factor by roughly 4% if we assume constant entropy. A proper theory about the QCD phase transition is required to address this issue, which is beyond the scope of this article. The theory we have presented here should be valid to a good approximation, before and after the QCD transition.

10. Conclusions

Our knowledge of the very first stages of Universe is limited. In order to know for sure what is happening at these extreme energies and temperatures, we want to recreate the conditions using particle accelerators. The Large Hadron Collider at CERN can collide protons together at energies of 13 TeV, and with their discovery of the Higgs boson, all the elementary particles predicted by the Standard Model of particle physics have been found. This is, however, most likely not the complete

story. Dark matter particles are the hottest candidates to be added to our list of particles, and there is almost sure to be more particles at even higher temperatures, such as at the Grand Unified Theory (GUT) scale of $T \sim 10^{16}$ GeV.

We have here used the statistical physics approach to counting the effective degrees of freedom in the early Universe at temperatures below 10 TeV. Some simplifications have been used, such as setting the chemical potential equal to zero for all particles. The aim of this article was to give a good qualitative introduction to the subject, as well as providing some quantitative data in the form of plots and tables.

The early Universe is often thought of as being pure radiation (just relativistic particles). However, when the temperature drops to approximately that of the rest mass of some massive particles, we get interesting results, where we have a mix of relativistic particles and semi- and non-relativistic ones. This mix is most prominent during the electron–positron annihilations, and just after the phase transition from a quark–gluon plasma to a hadron gas. Approaching this, using our “no-chemical potential” distribution functions shows us how the entropy per particle increases when the ratio of semi- and non-relativistic particles becomes significant.

The number of effective degrees of freedom for hadrons changes very quickly around the QCD transition temperature. We found a cross-over temperature of 214 MeV using the known baryons and mesons. As there could be many more possible hadronic states than we have accounted for, this cross-over temperature could be lower. This is not meant as a claim of a new QCD transition temperature, but rather as an interesting fact. Our first-order approach based purely on the distribution functions has inconsistencies at the cross-over temperature.

We have listed the effective degrees of freedom for number density (g_{*n}), energy density ($g_{*\epsilon}$), pressure (g_{*p}), entropy density (g_{*s}), and time (t) as function of temperature (T) in Table A1 in Appendix A. Table B1 in Appendix B lists the different effective contributions to a single intrinsic degree of freedom, corresponding to our plot in Figure 3.

Acknowledgments: The author would like to thank Jens O. Andersen, Iver Brevik, Kåre Olaussen, and Alireza Qaiumzadeh for fruitful discussions.

Conflicts of Interest: The authors declare no conflict of interest.

Appendix A. Table for Time, g_{*n} , $g_{*\epsilon}$, g_{*p} , and g_{*s}

Table A1. Values for time, g_{*n} , $g_{*\epsilon}$, g_{*p} , and g_{*s} from $T = 10$ TeV to 10 keV. In the region between 150–214 MeV, the values for all five quantities depend on the model’s transition temperature. We should emphasize that the values for this period are based on our simple no-chemical potential model.

$k_B T$ (eV)	T (K)	Time (s)	g_{*n}	$g_{*\epsilon}$	g_{*p}	g_{*s}	Tr. Temp.
10 TeV	1.16×10^{17}	2.32×10^{-15}	95.50	106.75	106.75	106.75	All
5 TeV	5.80×10^{16}	9.29×10^{-15}	95.49	106.75	106.75	106.75	All
2 TeV	2.32×10^{16}	5.81×10^{-14}	95.47	106.74	106.73	106.74	All
1 TeV	1.16×10^{16}	2.32×10^{-13}	95.39	106.72	106.65	106.70	All
500 GeV	5.80×10^{15}	9.30×10^{-13}	95.11	106.61	106.38	106.56	All
200 GeV	2.32×10^{15}	5.83×10^{-12}	93.55	105.90	104.75	105.61	All
100 GeV	1.16×10^{15}	2.36×10^{-11}	89.89	103.53	100.80	102.85	All
50 GeV	5.80×10^{14}	9.73×10^{-11}	83.53	97.40	93.94	96.53	All
20 GeV	2.32×10^{14}	6.40×10^{-10}	77.39	88.45	87.22	88.14	All
10 GeV	1.16×10^{14}	2.58×10^{-9}	76.20	86.22	85.85	86.13	All
5 GeV	5.80×10^{13}	1.04×10^{-8}	75.27	85.60	84.68	85.37	All
2 GeV	2.32×10^{13}	6.61×10^{-8}	71.14	82.50	79.69	81.80	All
1 GeV	1.16×10^{13}	2.75×10^{-7}	65.37	76.34	72.97	75.50	All
500 MeV	5.80×10^{12}	1.15×10^{-6}	59.69	69.26	66.43	68.55	All
214 ⁺ MeV	2.48×10^{12}	6.63×10^{-6}	55.37	62.49	61.52	62.25	All
214 ⁻ MeV	2.48×10^{12}	6.63×10^{-6}	30.27	62.49	33.88	54.80	214 MeV
		6.63×10^{-6}	55.37	62.49	61.52	62.25	170 + 150 MeV
200 MeV	2.32×10^{12}	8.42×10^{-6}	26.45	50.75	29.62	45.47	214 MeV

Table A1. Cont.

$k_B T$ (eV)	T (K)	Time (s)	g_{*n}	$g_{*\epsilon}$	g_{*p}	g_{*s}	Tr. Temp.
190 MeV	2.20×10^{12}	7.61×10^{-6}	55.21	62.21	61.34	61.99	170 + 150 MeV
		1.00×10^{-5}	24.14	44.01	27.04	39.77	214 MeV
180 MeV	2.09×10^{12}	8.44×10^{-6}	55.10	62.03	61.21	61.83	170 + 150 MeV
		1.20×10^{-5}	22.16	38.27	24.84	34.91	214 MeV
170 ⁺ MeV	1.97×10^{12}	9.42×10^{-6}	54.99	61.87	61.07	61.67	170 + 150 MeV
		1.44×10^{-5}	20.49	33.47	22.98	30.84	214 MeV
170 ⁻ MeV	1.97×10^{12}	1.06×10^{-5}	54.88	61.72	60.94	61.52	170 + 150 MeV
		1.44×10^{-5}	20.49	33.47	22.98	30.84	214 + 170 MeV
160 MeV	1.86×10^{12}	1.06×10^{-5}	54.88	61.72	60.94	61.52	150 MeV
		1.73×10^{-5}	19.09	29.51	21.42	27.49	214 + 170 MeV
150 ⁺ MeV	1.74×10^{12}	1.20×10^{-5}	54.77	61.58	60.80	61.38	150 MeV
		2.08×10^{-5}	17.93	26.31	20.13	24.77	214 + 170 MeV
150 ⁻ MeV	1.74×10^{12}	1.36×10^{-5}	54.65	61.45	60.65	61.25	150 MeV
		2.08×10^{-5}	17.93	26.32	20.13	24.77	All
140 MeV	1.62×10^{12}	2.51×10^{-5}	16.96	23.77	19.05	22.59	All
130 MeV	1.51×10^{12}	3.04×10^{-5}	16.16	21.76	18.16	20.86	All
100 MeV	1.16×10^{12}	5.66×10^{-5}	14.39	18.00	16.21	17.55	All
50 MeV	5.80×10^{11}	2.51×10^{-4}	11.87	14.63	13.40	14.32	All
20 MeV	2.32×10^{11}	1.78×10^{-3}	9.71	11.33	10.99	11.25	All
10 MeV	1.16×10^{11}	7.32×10^{-3}	9.50	10.76	10.75	10.76	All
5 MeV	5.80×10^{10}	2.93×10^{-2}	9.49	10.74	10.73	10.74	All
2 MeV	2.32×10^{10}	0.18	9.43	10.71	10.65	10.70	All
1 MeV	1.16×10^{10}	0.74	9.22	10.60	10.36	10.56	All
500 keV	5.80×10^9	3.11	8.53	10.16	9.43	10.03	All
200 keV	2.32×10^9	2.39×10^1	5.97	7.66	6.20	7.55	All
100 keV	1.16×10^9	1.22×10^2	4.03	4.46	3.84	4.78	All
50 keV	5.80×10^8	5.24×10^2	3.64	3.39	3.37	3.93	All
20 keV	2.32×10^8	3.27×10^3	3.64	3.36	3.36	3.91	All
10 keV	1.16×10^8	1.31×10^4	3.64	3.36	3.36	3.91	All

Appendix B. Effective Contribution to One Single Intrinsic Degree of Freedom

Table B1. The effective contribution to a single degree of freedom as function of temperature ($k_B T$) over mass (mc^2).

$\frac{k_B T}{mc^2}$	Number Density		Energy Density		Pressure		Entropy Density	
	Bosons	Fermions	Bosons	Fermions	Bosons	Fermions	Bosons	Fermions
∞	1	0.750	1	0.875	1	0.875	1	0.875
10:1	0.993	0.749	0.999	0.874	0.996	0.873	0.998	0.874
2:1	0.901	0.716	0.970	0.859	0.929	0.831	0.960	0.852
1:1	0.740	0.630	0.890	0.808	0.784	0.724	0.863	0.787
1:2	0.438	0.409	0.658	0.626	0.477	0.461	0.613	0.585
1:3	0.236	0.227	0.427	0.418	0.257	0.254	0.385	0.377
1:4	0.116	0.115	0.253	0.251	0.129	0.128	0.222	0.222
1:5	0.055	0.055	0.139	0.139	0.061	0.061	0.120	0.120
1:6	0.025	0.025	0.073	0.073	0.028	0.028	0.062	0.062
1:7	0.011	0.011	0.037	0.037	0.013	0.013	0.031	0.031
1:8	4.93×10^{-3}	4.93×10^{-3}	0.018	0.018	5.48×10^{-3}	5.48×10^{-3}	0.015	0.015
1:9	2.12×10^{-3}	2.12×10^{-3}	8.37×10^{-3}	8.37×10^{-3}	2.35×10^{-3}	2.35×10^{-3}	6.87×10^{-3}	6.87×10^{-3}
1:10	8.94×10^{-4}	8.94×10^{-4}	3.87×10^{-3}	3.87×10^{-3}	9.94×10^{-4}	9.94×10^{-4}	3.15×10^{-3}	3.15×10^{-3}
1:12	1.55×10^{-4}	1.55×10^{-4}	7.81×10^{-4}	7.81×10^{-4}	1.72×10^{-4}	1.72×10^{-4}	6.29×10^{-4}	6.29×10^{-4}
1:14	2.58×10^{-5}	2.58×10^{-5}	1.49×10^{-4}	1.49×10^{-4}	2.87×10^{-5}	2.87×10^{-5}	1.19×10^{-4}	1.19×10^{-4}
1:16	4.21×10^{-6}	4.21×10^{-6}	2.74×10^{-5}	2.74×10^{-5}	4.67×10^{-6}	4.67×10^{-6}	2.17×10^{-5}	2.17×10^{-5}
1:18	6.71×10^{-7}	6.71×10^{-7}	4.87×10^{-6}	4.87×10^{-6}	7.45×10^{-7}	7.45×10^{-7}	3.84×10^{-6}	3.84×10^{-6}
1:20	1.05×10^{-7}	1.05×10^{-7}	8.42×10^{-7}	8.42×10^{-7}	1.17×10^{-7}	1.17×10^{-7}	6.61×10^{-7}	6.61×10^{-7}
1:30	8.52×10^{-12}	8.52×10^{-12}	9.96×10^{-11}	9.96×10^{-11}	9.47×10^{-12}	9.47×10^{-12}	7.71×10^{-11}	7.71×10^{-11}
1:40	5.87×10^{-16}	5.87×10^{-16}	9.03×10^{-15}	9.03×10^{-15}	6.52×10^{-16}	6.52×10^{-16}	6.93×10^{-15}	6.93×10^{-15}
1:50	3.69×10^{-20}	3.69×10^{-20}	7.04×10^{-19}	7.04×10^{-19}	4.10×10^{-20}	4.10×10^{-20}	5.38×10^{-19}	5.38×10^{-19}
1:100	1.98×10^{-41}	1.98×10^{-41}	7.43×10^{-40}	7.43×10^{-40}	2.19×10^{-41}	2.19×10^{-41}	5.62×10^{-40}	5.62×10^{-40}

Appendix C. List of Mesons and Their Degeneracy

Table C1. Pseudoscalar mesons.

Symbol	Flavours	Spin States	Color States	Bose or Fermi	Mass
π^0	1	1	1	1	134.9766
π^\pm	2	1	1	1	139.57018
K^\pm	2	1	1	1	493.677
K^0, \bar{K}^0	2	1	1	1	497.614
K_S^0, K_L^0	2	1	1	1	497.614
η	1	1	1	1	547.862
η'	1	1	1	1	957.78
D^0, \bar{D}^0	2	1	1	1	1864.84
D^\pm	2	1	1	1	1869.61
D_s^\pm	2	1	1	1	1968.30
η_c	1	1	1	1	2983.6
B^\pm	2	1	1	1	5279.26
B^0, \bar{B}^0	2	1	1	1	5279.58
B_s^0, \bar{B}_s^0	2	1	1	1	5366.77
B_c^\pm	2	1	1	1	6275.6
η_b	1	1	1	1	9398.0
Pseudoscalar Mesons					g = 27

Table C2. Vector mesons.

Symbol	Flavours	Spin States	Color States	Bose or Fermi	Mass
ρ^\pm	2	3	1	1	775.11
ρ^0	1	3	1	1	775.26
ω	1	3	1	1	782.65
$K^{*\pm}$	2	3	1	1	891.66
K^{*0}, \bar{K}^{*0}	2	3	1	1	895.81
ϕ	1	3	1	1	1019.461
D^{*0}, \bar{D}^{*0}	2	3	1	1	2006.96
$D^{*\pm}$	2	3	1	1	2010.26
$D_s^{*\pm}$	2	3	1	1	2112.1
J/ψ	1	3	1	1	3096.916
$B^{*\pm}$	2	3	1	1	5325.2
B^{*0}, \bar{B}^{*0}	2	3	1	1	5325.2 ^a
B_s^{*0}, \bar{B}_s^{*0}	2	3	1	1	5415.4 ^a
$Y(1S)$	1	3	1	1	9460.30
Vector Mesons					g = 69

^a These are listed without 0 superscript by PDG [19].

Table C3. Excited unflavoured mesons.

Symbol	Flavours	Spin States	Color States	Bose or Fermi	Mass
$f_0(500)$	1	1	1	1	500
$f_0(980)$	1	1	1	1	980
$a_0(980)$	3	1	1	1	980
$h_1(1170)$	1	3	1	1	1170
$b_1(1235)$	3	3	1	1	1235
$a_1(1260)$	3	3	1	1	1260
$f_2(1270)$	1	5	1	1	1270
$f_1(1285)$	1	3	1	1	1285

Table C3. Cont.

Symbol	Flavours	Spin States	Color States	Bose or Fermi	Mass
$\eta(1295)$	1	1	1	1	1295
$\pi(1300)$	3	1	1	1	1300
$a_2(1320)$	3	5	1	1	1320
$f_0(1370)$	1	1	1	1	1370
$h_1(1380)$	1	3	1	1	1380
$\pi_1(1400)$	3	3	1	1	1400
$\eta(1405)$	1	1	1	1	1405
$f_1(1420)$	1	3	1	1	1420
$\omega(1420)$	1	3	1	1	1420
$f_2(1430)$	1	5	1	1	1430
$a_0(1450)$	3	1	1	1	1450
$\rho(1450)$	3	3	1	1	1450
$\eta(1475)$	1	1	1	1	1475
$f_0(1500)$	1	1	1	1	1500
$f_1(1510)$	1	3	1	1	1510
$f'_1(1525)$	1	3	1	1	1525
$f_2(1565)$	1	5	1	1	1565
$\rho(1570)$	3	3	1	1	1570
$h_1(1595)$	1	3	1	1	1595
$\pi_1(1600)$	3	3	1	1	1600
$a_1(1640)$	3	3	1	1	1640
$f_2(1640)$	1	5	1	1	1640
$\eta_2(1645)$	1	5	1	1	1645
$\omega(1650)$	1	3	1	1	1650
$\omega_3(1670)$	1	7	1	1	1670
$\pi_2(1670)$	3	5	1	1	1670
$\phi(1680)$	1	3	1	1	1680
$\rho_3(1690)$	3	7	1	1	1690
$\rho(1700)$	3	3	1	1	1700
$a_2(1700)$	3	5	1	1	1700
$f_0(1710)$	1	1	1	1	1710
$\eta(1760)$	1	1	1	1	1760
$\pi(1800)$	3	1	1	1	1800
$f_2(1810)$	1	5	1	1	1800
$\phi_3(1850)$	1	7	1	1	1850
$\eta_2(1870)$	1	5	1	1	1870
$\pi_2(1880)$	3	5	1	1	1880
$\rho(1900)$	3	1	1	1	1900
$f_2(1910)$	1	5	1	1	1910
$f_2(1950)$	1	5	1	1	1950
$\rho_3(1990)$	3	7	1	1	1990
$f_2(2010)$	1	5	1	1	2010
$f_0(2020)$	1	1	1	1	2020
$a_4(2040)$	3	9	1	1	2040
$f_4(2050)$	1	9	1	1	2050
$\pi_2(2100)$	3	5	1	1	2100
$f_0(2100)$	1	1	1	1	2100
$f_2(2150)$	1	5	1	1	2150
$\rho(2150)$	3	3	1	1	2150
$\phi(2170)$	1	3	1	1	2170
$f_0(2200)$	1	1	1	1	2200
$f_1(2220)$	1	9	1	1	2220 ^b
$\eta(2225)$	1	1	1	1	2225
$\rho_3(2250)$	3	7	1	1	2250
$f_2(2300)$	1	5	1	1	2300
$f_4(2300)$	1	9	1	1	2300
$f_0(2330)$	1	1	1	1	2330
$f_2(2340)$	1	5	1	1	2340
$\rho_5(2350)$	3	11	1	1	2350
$a_6(2450)$	3	13	1	1	2450
$f_6(2510)$	1	13	1	1	2510
Excited Unflavoured Mesons					g = 499

^b We have used the $(J^{PC}) = (4^{++})$ for f_j .

Table C4. Excited strange mesons.

Symbol	Flavours	Spin States	Color States	Bose or Fermi	Mass
K ₁ (1270)	2	3	1	1	1270
K ₁ (1400)	2	3	1	1	1400
K [*] (1410)	2	3	1	1	1410
K ₀ [*] (1430)	2	1	1	1	1430
K ₂ [*] (1430)	2	5	1	1	1430
K ₂ [*] (1430)	2	5	1	1	1430
K(1460)	2	1	1	1	1460
K ₂ (1580)	2	5	1	1	1580
K ₁ (1650)	2	3	1	1	1650
K [*] (1680)	2	3	1	1	1680
K ₂ (1770)	2	5	1	1	1770
K ₃ [*] (1780)	2	7	1	1	1780
K ₂ (1820)	2	5	1	1	1820
K(1830)	2	1	1	1	1830
K ₀ [*] (1950)	2	1	1	1	1950
K ₂ [*] (1980)	2	5	1	1	1980
K ₄ [*] (2045)	2	9	1	1	2045
K ₂ (2250)	2	5	1	1	2250
K ₃ (2320)	2	7	1	1	2320
K ₅ [*] (2380)	2	11	1	1	2380
K ₄ (2500)	2	9	1	1	2500
Excited Strange Mesons					g = 194

Appendix D. List of Baryons and Their Degeneracy**Table D1.** Spin ½ baryons.

Symbol	Flavours	Spin States	Color States	Bose or Fermi	Mass
p	2	2	1	7/8	938.272
n	2	2	1	7/8	939.565
Λ ⁰	2	2	1	7/8	1115.683
Σ ⁺	2	2	1	7/8	1189.37
Σ ⁰	2	2	1	7/8	1192.642
Σ ⁻	2	2	1	7/8	1197.449
Ξ ⁰	2	2	1	7/8	1314.86
Ξ ⁻	2	2	1	7/8	1321.71
Λ _c ⁺	2	2	1	7/8	2186.46
Σ _c ⁺	2	2	1	7/8	2452.9
Σ _c ⁰	2	2	1	7/8	2453.74
Σ _c ⁺⁺	2	2	1	7/8	2453.98
Ξ _c ⁺	2	2	1	7/8	2467.8
Ξ _c ⁰	2	2	1	7/8	2470.88
Ξ _c ⁺	2	2	1	7/8	2575.6
Ξ _c ⁰	2	2	1	7/8	2577.9
Ω _c ⁰	2	2	1	7/8	2695.2
Ξ _{cc} ⁺	2	2	1	7/8	3518.9
Λ _b ⁰	2	2	1	7/8	5619.4
Ξ _b ⁰	2	2	1	7/8	5787.8
Ξ _b ⁻	2	2	1	7/8	5791.1
Σ _b ⁺	2	2	1	7/8	5811.3
Σ _b ⁻	2	2	1	7/8	5815.5
Ω _b ⁻	2	2	1	7/8	6071
Spin ½ Baryons					g = 84

Table D2. Spin $\frac{1}{2}$ baryons.

Symbol	Flavours	Spin States	Color States	Bose or Fermi	Mass
Δ^{++}	2	4	1	$\frac{7}{8}$	1232
Δ^+	2	4	1	$\frac{7}{8}$	1232
Δ^0	2	4	1	$\frac{7}{8}$	1232
Δ^-	2	4	1	$\frac{7}{8}$	1232
Σ^{*+}	2	4	1	$\frac{7}{8}$	1382.8
Σ^{*0}	2	4	1	$\frac{7}{8}$	1383.7
Σ^{*-}	2	4	1	$\frac{7}{8}$	1387.2
Ξ^{*0}	2	4	1	$\frac{7}{8}$	1531.80
Ξ^{*-}	2	4	1	$\frac{7}{8}$	1535.0
Ω^-	2	4	1	$\frac{7}{8}$	1672.45
Σ_c^{*+}	2	4	1	$\frac{7}{8}$	2517.5
Σ_c^{*++}	2	4	1	$\frac{7}{8}$	2517.9
Σ_c^{*0}	2	4	1	$\frac{7}{8}$	2518.8
Ξ_c^{*+}	2	4	1	$\frac{7}{8}$	2645.9
Ξ_c^{*0}	2	4	1	$\frac{7}{8}$	2645.9
Ω_c^{*0}	2	4	1	$\frac{7}{8}$	2765.9
Σ_b^{*+}	2	4	1	$\frac{7}{8}$	5832.1
Σ_b^{*-}	2	4	1	$\frac{7}{8}$	5835.1
Ξ_b^{*-}	2	4	1	$\frac{7}{8}$	5945.5
Spin $\frac{1}{2}$ Baryons					g = 133

Table D3. Excited N baryons.

Symbol	Flavours	Spin States	Color States	Bose or Fermi	Mass
N(1440)	2	2	1	$\frac{7}{8}$	1440
N(1520)	2	4	1	$\frac{7}{8}$	1520
N(1535)	2	2	1	$\frac{7}{8}$	1535
N(1650)	2	2	1	$\frac{7}{8}$	1650
N(1675)	2	6	1	$\frac{7}{8}$	1675
N(1680)	2	6	1	$\frac{7}{8}$	1680
N(1700)	2	4	1	$\frac{7}{8}$	1700
N(1710)	2	2	1	$\frac{7}{8}$	1710
N(1720)	2	4	1	$\frac{7}{8}$	1720
N(1860)	2	6	1	$\frac{7}{8}$	1860
N(1875)	2	4	1	$\frac{7}{8}$	1875
N(1880)	2	2	1	$\frac{7}{8}$	1880
N(1895)	2	2	1	$\frac{7}{8}$	1895
N(1900)	2	4	1	$\frac{7}{8}$	1900
N(1990)	2	8	1	$\frac{7}{8}$	1990
N(2000)	2	6	1	$\frac{7}{8}$	2000
N(2040)	2	4	1	$\frac{7}{8}$	2040
N(2060)	2	6	1	$\frac{7}{8}$	2060
N(2100)	2	2	1	$\frac{7}{8}$	2100
N(2120)	2	4	1	$\frac{7}{8}$	2120
N(2190)	2	8	1	$\frac{7}{8}$	2190
N(2220)	2	10	1	$\frac{7}{8}$	2220
N(2250)	2	10	1	$\frac{7}{8}$	2250
N(2300)	2	2	1	$\frac{7}{8}$	2300
N(2570)	2	6	1	$\frac{7}{8}$	2570
N(2600)	2	12	1	$\frac{7}{8}$	2600
N(2700)	2	14	1	$\frac{7}{8}$	2700
Excited N Baryons					g = 248.5

Table D4. Excited Δ Baryons.

Symbol	Flavours	Spin States	Color States	Bose or Fermi	Mass
$\Delta(1600)$	2	4	1	$\frac{7}{8}$	1600
$\Delta(1620)$	2	2	1	$\frac{7}{8}$	1620
$\Delta(1700)$	2	4	1	$\frac{7}{8}$	1700
$\Delta(1750)$	2	2	1	$\frac{7}{8}$	1750
$\Delta(1900)$	2	2	1	$\frac{7}{8}$	1900
$\Delta(1905)$	2	6	1	$\frac{7}{8}$	1905
$\Delta(1910)$	2	2	1	$\frac{7}{8}$	1910
$\Delta(1920)$	2	4	1	$\frac{7}{8}$	1920
$\Delta(1930)$	2	6	1	$\frac{7}{8}$	1930
$\Delta(1940)$	2	4	1	$\frac{7}{8}$	1940
$\Delta(1950)$	2	8	1	$\frac{7}{8}$	1950
$\Delta(2000)$	2	6	1	$\frac{7}{8}$	2000
$\Delta(2150)$	2	2	1	$\frac{7}{8}$	2150
$\Delta(2200)$	2	8	1	$\frac{7}{8}$	2200
$\Delta(2300)$	2	10	1	$\frac{7}{8}$	2300
$\Delta(2350)$	2	6	1	$\frac{7}{8}$	2350
$\Delta(2390)$	2	8	1	$\frac{7}{8}$	2390
$\Delta(2400)$	2	10	1	$\frac{7}{8}$	2400
$\Delta(2420)$	2	12	1	$\frac{7}{8}$	2420
$\Delta(2750)$	2	14	1	$\frac{7}{8}$	2750
$\Delta(2950)$	2	16	1	$\frac{7}{8}$	2950
Excited Δ Baryons					g = 238

Table D5. Excited Λ baryons.

Symbol	Flavours	Spin States	Color States	Bose or Fermi	Mass
$\Lambda(1405)$	2	2	1	$\frac{7}{8}$	1405
$\Lambda(1520)$	2	4	1	$\frac{7}{8}$	1520
$\Lambda(1600)$	2	2	1	$\frac{7}{8}$	1600
$\Lambda(1670)$	2	2	1	$\frac{7}{8}$	1670
$\Lambda(1690)$	2	4	1	$\frac{7}{8}$	1690
$\Lambda(1710)$	2	2	1	$\frac{7}{8}$	1710
$\Lambda(1800)$	2	2	1	$\frac{7}{8}$	1800
$\Lambda(1810)$	2	2	1	$\frac{7}{8}$	1810
$\Lambda(1820)$	2	6	1	$\frac{7}{8}$	1820
$\Lambda(1830)$	2	6	1	$\frac{7}{8}$	1830
$\Lambda(1890)$	2	4	1	$\frac{7}{8}$	1890
$\Lambda(2020)$	2	8	1	$\frac{7}{8}$	2020
$\Lambda(2050)$	2	4	1	$\frac{7}{8}$	2050
$\Lambda(2100)$	2	8	1	$\frac{7}{8}$	2100
$\Lambda(2110)$	2	6	1	$\frac{7}{8}$	2110
$\Lambda(2325)$	2	4	1	$\frac{7}{8}$	2325
$\Lambda(2350)$	2	10	1	$\frac{7}{8}$	2350
Excited Λ Baryons					g = 133

Table D6. Excited Σ baryons.

Symbol	Flavours	Spin States	Color States	Bose or Fermi	Mass
$\Sigma(1580)$	2	4	1	$\frac{7}{8}$	1580
$\Sigma(1620)$	2	2	1	$\frac{7}{8}$	1620
$\Sigma(1660)$	2	2	1	$\frac{7}{8}$	1660
$\Sigma(1670)$	2	4	1	$\frac{7}{8}$	1670
$\Sigma(1730)$	2	4	1	$\frac{7}{8}$	1730
$\Sigma(1750)$	2	2	1	$\frac{7}{8}$	1750
$\Sigma(1770)$	2	2	1	$\frac{7}{8}$	1770
$\Sigma(1775)$	2	6	1	$\frac{7}{8}$	1775
$\Sigma(1840)$	2	4	1	$\frac{7}{8}$	1840
$\Sigma(1880)$	2	2	1	$\frac{7}{8}$	1880
$\Sigma(1900)$	2	2	1	$\frac{7}{8}$	1900
$\Sigma(1915)$	2	6	1	$\frac{7}{8}$	1915
$\Sigma(1940^+)$	2	4	1	$\frac{7}{8}$	1940
$\Sigma(1940^-)$	2	4	1	$\frac{7}{8}$	1940
$\Sigma(2000)$	2	2	1	$\frac{7}{8}$	2000
$\Sigma(2030)$	2	8	1	$\frac{7}{8}$	2030
$\Sigma(2070)$	2	6	1	$\frac{7}{8}$	2070
$\Sigma(2080)$	2	4	1	$\frac{7}{8}$	2080
$\Sigma(2100)$	2	8	1	$\frac{7}{8}$	2100
Excited Σ Baryons					g = 133

Table D7. Excited Ξ baryons.

Symbol	Flavours	Spin States	Color States	Bose or Fermi	Mass
$\Xi(1820)$	2	4	1	$\frac{7}{8}$	1820
$\Xi(2030)$	2	6	1	$\frac{7}{8}$	2030
Excited Ξ Baryons					g = 17.5

References

1. Penzias, A.A.; Wilson, R.W. A Measurement of Excess Antenna Temperature at 4080 Mc/s. *Astrophys. J.* **1965**, *142*, 419–421.
2. Ade, P.A.R.; Aghanim, N.; Arnaud, M.; Ashdown, M.; Aumont, J.; Baccigalupi, C.; Banday, A.J.; Barreiro, R.B.; Bartlett, J.G.; Bartolo, N.; et al. Planck 2015 Results. XIII. Cosmological Parameters. *Astron. Astrophys.* **2016**, *594*, A13.
3. Trodden, M.; Carroll, S.M. TASI lectures: Introduction to cosmology. In Proceedings of the Progress in String Theory, Summer School, TASI 2003, Boulder, CO, USA, 2–27 June 2003; pp. 703–793.
4. Baumann, D. Cosmology Lectures. Available online: www.damtp.cam.ac.uk/user/db275/Cosmology.pdf (accessed on 15 December 2016).
5. Kurki-Suonio, H. Cosmology I Lectures. Available online: <http://www.helsinki.fi/~hkurkisu/> (accessed on 15 December 2016).
6. Weinberg, S. *Cosmology*; Oxford University Press: Oxford, UK, 2008.
7. Weinberg, S. *Gravitation and Cosmology*; John Wiley & Sons: New York, NY, USA, 1972.
8. Kolb, E.W.; Turner, M.S. *The Early Universe*; Westview Press: Boulder, CO, USA, 1990.
9. Dodelson, S. *Modern Cosmology*; Academic Press: San Diego, CA, USA, 2003.
10. Ryden, B. *Introduction to Cosmology*; Addison-Wesley: San Francisco, CA, USA, 2003.
11. Lesgourgues, J.; Mangano, G.; Miele, G.; Pastor, S. *Neutrino Cosmology*; Cambridge University Press: Cambridge, UK, 2013.
12. Husdal, L. Viscosity in a Lepton-Photon Universe. *Astrophys. Space Sci.* **2016**, doi:10.1007/s10509-016-2847-4.
13. Hoogeveen, F.; Leeuwen, W.V.; Salvati, G.; Schilling, E. Viscous phenomena in cosmology: I. Lepton era. *Phys. A Stat. Mech. Appl.* **1986**, *134*, 458–473.

14. Caderni, N.; Fabbri, R. Viscous Phenomena and Entropy Production in the Early Universe. *Phys. Lett. B* **1977**, *69*, 508–511.
15. Aad, G.; Abajyan, T.; Abbott, B.; Abdallah, J.; Khalek, S.A.; Abdelalim, A.A.; Abidinov, O.; Aben, R.; Abi, B.; Abolins, M.; et al. Observation of a new particle in the search for the Standard Model Higgs boson with the ATLAS detector at the LHC. *Phys. Lett. B* **2012**, *716*, 1–29.
16. Chatrchyan, S.; Khachatryan, V.; Sirunyan, A.M.; Tumasyan, A.; Adam, W.; Aguilo, E.; Bergauer, T.; Dragicevic, M.; Erö, J.; Fabjan, C.; et al. Observation of a new boson at a mass of 125 GeV with the CMS experiment at the LHC. *Phys. Lett. B* **2012**, *716*, 30–61.
17. Lesgourgues, J.; Pastor, S. Neutrino mass from Cosmology. *Adv. High Energy Phys.* **2012**, *2012*, 608515.
18. Bennett, C.L.; Larson, D.; Weiland, J.L.; Jarosik, N.; Hinshaw, G.; Odegard, N.; Smith, K.M.; Hill, R.S.; Gold, B.; Halpern, M.; et al. Nine-Year Wilkinson Microwave Anisotropy Probe (WMAP) Observations: Final Maps and Results. *Astrophys. J. Suppl.* **2013**, *208*, 20.
19. Olive, K.A.; Particle Data Group. Review of Particle Physics. *Chin. Phys. C* **2014**, *38*, 090001.
20. Lesgourgues, J.; Pastor, S. Cosmological implications of a relic neutrino asymmetry. *Phys. Rev. D* **1999**, *60*, 103521.
21. Mangano, G.; Miele, G.; Pastor, S.; Pisanti, O.; Sarikas, S. Constraining the cosmic radiation density due to lepton number with Big Bang Nucleosynthesis. *J. Cosmol. Astropart. Phys.* **2011**, *2011*, 035.
22. Petreczky, P. Lattice QCD at non-zero temperature. *J. Phys. G* **2012**, *39*, 093002.
23. Kapusta, J.; Muller, B.; Rafelski, J. *Quark Gluon Plasma: Theoretical Foundations: An Annotated Reprint Collection*; Elsevier: Amsterdam, The Netherlands, 2003.
24. Griffiths, D.J. *Introduction to Elementary Particles*, 2nd ed.; Wiley: New York, NY, USA, 2008.
25. Beringer, J.E.A. Review of Particle Physics. *Phys. Rev. D* **2012**, *86*, 010001.
26. Mangano, G.; Miele, G.; Pastor, S.; Pinto, T.; Pisanti, O.; Serpico, P.D. Relic neutrino decoupling including flavor oscillations. *Nucl. Phys.* **2005**, *B729*, 221–234.
27. De Salas, P.F.; Pastor, S. Relic neutrino decoupling with flavour oscillations revisited. *J. Cosmol. Astropart. Phys.* **2016**, *2016*, 051.
28. Fixsen, D.J. The Temperature of the Cosmic Microwave Background. *Astrophys. J.* **2009**, *707*, 916–920.
29. Liddle, A.R. *An Introduction to Modern Cosmology*; Wiley: Chichester, UK, 2003.
30. Rahvar, S. Cooling in the universe. *arXiv* **2006**, arXiv:physics/0603087.



© 2016 by the author; licensee MDPI, Basel, Switzerland. This article is an open access article distributed under the terms and conditions of the Creative Commons Attribution (CC-BY) license (<http://creativecommons.org/licenses/by/4.0/>).

Paper II

Viscosity in a Lepton-Photon Universe

Astrophysics and Space Science **361** (2016) no. 8

Viscosity in a lepton-photon universe

Lars Husdal¹ 

Received: 23 May 2016 / Accepted: 27 June 2016
© Springer Science+Business Media Dordrecht 2016

Abstract We look at viscosity production in a universe consisting purely of leptons and photons. This is quite close to what the universe actually look like when the temperature was between 10^{10} K and 10^{12} K (1–100 MeV). By taking the strong force and the hadronic particles out of the equation, we can examine how the viscous forces behave with all the 12 leptons present. By this we study how shear- and (more interestingly) bulk viscosity is affected during periods with particle annihilation. We use the theory given by Hoogeveen et al. from 1986, replicate their 9-particle results and expanded it to include the muon and tau particles as well. This will impact the bulk viscosity immensely for high temperatures. We will show that during the beginning of the lepton era, when the temperature is around 100 MeV, the bulk viscosity will be roughly 100 million times larger with muons included in the model compared to a model without.

Keywords Viscous cosmology · Shear viscosity · Bulk viscosity · Lepton era · Relativistic kinetic theory

1 Introduction

Viscosity, the resistance to gradual deformation, is a well-described phenomenon in classical fluid dynamics. Shear (or dynamic) viscosity is the resistance to shearing flows, and occurs when adjacent layers of a fluid, which are parallel to each other, move at different velocities, or have different temperatures. Bulk (or volume) viscosity is the internal resistance for a fluid to evenly expand (or compress). Both

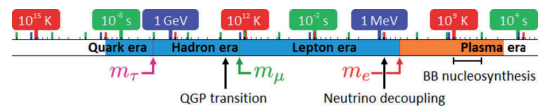


Fig. 1 The temperature (in kelvin and MeV), and time scales used in our paper

types of viscosity played an important role in the early universe. See Fig. 1.

Several papers about viscous cosmology have been published over the years (Hoogeveen et al. 1986a; Treciokas and Ellis 1971; Grøn 1990; Brevik 2015). Most of them have looked upon it from a phenomenological point of view.

But what does this all mean in a cosmological framework? Or more specifically during the lepton era? At this time the universe consisted of photons, charged leptons and neutrinos—more or less acting as ideal (relativistic and non-relativistic) gases. The early universe was also very close to being in local (and global) thermal equilibrium, it was almost completely isotropic.

Let us give a simple qualitative description of how the two previously mentioned types of viscosities acted in this era: Any stress forces driving the system towards anisotropy is countered and resisted by viscous forces. In the first case we have shear stress due to regional differences in flow or temperature. The way shear viscosity drives the system back towards equilibrium is through momentum transfer between the regions. See Fig. 2. This is proportional to the mean free path of the momentum-carrying particles. Because the weak nuclear force is so much weaker than the electromagnetic force at this time, the mean free path of neutrinos are much larger than those of the electromagnetic interacting particles. Practically, all the action of shear viscosity is due the interactions between neutrinos and other particles.

✉ L. Husdal
lars.husdal@ntnu.no

¹ Department of Physics, Norwegian University of Science and Technology, Trondheim, Norway

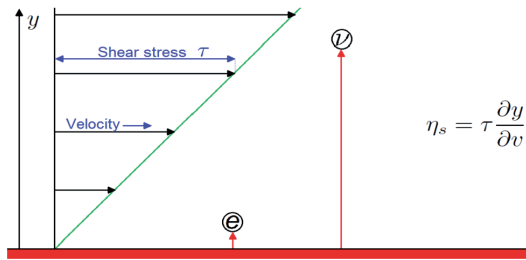


Fig. 2 A simple illustration of shear viscosity. The weakly interaction neutrinos have a much longer mean free path than the electromagnetic interacting particles (e.g. like electrons). They will thus travel much farther in the perpendicular direction (y) of the flow

Bulk viscosity arises due to the fact that non-relativistic and relativistic gases behave adiabatically differently. During expansion, relativistic gases drop in temperature as a^{-1} , while non-relativistic gases drop as a^{-2} (where a is the scale factor). The system as a whole will try to bring these two components into equilibrium by heat transfer. Also here the main component of the momentum transfer is due to the neutrinos, but is a bit more complicated. As the temperature of the universe cools, and some particles transition towards non-relativistic velocities they will start to drop in temperature according to the aforementioned a^{-2} . They will be heated up by all the relativistic particles (which themselves will be cooled down). The electromagnetic interacting particles will never have time to gain any real temperature difference and they collectively will cool down a bit faster. The neutrinos on the other hand, because of their weakly interacting nature, have a longer mean life time resulting in a larger temperature difference before they interact. This will lead to a larger momentum transfer and a resulting larger viscous effect. In this way the photons play an indirect role as they help heat up the non-relativistic particles such that the temperature difference between them and the neutrinos are smaller than it would be the case in a no-photon case. See Fig. 3. From the same argument it follows that compared to the neutrinos, the muons should drop faster in temperature than the tau-leptons, and the electrons even faster. We will later see that bulk viscosity also has another impact as it is associated with a pressure.

Being interested in the underlying physics, we looked at some earlier papers with a focus on the origins for shear and bulk viscosity, including Misner (1967, 1968, 1969), Caderni and Fabbri (1977), van Erkelens and van Leeuwen (1978), van Leeuwen et al. (1986) and Hoogeveen et al. (1986a) with a special focus on the latter (“Viscous Phenomena in Cosmology. I. Lepton Era”). We used their model, reproduced their result and took a closer look at the transition temperatures towards the colder plasma era and the warmer hadron and quark eras. We were interested in the evolution of the two viscosity coefficients.

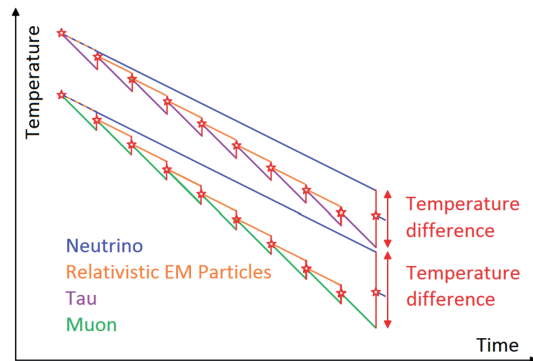


Fig. 3 A simplified illustrating of bulk viscosity. The electromagnetic interacting particles (γ, e, μ, τ) all have a short mean life time, resulting in a small momentum transfer. The longer lived neutrinos provide a much larger momentum transfer since the temperature difference is bigger. The heavier leptons (here illustrated by the purple τ and $\bar{\tau}$ particles) cool down slower compared to the a lighter lepton (here illustrated by the green μ and $\bar{\mu}$ particles), since they are heated up by more relativistic particles

The main purpose with this work is to study the impact of including all three lepton generations. As these will annihilate at different times, we can study the build-up and fall-down of the two viscosity coefficients. We will also look at some aspects where this model comes short.

2 Setup and constraints

2.1 Definition of lepton era

The lepton era (or epoch) follows not long after the end of the phase transition from quark gluon plasma to hot hadron gas at roughly 170 MeV (1.9×10^{12} K) (Kapusta et al. 2003). At this time, the free quarks and gluons bound together to form mesons and baryons. Because the temperature is too low for most pair productions, the more massive baryons quickly die out, and soon only the lightest mesons—the pions, have a significant contribution to the particle-mix. Already at the time of this phase transition, the number of leptons (e, μ, τ, ν) equals that of the hadrons, and the energy density is soon after (~ 140 MeV) dominated by the leptons. The rounded down temperature of 100 MeV is a good definition for the start of the lepton era. From here on the universe is mainly filled with electrons, positrons, the 6 neutrinos, and the photons. At around 1 MeV (10^{10} K), two coinciding events take place: the neutrinos decouple from matter, and soon after the temperature drops below the threshold for e^-e^+ production, so they will start to annihilate. As the last positrons die out we enter the plasma era, where the universe is filled with a hot plasma of photons and the residual matter consisting of nuclei and electrons.

2.2 Constraints in our model

For our model we use theories which is constrained to the lepton era. Hence its validity drops as we cross over from both sides: going to higher temperatures leading into the hadron era, and dropping to lower temperatures leading into the plasma era. Expanding out of the (more) valid lepton-era can still show us some interesting physics worth exploring. We use the following constraints/simplifications in our model:

A hadron-less universe: At temperatures of 100 MeV (10^{12} K) the hadronic content of the universe is mainly pions ($m_{\pi^0} = 135.0$ MeV/ c^2 , $m_{\pi^\pm} = 139.6$ MeV/ c^2) and only to a smaller extent other heavier hadrons, like kaons, protons and neutrons. Going above the phase transition at $T \approx 170$ MeV there will be a quark-gluon plasma with all its implications. This requires taking QCD theory into account. For simplicity we disregard all quarks, gluons, and hadrons. This will give a better understanding of the consequences by adding a single particle pair to our model.

Matter-antimatter neutral universe: Data from WMAP (Bennett et al. 2012) suggest a baryon-to-photon ratio of $(6.079 \pm 0.090) \times 10^{-10}$, which roughly corresponds to the matter over antimatter difference. This hardly plays any role when the universe is still hot enough to produce particle pairs, but this asymmetry have to be taken into consideration as we enter the plasma era, when all antimatter is annihilated, and we are left with the residual matter.

No neutrino decoupling: Neutrinos have a very long mean free path, which makes them the primary source for momentum transfer. Being the main contributor to both shear and bulk viscosity, an accurate model of the neutrino density is important. As the rate of the (weak) neutrino interactions becomes slower than the rate of expansion of the universe the neutrinos will decouple. This happens at $\Gamma_\nu/H \approx [G_\nu^2/(\hbar c)^6]\sqrt{\hbar c/G}(k_B T)^3 \simeq (T/10^{10} \text{ K})^3$ (see Sect. 3.4). We have neglected the neutrinos in our calculations, but marked the decoupling temperature in our figures.

No electromagnetic contribution: Particle interaction in the lepton era is dominated by the weak and electromagnetic forces. Viscous effects are related to momentum transfer. The long mean free path of the neutrinos ensures that its momentum transfer is several orders of magnitude larger to those of electromagnetic origin during this era. Electromagnetic interactions do however play a role at low temperatures after the neutrinos decouples (plasma era) and at high temperatures when the weak and electromagnetic forces are closer in strength (electroweak scale). This argument should be valid at temperatures beneath 10^{13} K, but become more questionable as we get towards 10^{14} K (Hoogeveen et al. 1986b).

No reheating from annihilations: The decay of heavier particles to lighter particles result in a temperature increase, as the rest masses are converted to kinetic energy. Any out-of-equilibrium effects of this origin has not been considered in this paper.

Elastic collisions and no chemical potential: As is done in earlier writings, we only use elastic collisions in our calculations. The cross-section of inelastic collisions is of comparable sizes, so this approximation should not affect the results considerably (Hoogeveen et al. 1986a). The chemical potentials of all particles is set to zero.

3 Viscous theory

Two factors which play a role in viscosity are, first the state of the system—which for our case is the particle composition of the system, and secondly the transport equation for the system. We use the theory as described by Hoogeveen et al. (1986a). The core theory and equations for shear (η_s) and bulk (η_v) viscosities are given below, and a more thorough description of the linear equations is described in Appendix A. First of, the shear and bulk viscosities are found using the Chapman-Enskog approximation (van Erkelens and van Leeuwen 1978; Groot et al. 1980):

$$\eta_s = \frac{1}{10}cn \left(\frac{k_B T}{c}\right)^3 \sum_k c_k \gamma_k, \tag{1}$$

$$\eta_v = nk_B T \sum_k a_k \alpha_k, \tag{2}$$

where c is the speed of light, n is total particle density, k_B is Boltzmann’s constant, and T is temperature. The coefficients c_k and a_k originate from the linearized relativistic Boltzmann equations. These transport equations describe the energy-momentum transfer, essentially the “force” trying to drive the system back to equilibrium. The two sets of linear equations are given in Appendix A for particle k . $\gamma_k(n_k, T)$ and $\alpha_k(n_k, T)$ are functions of the particle densities and temperature and describe the state of the system. For the shear viscosity case this is a product of the particle composition (fraction) and enthalpy of the system, while for the bulk case it is a more complex function of these. The two functions are given by:

$$\gamma_k = 10x_k \hat{h}_k, \tag{3}$$

$$\alpha_k = -x_k [\gamma - (\gamma - 1)(z_k^2 + 5\hat{h}_k - \hat{h}_k^2)], \tag{4}$$

where x_k , z_k and \hat{h}_k are partial fraction, inverse dimensionless temperature and dimensionless partial specific enthalpy respectively, and are defined as:

$$x_k \equiv \frac{n_k}{n}, \tag{5a}$$

$$z_k \equiv \frac{m_k c^2}{k_B T}, \tag{5b}$$

$$\hat{h}_k \equiv z_k \frac{K_3(z_k)}{K_2(z_k)}. \tag{5c}$$

Here K_3 and K_2 are the modified Bessel functions of the second kind. $(z_k^2 + 5\hat{h}_k - \hat{h}_k^2)$ is actually the specific heat capacity per particle for constant pressure, \hat{c}_P . The γ in Eq. (4) is the heat capacity ratio (also known as the adiabatic index) and is given by¹

$$\frac{\gamma}{\gamma - 1} = \sum_{k=1}^N x_k (z_k^2 + 5\hat{h}_k - \hat{h}_k^2). \tag{6}$$

For low temperatures the heat capacity ratio should coincide with the classical value for a non-relativistic gas and approach 5/3. For massless particles, the average kinetic energy per particle is $3k_B T$, the enthalpy per particle is $4k_B T$, such that γ should approach 4/3 in the relativistic limit. We look closer at $\hat{c}_P = (z^2 + 5\hat{h} - \hat{h}^2)$ and α_k and their properties in Fig. 6. The partial fractions x_k , depends solely on the particle densities.

3.1 Particle densities

The particle density for a particle k is given by Andersen (2012), Hoogeveen et al. (1986a) as

$$n_k(T) = \frac{g_k}{2\pi^2(\hbar)^3} \int_{m_k c^2}^{\infty} \frac{E \sqrt{E^2 - m_k^2 c^4}}{e^{E/k_B T} - \delta_k} dE, \tag{7a}$$

where g is the number of possible spin states for particle k and δ is +1 for bosons and -1 for fermions, which gives us the expressions for the 13 different particles:

$$n_{e^\pm, \mu^\pm, \tau^\pm}(T) = \frac{1}{\pi^2} \left(\frac{k_B T}{\hbar c}\right)^3 \int_{z_k}^{\infty} \frac{u \sqrt{u^2 - z_k^2}}{e^u + 1} du, \tag{7b}$$

$$n_\gamma(T) = \frac{1}{\pi^2} \left(\frac{k_B T}{\hbar c}\right)^3 2\zeta(3), \tag{7c}$$

$$n_{\nu_e, \bar{\nu}_e, \nu_\mu, \bar{\nu}_\mu, \nu_\tau, \bar{\nu}_\tau}(T) = \frac{1}{\pi^2} \left(\frac{k_B T}{\hbar c}\right)^3 \frac{3}{4}\zeta(3), \tag{7d}$$

where $\zeta(3) \approx 1.202$ is the Riemann zeta function and u (just as z) is a dimensionless inverse temperatures defined by

$$u \equiv \frac{E}{k_B T}. \tag{8}$$

¹From Groot et al. (1980) we have $\gamma = c_P/c_V = (\frac{\partial h}{\partial T})_P / (\frac{\partial e_k}{\partial T})_V$, where $e_k = mc^2 \frac{K_1(z)}{K_2(z)} + 3k_B T = mc^2 \frac{K_3(z)}{K_2(z)} - k_B T$ and $h = e_k + \frac{P}{n} = mc^2 \frac{K_3(z)}{K_2(z)}$.

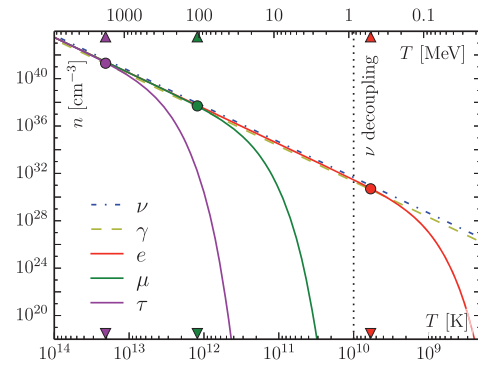


Fig. 4 Particle densities n_k as functions of temperature. Similar particles (i.e. 1 photon, 6 neutrinos, 2 electrons, 2 muons and 2 taus) are added together. Rest mass of particles are marked by triangles and circles

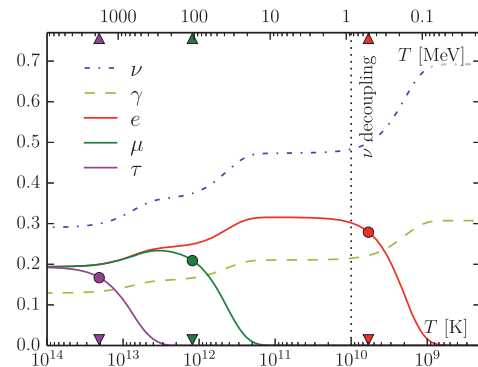


Fig. 5 Particle fractions x_k as functions of temperature

Using dimensionless numbers in Eq. (7a), the integrals themselves will vary from 0 (low temperature) to $3\zeta(3)/2$ for fermions and $2\zeta(3)$ for bosons at high temperatures. The numerical solutions for the particles densities are given in Fig. 4, and that for the particle fractions in Fig. 5. It is worth noting how late the pair production of massive particles is maintained. Their contribution is significant at temperatures well below the pair production energy threshold of $2m_k$.

3.2 Bulk viscosity and its terms

Let us revisit the concept of bulk viscosity by giving a few examples. During expansion relativistic and a non-relativistic gases drop differently in temperature. For relativistic gases we have $T \propto a^{-1}$, while the case for non-relativistic gases is $T \propto a^{-2}$. Since non-relativistic gases drop quicker in temperature we will have heat transfer from the warmer relativistic gas to the colder non-relativistic gas in order to regain a thermal equilibrium in the mixture. Bulk

viscosity increases with the temperature difference. Neutrinos have a long mean free path, resulting in a longer mean life time than the charged leptons and the photon which interact much stronger, and hence the neutrinos are the primary contributor to the bulk viscous term.

As mentioned earlier, the α_k coefficients tells us about the state of the system, more specifically it tells us about the ratio of particles which want to drop faster (non-relativistic particles) in temperature to those who want to drop slower (relativistic particles). Particles, or the particle specie as a whole to be more specific, with a positive α_k are above the equilibrium temperature, and the other way around for particles with a negative α_k , and the sum of all α_k 's is zero. Since massive particles gradually change from behaving (ultra-)relativistic, to non-relativistic, and finally annihilation, the “sweet spot” should therefor be somewhere in between. Looking at Fig. 6(c) we see this peak in α when the ratio of non-relativistic (nr) to relativistic particles (r) is $\sqrt{2} : 1$. For $n_r \gg n_{nr}$ we have $\alpha \propto n_r/n_{nr}$, and will decrease in the same manner for $n_r \ll n_{nr}$. For ratios of 1 : 1 and 2 : 1 α will be 1/6, while the peak at $\sqrt{2} : 1$ will be just slightly larger.

In Fig. 6(d) we have shown a case with one massive and one massless particle with no particle decay (such that each particle number stays constant). At high temperature most of the massive particles move at relativistic velocities, and the mixture expands with negligible bulk viscosity. As the temperature drops, a bigger and bigger portion of the massive particles will behave more non-relativistic, and α will grow as T^{-2} until we reach a temperature roughly equal that of the particle mass. The growth in α will slow down and converge towards 1/6 as the ratio of relativistic to non-relativistic particles goes towards 1 : 1.

The complete functions of γ_k and α_k are plotted in Fig. 7.

3.3 Viscous pressure

For a system in thermodynamic equilibrium, the energy density² ϵ and pressure P is found by adding together the individual pressures from all particle types k :

$$\epsilon(T) = \sum_k \frac{g_k}{2\pi^2 \hbar^3} \int_{m_k c^2}^{\infty} \frac{E^2 \sqrt{E^2 - m_k^2 c^4}}{e^{E/k_B T} \pm 1} dE, \tag{9}$$

$$P(T) = \sum_k \frac{g_k}{6\pi^2 \hbar^3} \int_{m_k c^2}^{\infty} \frac{(E^2 - m_k^2 c^4)^{3/2}}{e^{E/k_B T} \pm 1} dE. \tag{10}$$

Equation (10) is normally written in a simplified version as

$$P(T) = g_{*p}(T) \frac{\pi^2 (k_B T)^4}{90 (\hbar c)^3} \equiv P_{TE}. \tag{11}$$

²As not to be confused with the mass density $\rho = \epsilon/c^2$.

where $g_{*p}(T)$ is the relativistic degrees of freedom for pressure (compared to that of the photon). For periods where the particle fractions stay constant the degrees of freedom stay constant as well (for example just before neutrino decoupling $g_{*p} = 10.75$). The evolution of g_{*p} for all particles in the standard model is plotted in the upper right corner of Fig. 10. We will define this thermodynamic equilibrium pressure for P_{TE} , making the temperature dependence implicit.

The viscous pressure is (Brevik and Gorbunova 2005):

$$P_{\text{visc}} = -\eta_v u^\mu_{;\mu} = -3\eta_v H, \tag{12}$$

where H is the Hubble constant given by

$$H = \sqrt{\frac{8\pi G}{3}} \rho = \sqrt{\frac{8\pi G}{3}} \frac{\epsilon}{c^2}. \tag{13}$$

The effective pressure is found by

$$P_{\text{eff}} = P_{TE} + P_{\text{visc}} = \frac{\epsilon}{3} - 3\eta_v H. \tag{14}$$

3.4 Neutrino decoupling

As the rate of the neutrino interactions, Γ_v , becomes slower than the rate of expansion of the universe, H , the neutrinos will decouple. The collision rate of neutrinos with electrons and positrons is (Weinberg 2008):

$$\begin{aligned} \Gamma_v &= n_e \sigma_{\text{wk}} \approx \left(\frac{k_B T}{\hbar c}\right)^3 (\hbar c G_{\text{wk}} k_B T)^2 \\ &\approx \frac{G_{\text{wk}}^2 (k_B T)^5}{\hbar c}, \end{aligned} \tag{15}$$

where n_e is the number density of electrons and σ_{wk} is the neutrino-electron scattering. $G_{\text{wk}} = G_F/(\hbar c)^3 \approx 1.166 \times 10^{-5} \text{ GeV}^{-2}$ (Griffiths 2008; Beringer 2012) is the weak coupling constant. By using the energy density as given in Eq. (9), the expansion rate at the same time is

$$\begin{aligned} H &= \sqrt{\frac{8\pi G}{3c^2}} \epsilon = \sqrt{\frac{8\pi G}{3c^2}} g_* \frac{\pi^2 (k_B T)^4}{30 (\hbar c)^3} \\ &\approx \sqrt{\frac{G (k_B T)^4}{(\hbar c)^3}}, \end{aligned} \tag{16}$$

where g_* is the effective degrees for freedom for energy density. The prefactors in Γ_v and H roughly cancel each other out, such that we end up with

$$\frac{\Gamma_v}{H} \approx G_{\text{wk}}^2 \sqrt{\frac{\hbar c}{G}} (k_B T)^3 \approx \left(\frac{T}{10^{10} \text{ K}}\right)^3. \tag{17}$$

It is worth noting that without taking neutrino decoupling into account, our equations would result in the shear viscosity going towards infinity as T goes towards zero. However

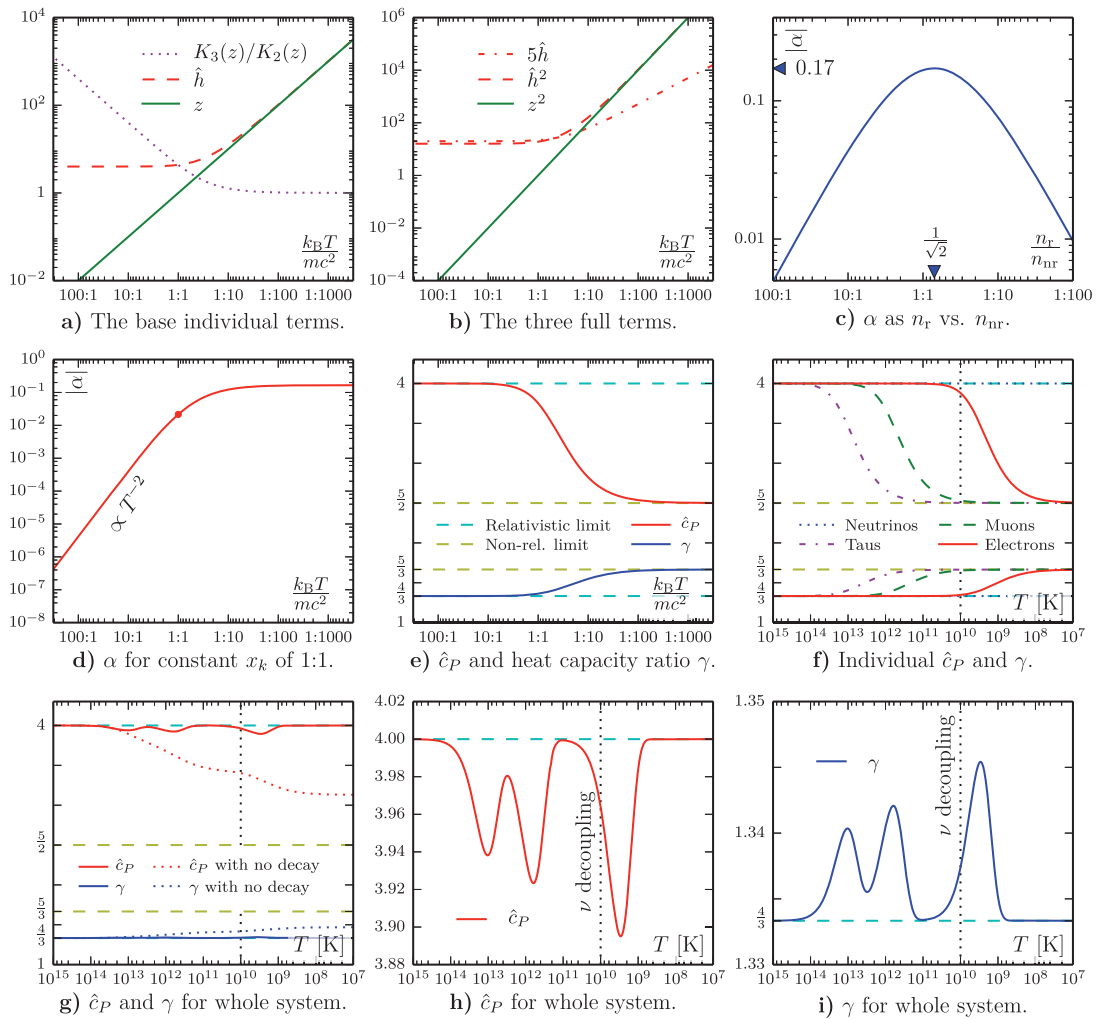


Fig. 6 A more thorough look at the specific heat capacity per particle (\hat{c}_P), the heat capacity ratio (γ), and α , as they are decomposed into its basic constituents. Subfigures (a) and (b) show functions of z , \hat{h} and the Bessel functions, which make up \hat{c}_P . (c) shows α as a function of the amount of relativistic to non-relativistic particles. The momentum transfer is biggest when the ratio is $2^{-1/2}$. (d) shows a system with one massless and one massive particle specie in equal amount.

α will increase as the massive particles go from being relativistic to non-relativistic. (e) shows \hat{c}_P and γ as function of $k_B T/mc^2$, and (f) shows the complete functions of \hat{c}_P and γ . For (g) we have included a hypothetical scenario with no particle annihilation (decay). \hat{c}_P (shown in (h)) drops almost 7 % towards the non-relativistic limit of $5/2$, while γ (shown in (i)) rise almost 3.5 % towards the non-relativistic of $5/3$

the bulk viscosity would still drop as it relies on the ratio of relativistic to non-relativistic particles.

4 Numerical model

Our model is made with *Mathematica 9* using standard precision. We calculate the shear viscosity for 6, 9, 11 and 13

particles. For bulk viscosity we use 9, 11 and 13 particles. This refers to: pure neutrino model ($\nu_e, \bar{\nu}_e, \nu_\mu, \bar{\nu}_\mu, \nu_\tau, \bar{\nu}_\tau = 6$), plus electron/positron and photon (plus $e^-, e^+, \gamma = 9$), plus muons (plus $\mu^-, \mu^+ = 11$), plus taus (plus $\tau^-, \tau^+ = 13$). We use the particle and physical constants from PDG’s “Review of Particle Physics (Beringer 2012). The Weinberg angle ($\sin^2 \theta_W$) is set to 0.229, as it was in the original 1986

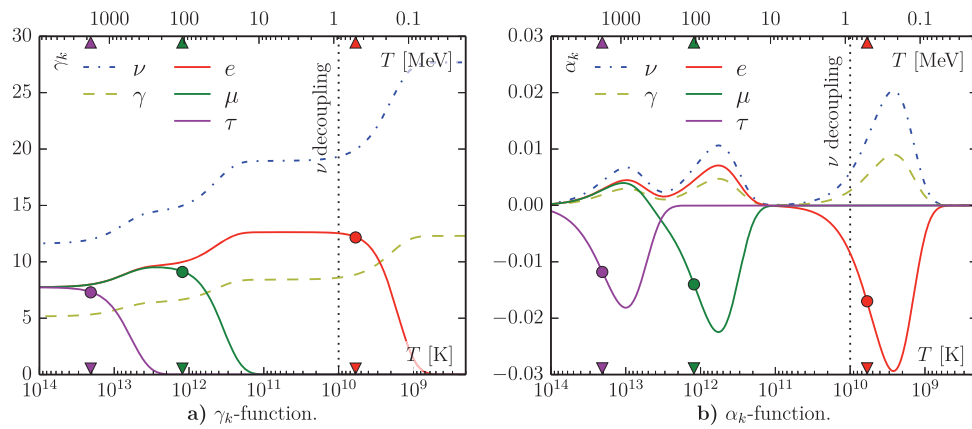


Fig. 7 γ_k (a) and α_k (b) as functions of temperature. We clearly see how γ_k correlates to the particle fraction plot of Figure 5 (just slightly shifted to the left). α_k peaks at temperatures where there is a good por-

tion of both relativistic particles and non-relativistic particles. In practice this is the periods from when, in order, the tau, muon and electron particles become non-relativistic until they annihilate

paper. The expanded parameters including τ^- , τ^+ for differential cross-sections in elastic collisions are given in Appendix B, Table 3.

Using these new parameters, we have solved the coefficients as given in Appendix A in Hoogeveen et al. (1986a). The equations used are reprinted in Appendix A.

Some integrals have been solved numerically instead of analytically. This has resulted in some high precision errors (e.g. when α_k goes towards zero). This affected the calculations at low temperatures when including the tau and muon particles. The results did however converge to the “2-particle-less” models beforehand, and hence these errors can be disregarded. For low temperature where these are the cases, the cells in Table 2 are left blank.

The particle densities, and the α_k and γ_k terms were calculated and plotted continuously, the viscosity terms themselves consist of a series of single calculations over 74 different temperatures and 7 particle models (4 for shear and 3 for bulk viscosities).

Readers interested in the *Mathematica* code are encouraged to email the author.

5 Results

All calculations in this article are given in CGS units. Our main results are given in Table 2, where we have organized the shear and bulk viscosities by numbers of particles used in the model. For shear viscosity, this is with 7, 9, 11 and 13 particles. Since photons have no impact on the shear viscosity, we might as well have written 6, 8, 10 and 12. As bulk viscosity requires both a relativistic and a non-relativistic

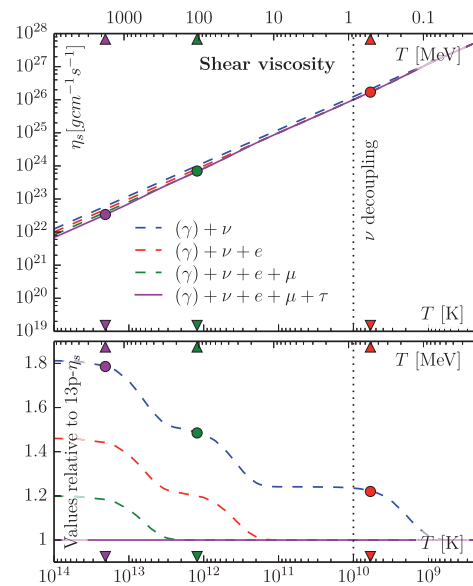


Fig. 8 *Top*: Absolute value of η_s . Its value increases slightly more rapidly in the regions where heavier particles annihilate. In “particle-stable” regions η_s goes as $\propto T^{-1}$. The *bottom plot* shows the deviations from the 13 particle model

part, we only have 9, 11 and 13 particle models. Our results are graphed in Figs. 8, 9, ranging from 2×10^8 to 10^{14} K (≈ 20 keV to 10 GeV). Everything below the neutrino decoupling temperature should be considered non-physical. We have included them in our calculations and plot as they still give us some input on the behavior of the two viscous terms.

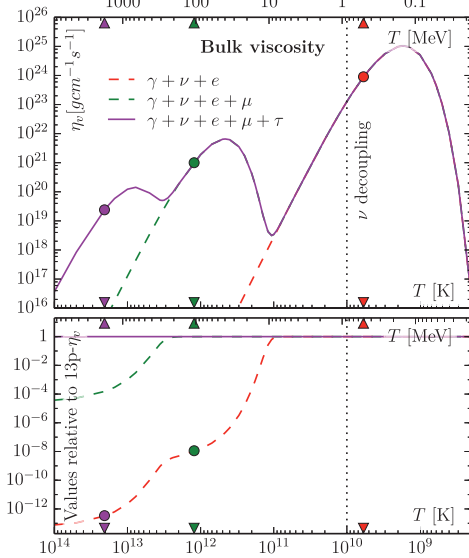


Fig. 9 Top plot show the bulk viscosity, η_v . In the particle-fraction-stable regions the bulk viscosity increases rapidly as $\eta_v \propto T^{-5}$, and then drop quickly as the heavier particles dies out. The local maxima's (peaks) corresponding to the three lepton generations show that three peaks in η_v goes as $\propto T^{-4/3}$. The bottom plot shows the deviations from the 13 particle model

Table 1 Local maxima peaks in α_k and η_v

(a) α_k related peaks			
e peak	$T = 2.642\text{E}9$ K	227.7 keV	$0.4455 m_e$
μ peak	$T = 5.763\text{E}11$ K	49.66 MeV	$0.4700 m_\mu$
τ peak	$T = 9.718\text{E}12$ K	837.4 MeV	$0.4713 m_\tau$
(b) η_v related peaks			
e peak	$T = 1.698\text{E}9$ K	146.3 keV	$0.2863 m_e$
μ peak	$T = 4.597\text{E}11$ K	39.61 MeV	$0.3749 m_\mu$
τ peak	$T = 7.710\text{E}12$ K	664.4 MeV	$0.3739 m_\tau$

For Table 2 the range is increased one order of magnitude to 10^{15} K (which is uncomfortable close to the electroweak scale).

The peaks in α_k and related peaks in the bulk viscosity, η_v , are given in Table 1. The associated electron peaks are found at $0.44 m_e$ for α and $0.29 m_e$ for η_v . For the muon and tau particles they both peak at $0.47 m_{\mu,\tau}$ for α and $0.37 m_{\mu,\tau}$ for η_v .

Our results using a 9-particle model are very similar to those found by Hoogeveen et al., only differing by around 1 %—which is within uncertainty. However, for our more particle-rich models the differences are quite significant in the high temperature regions. Plotting the pressures (Fig. 10) shows that the viscous pressure has a negligible contribution

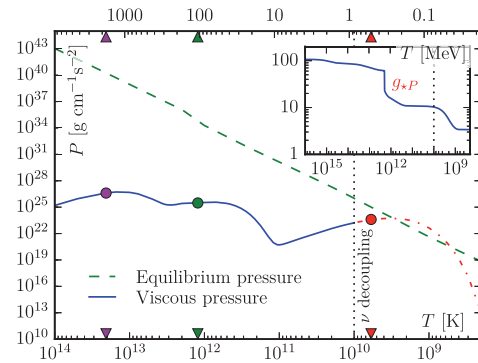


Fig. 10 Thermodynamic equilibrium pressure and viscous pressure. The calculations for the latter pressure does not make sense after the neutrinos decouple and are plotted as red dash-dots. The thermodynamic pressure P_{TE} is as a function of g_{*P} (shown in the subplot)

at high temperatures, and is at its highest at the time of the neutrino decoupling (and is actually larger than the thermodynamic pressure if we disregard the decoupling).

The rest of our results from Fig. 8, 9 and Table 2 will be divided into a shear and bulk viscosity part. As a side note we should say that by using PDG's (Beringer 2012) entry for $\sin^2 \theta_W$ will keep α_k unchanged, but the values of η_s and η_v will decrease by roughly 1 %.

5.1 Shear viscosity

- The photon contribution to shear viscosity is negligible, so removing them and making models for 6, 8, 10 and 12 particles gives the same results.
- Shear viscosity goes as T^{-1} as long as the particle fractions stays constant. This can be understood by the fact that energy density (for relativistic particles) goes as T^4 while the interaction rate, Γ goes as T^5 . As shear viscosity depends on the mean free path of the particles, this is the inverse of the interaction rate.
- At high temperatures where all charged leptons are present we get a drop of η_s by including the extra leptons in our model. For every particle pair we include in our model, η_s drops by roughly 20 %, or more specifically

$$\eta_{s(7p)} \xrightarrow{19\%} \eta_{s(9p)} \xrightarrow{18\%} \eta_{s(11p)} \xrightarrow{17\%} \eta_{s(13p)}. \quad (18)$$

5.2 Bulk viscosity

- Bulk viscosity is much more sensitive to temperature and number densities of the different particles.
- Photons contribute to bulk viscosity indirectly as they heat up the non-relativistic leptons. Removing the photon from our model would decreased η_v by 38 %, 29 % and 24 % for our 9, 11 and 13 particle models.

Table 2 Numerical values for shear and bulk viscosities for 7, 9, 11 and 13 particles. The local maximas and minimas in the bulk viscosities are marked by † and ‡, respectively. Everything after neutrinos decoupling should be considering non-physical and are marked in a red color. At temperatures of 10^{14} K and above, the viscosity due to electromagnetic interacting particles should be considered (shown in orange)

T (K)	T (eV)	η_s [g/cm s]				η_v [g/cm s]		
		7p	9p	11p	13p	9p	11p	13p
1.000E15	86.17 GeV	1.241E21	9.997E20	8.208E20	6.843E20	2.824E-2	1.379E7	4.445E11
1.000E14	8.617 GeV	1.241E22	9.997E21	8.208E21	6.846E21	2.823E3	1.376E12	3.658E16
5.000E13	4.309 GeV	2.481E22	1.999E22	1.642E22	1.371E22	9.033E4	4.385E13	8.423E17
2.000E13	1.723 GeV	6.204E22	4.998E22	4.104E22	3.469E22	8.821E6	4.182E15	2.656E19
1.000E13	861.7 MeV	1.241E23	9.997E22	8.209E22	7.213E22	2.823E8	1.260E17	1.227E20
7.710E12†	664.4 MeV	1.609E23	1.297E23	1.065E23	9.613E22	1.036E9	4.423E17	1.428E20
5.000E12	430.9 MeV	2.481E23	1.999E23	1.643E23	1.564E23	9.033E9	3.419E18	9.135E19
3.354E12‡	289.0 MeV	3.699E23	2.981E23	2.451E23	2.419E23	6.650E10	2.082E19	5.027E19
2.000E12	172.3 MeV	6.204E23	4.998E23	4.124E23	4.122E23	8.820E11	1.800E20	1.831E20
1.000E12	86.17 MeV	1.241E24	9.997E23	8.381E23	8.381E23	2.821E13	1.898E21	1.898E21
5.000E11	43.09 MeV	2.481E24	1.999E24	1.769E24	1.769E24	9.017E14	6.422E21	6.422E21
4.597E11†	39.61 MeV	2.699E24	2.175E24	1.944E24	–	1.372E15	6.544E21	–
2.000E11	17.23 MeV	6.204E24	4.998E24	4.925E24	–	8.744E16	4.251E20	–
1.069E11‡	9.212 MeV	1.161E25	9.352E24	9.350E24	–	1.972E18	3.145E18	–
1.000E11	8.617 MeV	1.241E25	9.997E24	9.996E24	–	2.745E18	3.418E18	–
5.000E10	4.309 MeV	2.481E25	2.000E25	2.000E25	–	8.300E19	8.300E19	–
2.000E10	1.723 MeV	6.204E25	5.004E25	5.004E25	–	6.372E21	6.372E21	–
1.000E10	861.7 keV	1.241E26	1.005E26	–	–	1.263E23	–	–
5.000E9	430.9 keV	2.481E26	2.042E26	–	–	1.514E24	–	–
2.000E9	172.3 keV	6.204E26	5.564E26	–	–	9.795E24	–	–
1.698E9†	146.3 keV	7.307E26	6.716E26	–	–	1.037E25	–	–
1.000E9	86.17 keV	1.241E27	1.217E27	–	–	5.107E24	–	–
5.000E8	43.09 keV	2.481E27	2.481E27	–	–	1.063E23	–	–
2.000E8	17.23 keV	6.204E27	6.204E27	–	–	3.120E16	–	–

- Bulk viscosity goes as T^{-5} as long as the particle number stays constant. When a particle species dies out η_v drops as the particle density function (which is exponential decay).
- At high temperatures where all charged leptons are present we get a significant increase in η_v by including the extra leptons in our model. Specifically the two jumps are:

$$\eta_{v(9p)} \xrightarrow{4.88E9} \eta_{v(11p)} \xrightarrow{3.22E4} \eta_{v(13p)}. \tag{19}$$

- The peaks for the local maximas of η_v goes roughly as $T^{-4/3}$ (within 6 %). The maximas and minimas are marked by † and ‡ in Table 2. (A newer value for $\sin^2 \theta_W$ from PDG (Beringer 2012) will shift the local maxima and minimum peaks by less than 0.1 %.)
- To understand why the peaks in bulk viscosity are as they are we have to look at several factors. Just as shear viscosity, the interacting rate vs. energy density should go as T^{-1} . To give an example of this: If the electron was

10 times heavier, the bulk viscosity would be a 10 times lower. That is: Changing the masses of particles changes the peaks as T^{-1} .

- The remaining T^{-4} comes from the product of the transport equations (α_k) and the α_k parameters. Each of which goes as T^{-2} .

6 Conclusions

The model universe we have presented here is a very simplified version of how the universe actually were at temperatures above 10^{12} K = 100 MeV. Our aim for this paper is to give a more illustrative description of early universe viscosity, particularly how it behaves with a multiple of different particles.

One important event which should be included however is the reheating effect during particle annihilations. Another interesting thought is whether we can use the same trans-

port equations to get a better understanding of the neutrino decoupling?

This extended model could be used to include new exotic particles, like dark matter candidates, or as a basis for an extended model using strongly interacting particles (e.g. pions) as well.

Acknowledgements Thanks to my supervisor Kåre Olaussen for giving me the project, and for helping me throughout this work. His help has been invaluable for understanding the concepts and the underlying mathematics. Thanks also to Iver Brevik for introducing us to the field of viscous cosmology, and for fruitful discussions on this paper.

Appendix A: Coefficients occurring in the linear equations

We begin by rewriting the equations for shear and bulk viscosities

$$\eta_s = \frac{1}{10}cn \left(\frac{k_B T}{c}\right)^3 \sum_k c_k \gamma_k, \tag{A.1}$$

$$\eta_v = nk_B T \sum_k a_k \alpha_k, \tag{A.2}$$

The c_k and a_k coefficients are solutions to the linearized relativistic Boltzmann (transport) equation for the shear and bulk cases are given as follows:

$$c_k = \frac{1}{n} \left(\frac{k_B T}{c}\right)^2 c_{kl}^{-1} \gamma_k, \tag{A.3}$$

$$a_k = \frac{1}{n} a_{kl}^{-1} \alpha_k, \tag{A.4}$$

where

$$c_{kl} = x_k \left(x_l c'_{kl} + \delta_{kl} \sum_{m=1}^N x_m c''_{km} \right), \tag{A.5}$$

$$a_{kl} = x_k \left(x_l a'_{kl} + \delta_{kl} \sum_{m=1}^N x_m a''_{km} \right) \tag{A.6}$$

are matrix elements related to the differential cross-sections in the frame of the center of momentum of the system. The primes and double primes are defined as

$$c'_{kl} = \frac{1}{3} \left(\frac{k_B T}{c}\right)^4 (-40I_{12110}^1 - 80I_{13110}^1 + 6I_{21000}^2 + 12I_{22000}^2 + 8I_{23000}^2), \tag{A.7}$$

$$c''_{kl} = \frac{1}{3} \left(\frac{k_B T}{c}\right)^4 (40I_{12200}^1 + 80I_{13200}^1 + 6I_{21000}^2 + 12I_{22000}^2 + 8I_{23000}^2), \tag{A.8}$$

$$a'_{kl} = -2I_{12000}, \tag{A.9}$$

$$a''_{kl} = 2I_{12000} = -a'_{kl}. \tag{A.10}$$

Here, as in the Hoogeveen article, the particle indexes k and l are suppressed on the right sides of the equations. The $10+2$ I-integrals described above are collision integrals, and have dimension σc [cm^3/s] and are defined by van Erkelens and van Leeuwen (1980):

$$I_{ij\kappa\lambda h}^\mu(k, l) = \left(\frac{c\pi}{z_k^2 z_l^2 K_2(z_k) K_2(z_l)}\right) \left(\frac{c}{k_B T}\right)^{2i-j+\kappa+\lambda+6} \times \int_{(m_k+m_l)c}^\infty dP_{kl} g_{kl}^{2i+2} P_{kl}^{-j+3} (g_{kl}^2 + m_k^2 c^2)^{\kappa/2} \times (g_{kl}^2 + m_l^2 c^2)^{\lambda/2} \times K_{j+h} \left(\frac{cP_{kl}}{k_B T}\right) \int_0^\pi (1 - \cos^\mu \theta_{kl}) \frac{d\sigma_{kl}}{d\Omega_{\text{CM}}}(P_{kl}, \theta_{kl}) \times \sin \theta_{kl} d\theta_{kl}, \tag{A.11}$$

where

$$g_{kl} = P_{kl}^{-1} \sqrt{\frac{1}{4}(P_{kl}^2 - m_k^2 c^2 - m_l^2 c^2)^2 - m_k^2 m_l^2 c^4} \tag{A.12}$$

is the invariant relative momentum.

Appendix B: Weak interaction cross-sections

The weak interaction cross-sections are given in Appendix C in Hoogeveen et al. (1986a). However we have included the tau particles in our model to give us the differential cross-sections for 68 (compared to 45) elastic collisions

$$k + l \rightarrow k + l, \tag{B.1}$$

where

$$k = \nu_e, \bar{\nu}_e, \nu_\mu, \bar{\nu}_\mu, \nu_\tau, \bar{\nu}_\tau, \tag{B.2}$$

$$l = \nu_e, \bar{\nu}_e, \nu_\mu, \bar{\nu}_\mu, \nu_\tau, \bar{\nu}_\tau, e^-, e^+, \mu^-, \mu^+, \tau^-, \tau^+. \tag{B.3}$$

The weak interaction cross-sections from Eq. (A.11) is given as:

$$\frac{d\sigma_{kl}}{d\Omega_{\text{CM}}} = \frac{G_F^2 S}{32\pi^2 \hbar^4 c^2} S f(s, t), \tag{B.4}$$

where S is equal to the product of the usual symmetry factor $1/n_f!$, where n_f is the number of identical particles in the final state, and a factor 2 for each incoming neutrino, so e.g. for $e^+ e^+ \rightarrow e^+ e^+$ we have $S = (1 \times 1)/2!$ and for $\nu_e \nu_e \rightarrow$

Table 3 v and a matrices. w^+ and w^- is abbreviation for $\sin^2 \theta_W +1/2$ and $\sin^2 \theta_W -1/2$, respectively. The electromagnetic contribution is so small it can be ignored. The crossection $\sigma_{\gamma\nu}$ is zero

(a) a matrix													(b) v matrix															
	γ	ν_e	$\bar{\nu}_e$	ν_μ	$\bar{\nu}_\mu$	ν_τ	$\bar{\nu}_\tau$	e^-	e^+	μ^-	μ^+	τ^-	τ^+		γ	ν_e	$\bar{\nu}_e$	ν_μ	$\bar{\nu}_\mu$	ν_τ	$\bar{\nu}_\tau$	e^-	e^+	μ^-	μ^+	τ^-	τ^+	
γ	-	0	0	0	0	0	0	-	-	-	-	-	-	γ	-	0	0	0	0	0	0	-	-	-	-	-	-	
ν_e	0	1	-1	1/2	-1/2	1/2	-1/2	1/2	-1/2	-1/2	1/2	-1/2	1/2	ν_e	0	1	1	1/2	1/2	1/2	1/2	w^+	w^+	w^-	w^-	w^-	w^-	
$\bar{\nu}_e$	0	-1	1	-1/2	1/2	-1/2	1/2	-1/2	1/2	1/2	-1/2	-1/2	1/2	$\bar{\nu}_e$	0	1	1	1/2	1/2	1/2	1/2	w^+	w^+	w^-	w^-	w^-	w^-	
ν_μ	0	1/2	-1/2	1	-1	1/2	-1/2	-1/2	1/2	1/2	-1/2	-1/2	1/2	ν_μ	0	1/2	1/2	1	1	1/2	1/2	w^-	w^-	w^+	w^+	w^-	w^-	
$\bar{\nu}_\mu$	0	-1/2	1/2	-1	1	-1/2	1/2	1/2	-1/2	-1/2	1/2	1/2	-1/2	$\bar{\nu}_\mu$	0	1/2	1/2	1	1	1/2	1/2	w^-	w^-	w^+	w^+	w^-	w^-	
ν_τ	0	1/2	-1/2	1/2	-1/2	1	-1	-1/2	1/2	-1/2	1/2	1/2	-1/2	ν_τ	0	1/2	1/2	1/2	1/2	1	1	w^-	w^-	w^-	w^-	w^+	w^+	
$\bar{\nu}_\tau$	0	-1/2	1/2	-1/2	1/2	-1	1	1/2	-1/2	1/2	-1/2	-1/2	1/2	$\bar{\nu}_\tau$	0	1/2	1/2	1/2	1/2	1	1	w^-	w^-	w^-	w^-	w^+	w^+	
e^-	-	1/2	-1/2	-1/2	1/2	-1/2	1/2	-	-	-	-	-	-	e^-	-	w^+	w^+	w^-	w^-	w^-	-	-	-	-	-	-	-	
e^+	-	-1/2	1/2	1/2	-1/2	1/2	-1/2	-	-	-	-	-	-	e^+	-	w^+	w^+	w^-	w^-	w^-	-	-	-	-	-	-	-	
μ^-	-	-1/2	1/2	1/2	-1/2	-1/2	1/2	-	-	-	-	-	-	μ^-	-	w^-	w^-	w^+	w^+	w^-	-	-	-	-	-	-	-	
μ^+	-	1/2	-1/2	-1/2	1/2	1/2	-1/2	-	-	-	-	-	-	μ^+	-	w^-	w^-	w^+	w^+	w^-	-	-	-	-	-	-	-	
τ^-	-	-1/2	1/2	-1/2	1/2	1/2	-1/2	-	-	-	-	-	-	τ^-	-	w^-	w^-	w^-	w^-	w^+	w^+	-	-	-	-	-	-	-
τ^+	-	1/2	-1/2	1/2	-1/2	-1/2	1/2	-	-	-	-	-	-	τ^+	-	w^-	w^-	w^-	w^-	w^+	w^+	-	-	-	-	-	-	-

$\nu_e \nu_e$ we have $S = (2 \times 2)/2!$. $f(s, t)$ is a collisions function for the two incoming particles and is given by:

$$\begin{aligned}
 f(s, t) = & (v + a)^2 \left(\frac{s - m^2 c^2}{s} \right)^2 \\
 & + (v - a)^2 \left(\frac{s + t - m^2 c^2}{s} \right)^2 \\
 & + (v^2 - a^2) \frac{2m^2 c^2 t}{s^2}, \tag{B.5}
 \end{aligned}$$

with the a and v matrices are related to the neutral current coupling (Hoogeveen et al. 1986a), basically how neutrinos couples to the other particles. They are listen in Table 3. The s and t being the Mandelstam variables:

$$s \equiv (p_k + p_l)^2 = P_{kl}^2, \tag{B.6}$$

$$t \equiv (p_k - p'_k)^2, \tag{B.7}$$

where s is the square of the center-of-mass energy (invariant mass) for the two incoming particles k and l . t is the square of the four-momentum transfer, and is related to the scattering angle in the center of momentum system, being defined below. p'_k is the four-momentum of particle k after collision, such that

$$\begin{aligned}
 t = & m_k^2 c^2 + m_l^2 c^2 - P_{kl}^2 \\
 & + \frac{(P_{kl}^2 + m_k^2 c^2 - m_l^2 c^2)(P_{kl}^2 - m_k^2 c^2 + m_l^2 c^2)}{2P_{kl}^2} \\
 & + \frac{[P_{kl}^2 - (m_k c + m_l c)^2][P_{kl}^2 - (m_k c - m_l c)^2]}{2P_{kl}^2} \cos \theta_{kl}, \tag{B.8}
 \end{aligned}$$

with θ_{kl} being the scattering angle of the CM-system.

References

Andersen, J.O.: Introduction to Statistical Mechanics. Akademika Publishing, Trondheim (2012)

Bennett, C.L., Larson, D., Weiland, J.L., Jarosik, N., Hinshaw, G., et al.: Nine-Year Wilkinson Microwave Anisotropy Probe (WMAP) Observations: Final Maps and Results (2012). [1212.5225](https://doi.org/10.1007/s10509-014-2162-x)

Beringer, J.e.a.: Phys. Rev. D **86**, 010001 (2012). doi:[10.1103/PhysRevD.86.010001](https://doi.org/10.1103/PhysRevD.86.010001)

Brevik, I.: Astrophys. Space Sci. **355**(1), 179 (2015). [1410.2069](https://doi.org/10.1007/s10509-014-2162-x). doi:[10.1007/s10509-014-2162-x](https://doi.org/10.1007/s10509-014-2162-x)

Brevik, I., Gorbunova, O.: Gen. Relativ. Gravit. **37**, 2039 (2005). [gr-qc/0504001](https://doi.org/10.1007/s10714-005-0178-9). doi:[10.1007/s10714-005-0178-9](https://doi.org/10.1007/s10714-005-0178-9)

Caderni, N., Fabbri, R.: Phys. Lett. B **69**, 508 (1977). doi:[10.1016/0370-2693\(77\)90856-5](https://doi.org/10.1016/0370-2693(77)90856-5)

Griffiths, D.: Introduction to Elementary Particles, 2nd edn. Wiley, Weinheim (2008)

Grøn, Ø.: Astrophys. Space Sci. **173**, 191 (1990). doi:[10.1007/BF00643930](https://doi.org/10.1007/BF00643930)

Groot, S.R., Leeuwen, W.A., van Weert, C.G.: Relativistic Kinetic Theory: Principles and Applications. North-Holland, Amsterdam (1980)

Hoogeveen, F., Leeuwen, W.A.V., Salvati, G.A.Q., Schilling, E.E.: Phys. A, Stat. Mech. Appl. **134**(2), 458 (1986a). doi:[10.1016/0378-4371\(86\)90059-2](https://doi.org/10.1016/0378-4371(86)90059-2)

Hoogeveen, F., Leeuwen, W.A.V., Salvati, G.A.Q., Schilling, E.E.: Phys. A, Stat. Mech. Appl. **134**(2), 463 (1986b). Equation 3.12

Kapusta, J., Muller, B., Rafelski, J.: Quark Gluon Plasma: Theoretical Foundations: An Annotated Reprint Collection. Elsevier, Amsterdam (2003)

Misner, C.W.: Phys. Rev. Lett. **19**, 533 (1967). doi:[10.1103/PhysRevLett.19.533](https://doi.org/10.1103/PhysRevLett.19.533)

- Misner, C.W.: *Astrophys. J.* **151**, 431 (1968). doi:[10.1086/149448](https://doi.org/10.1086/149448)
- Misner, C.W.: *Phys. Rev. Lett.* **22**, 1071 (1969). doi:[10.1103/PhysRevLett.22.1071](https://doi.org/10.1103/PhysRevLett.22.1071)
- Treciokas, R., Ellis, G.F.R.: *Commun. Math. Phys.* **23**(1), 1 (1971)
- van Erkelens, H., van Leeuwen, W.A.: *Phys. A, Stat. Mech. Appl.* **91**(1–2), 88 (1978)
- van Erkelens, H., van Leeuwen, W.A.: *Phys. A, Stat. Mech. Appl.* **101**(1), 205 (1980)
- van Leeuwen, W.A., Salvati, G.A.Q., Schelling, E.E.: *Phys. A, Stat. Mech. Appl.* **136**(2–3), 417 (1986). doi:[10.1016/0378-4371\(86\)90259-1](https://doi.org/10.1016/0378-4371(86)90259-1)
- Weinberg, S.: *Cosmology*. Oxford University Press, New York (2008)

Paper III

Entropy in a Lepton-Photon Universe

Astrophysics and Space Science **362** (2017) no. 2



Entropy production in a lepton-photon universe

Lars Husdal¹  · Iver Brevik²

Received: 14 October 2016 / Accepted: 19 January 2017
© Springer Science+Business Media Dordrecht 2017

Abstract We look at the entropy production during the lepton era in the early universe by using a model where we exclude all particles except the leptons and photons. We assume a temperature dependent viscosity as calculated recently by one of us (Husdal in *Astrophys. Space Sci.* 361(8):1, 2016b) with the use of relativistic kinetic theory. We consider only the bulk viscosity, the shear viscosity being omitted because of spatial isotropy. The rate of entropy production is highest just before the neutrinos decouple. Our results show that the increase in entropy during the lepton era is quite small, about 0.071 % at a decoupling temperature of $T = 10^{10}$ K. This result is slightly smaller than that obtained earlier by Caderni and Fabbri (*Phys. Lett. B* 69:508, 1977). After the neutrino decoupling, when the Universe has entered the photon era, kinetic theory arguments no longer support the appearance of a bulk viscosity. At high temperatures and a stable particle ratio, entropy production ($d\sigma/dT$) goes as T^{-8} , with the total entropy ($\Delta\sigma$) increasing as T^{-7} . These rates go slightly down just before the neutrinos decouple, where $\Delta\sigma \propto T^{-6.2}$.

Keywords Viscous cosmology · Bulk viscosity · Lepton era · Relativistic kinetic theory · Entropy · Entropy production

✉ L. Husdal
lars.husdal@ntnu.no
I. Brevik
iver.h.brevik@ntnu.no

¹ Department of Physics, Norwegian University of Science and Technology, Høgskoleringen 5, 7491 Trondheim, Norway

² Department of Energy and Process Engineering, Norwegian University of Science and Technology, Kolbjørn Hejes vei 1B, 7491 Trondheim, Norway

1 Introduction

In an isotropic adiabatic expanding universe the entropy remains constant. However, for periods where there is a mixture of relativistic and non-relativistic particles, bulk viscous effects will arise, leading to an increase of the entropy. The magnitude of these depend strongly on the mean free paths of the particles. For the early universe, the bulk viscosity and resulting entropy production is at their highest just before the neutrinos decouple.

Back in 1977, Caderni and Fabbri calculated the entropy production to be 0.11 % during the lepton era (Caderni and Fabbri 1977). Nine years later, in 1986, Hoogeveen et al., used a more rigorous theory to calculate the viscosity, and obtained a result about 4.5 times larger (Hoogeveen et al. 1986). This work was based on the relativistic kinetic theory developed by, among others, de Groot et al. (1980), van Erkelens and van Leeuwen (1978, 1980), and van Leeuwen et al. (1986).

In a previous paper (Husdal 2016b) one of us used the paper by Hoogeveen et al. as a reference and expanded their model to include all three of the charged lepton pairs. This was done in a hypothetical universe where all particles except the leptons and photons were omitted. This allowed us to perform an isolated study of the viscous phenomena at temperatures where, strictly speaking, other particles would interfere.

In this paper we use the theory by Brevik and Heen (1994) to calculate the entropy production for the same scenario, in a lepton-photon universe. We include all the charged leptons and look at entropy production caused by each of the three species.

2 Setup and assumptions

2.1 Definition of lepton era

The lepton era is normally defined to be between $T = 10^{12}$ K and $T = 10^{10}$ K ($k_B T = 100$ MeV to $k_B T = 1$ MeV). At these temperatures the Universe is populated by photons, neutrinos, electrons and their antiparticles, and at the warmer end of the period, also some muons and pions. At approximately $T = 10^{10}$ K the neutrinos decouple and for lower temperatures we enter the photon era. For $T > 10^{12}$ K the appearance of baryons will increase rapidly, and at roughly $k_B T = 170$ MeV (Kapusta et al. 2003) there is a phase transition to a quark-gluon plasma. At this time the energy content of the Universe is dominated by quarks and is hence called the quark era. In this paper, we disregard all particles except leptons and photons, and for our purposes, the lepton era is considered as the cosmic fluid before the neutrinos decouple.

2.2 Assumptions in our model

The data for bulk viscosity are taken from Husdal (2016b). We use the same assumptions, for the same reasons, as given in that paper. Since our study goes beyond the “textbook” lepton-era, our results for these high temperatures do not necessarily represent the real world. However, exploring this region in our modified universe gives us a better understanding of the entropy production with multiple particles. We make the following assumptions:

Pure lepton-photon universe: We exclude all other particles to get a more isolated study of the entropy production at high temperatures. This leaves out any entropy production caused by the hadronic particles just after the quark-gluon plasma to hadron gas transition. At this time there would exist a large number of semi- and non-relativistic baryons and mesons, which we expect would create a significant viscous term. We recommend the paper by Dobado et al. (2016) which discusses this era.

No chemical potential: The chemical potential for all particles is set to zero. This also excludes the asymmetry between matter and antimatter. This ratio is believed to be less than 10^{-9} (Bennett et al. 2013), making it negligible for our study.

No electromagnetic contribution to viscosity: The much larger cross sections for electromagnetic interactions compared to weak interactions mean that the weakly interacting neutrinos get a much larger mean free path, and resulting momentum transfer. We can disregard the viscous contribution from electromagnetic interactions for temperatures close up to 10^{14} K when the electromagnetic and weak forces approach each other in strength.

No reheating from annihilation processes: When the massive particles annihilate they should heat up the rest of the particles. This effect is not considered in our paper.

Only elastic collisions: We only consider elastic collisions in our calculations. The cross sections for inelastic collisions are of comparable sizes, and should thus not alter our results considerably (Hoogeveen et al. 1986).

Simple neutrino decoupling: We use a simple cut-off for the neutrino interactions, which means they interact 100 % until a decoupling temperature and then 0 % thereafter.

3 Conditions in the early universe

For a universe in thermal equilibrium (which is quite accurate for the early universe), the number density, n ,¹ and energy density, $\epsilon = \rho c^2$, is given by the thermodynamic functions (Husdal 2016a)

$$\text{Number density: } n = \frac{\zeta(3)}{\pi^2} g_{*n}(T) \frac{(k_B T)^3}{(\hbar c)^3}, \quad (1)$$

$$\text{Energy density: } \epsilon = \frac{\pi^2}{30} g_{*\epsilon}(T) \frac{(k_B T)^4}{(\hbar c)^3}, \quad (2)$$

where k_B , \hbar , c , and $\zeta(3)$ are the Boltzmann constant, reduced Planck constant, speed of light, and the Riemann zeta function of value 3, respectively. g_{*n} and $g_{*\epsilon}$ are the effective degrees of freedom for number density and energy density.² For high temperatures, when all particle species are created and destroyed at the same rate, we have $g_{*n} = 15.5$ and $g_{*\epsilon} = 17.25$. This is equal to the internal degrees of freedom for the particles, and is found by counting all the states of the particles, like spin, antiparticles, and including the distributional difference between fermions and bosons. This latter property results in fermions only contributing 3/4 (number density) and 7/8 (energy density) compared to bosons—hence the difference in g_{*n} and $g_{*\epsilon}$. The taus, muons, and electrons all contribute by 3 to g_{*n} and 3.5 to $g_{*\epsilon}$ at high temperatures, but as the temperature decreases and the annihilation rate becomes faster than the creation rate for these particles their effective contribution will decline. In a lepton-photon universe the evolution of g_{*n} and $g_{*\epsilon}$ is given in Fig. 1. In this and the following figures we use colored circles (\circ) in the graph, and triangles (Δ , ∇) on the axes, to mark the location where the rest mass of the taus, muons, and electrons equals that of the temperature ($mc^2 = k_B T$). We use magenta (taus), green (muons), and red (electrons) colors to represent the three different massive particle pairs.

¹The number density, n , is for all particles, not the net baryon number as in e.g. Weinberg (1971).

² $g_{*\epsilon}$ is normally written without the ϵ subscript, as g_* .

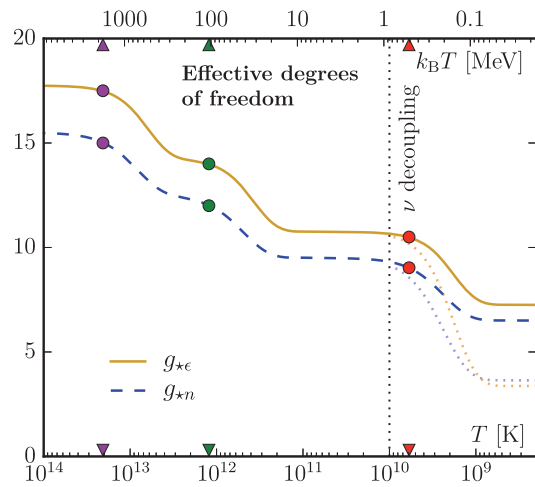


Fig. 1 Effective degrees of freedom for energy density and number density. As the temperature decreases below the mass equivalent for the taus, muons, and electrons, their contributions to g_{*n} and $g_{*ε}$ will drop, as we see as three dips in the two curves. The effective degrees of freedom from the neutrinos decrease after they decouple (as they are not heated by the decaying electrons and positrons). As we are interested in the difference in entropy production for slightly different decoupling temperatures, we keep the neutrino contribution to g_{*n} and $g_{*ε}$ constant in our calculations. The dotted curves show the standard representation of $g_{*ε}$ and g_{*n} where the neutrinos are not heated by the electron-positron annihilations, and is thus lower. The masses of the three massive leptons are marked with magenta, green, and red circles (○) and triangles (Δ, ▽)

Assuming that the early universe was flat and with negligible vacuum energy (cosmological constant equal to zero), we can write the first Friedmann equation as

$$H^2 \equiv \left(\frac{\dot{a}}{a}\right)^2 = \frac{8\pi G}{3c^2} \epsilon, \tag{3}$$

where G is the gravitational constant. We can use the energy density found in Eq. (2), such that

$$H^2 = \frac{8\pi G}{3c^2} \frac{\pi^2}{30} g_{*ε}(T) \frac{(k_B T)^4}{(\hbar c)^3}. \tag{4}$$

For a lepton-photon universe $g_{*ε}$ will vary between 17.75 and 3.36, with a value of roughly 10.75 at the time of the neutrino decoupling.

For a radiation dominated era, time can be calculated as a function of $g_{*ε}$ as follows (Olive et al. 2014):

$$t = \sqrt{\frac{90\hbar^3 c^5}{32\pi^3 G g_{*ε}}} (k_B T)^{-2}. \tag{5}$$

4 The appearance of bulk viscosity

Bulk viscous phenomena arise when two gas components expand differently. An expanding relativistic gas decreases in temperature as a^{-1} , while a non-relativistic gas decreases as a^{-2} . For semi-relativistic particles, we have something in between. Whenever we have a mixture at different temperatures there will be a heat transfer between the warmer components and the colder ones. The magnitude of this viscous factor depends on the temperature difference between the two components as well as the number ratio between them. The electromagnetic particles will interact frequently and never have time to build up a temperature difference, resulting in a negligible momentum transfer. The neutrinos, on the other hand, travel much further before interacting and thus gain a larger temperature difference. The main component of the heat transfer is therefore due to the transfer of momentum from the neutrinos to the EM-coupled particles.

We emphasize that the number of particles in the mixture plays a big role. When one of the charged (massive) lepton species starts to drop quicker in temperature, it is almost instantaneously heated by all the remaining charged leptons and the photons. All the EM-coupled particles will thus collectively decrease in temperature a bit faster than the neutrinos. How fast depends on the number of EM-coupled particles. The decrease in temperature will though happen faster during e^+e^- annihilations than during the $\mu^+\mu^-$, which again is faster than during $\tau^+\tau^-$ annihilations.

The bulk viscosity can be calculated as (van Erkelens and van Leeuwen 1978; de Groot et al. 1980; Husdal 2016b):

$$\eta_v(T) = nk_B T \sum_k a_k \alpha_k, \tag{6}$$

where a_k are coefficients for particle k for the linearized relativistic Boltzmann equations, describing the energy and momentum transfer, and $\alpha_k(n_k, T)$ describes the state of the system. a_k and α_k are proportional to T^{-7} and T^{-2} for $k_B T \gg mc^2$, and as we see in Fig. 2, the bulk viscosity (η_v) builds up as T^{-5} as the massive leptons change to semi- and non relativistic velocities. However, as they eventually disappear we get an exponential decay of η_v .

5 Entropy production

To begin with, let us sketch the general relativistic formalism leading to the expression for the local rate of entropy production in the cosmic fluid. We assume a spatially flat FRW universe, and for simplicity, we put $c = 1$ in this section where we are dealing with the general formalism. We include at first both the bulk viscosity η_v and the shear viscosity η_s , but omit heat conduction. This kind of formalism can be found in various places, for instance in Weinberg

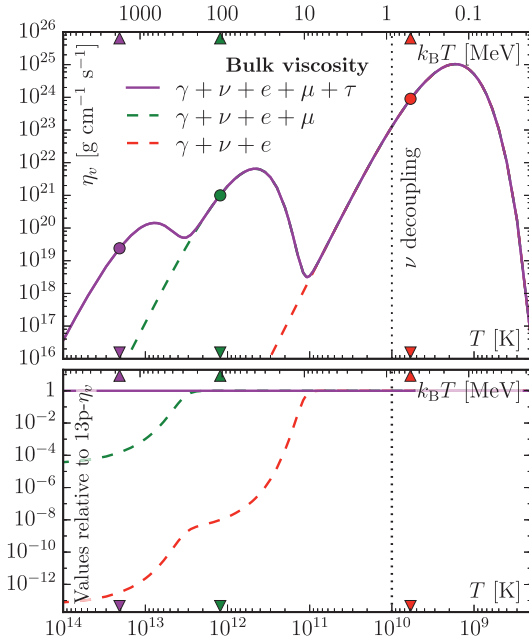


Fig. 2 Bulk viscosity for models using two, four, or all six of the charged leptons in addition to the neutrinos and photon. The viscous effect is at its greatest when there is a large contribution of semi- and non-relativistic particles (which cool faster), and a long mean free path for the neutrinos (such that the temperature difference has time to build up). At $k_B T$ high above $m_{\tau,\mu,e} c^2$ the viscosity grows as T^{-5} . After reaching local maxima at around $1/3$ of the rest mass of the particle in question, there will be an exponential drop. The viscosity at these local maxima goes roughly as $T^{-4/3}$ (Husdal 2016b)

(1971). Here, we follow the formalism as given in Brevik and Heen (1994).

If $U^\mu = (U^0, U^i)$ is the four-velocity of the fluid satisfying $U^\mu U_\mu = -1$, and if $h_{\mu\nu} = g_{\mu\nu} + U_\mu U_\nu$ is the projection tensor, we may write the energy-momentum tensor as

$$T_{\mu\nu} = \rho U_\mu U_\nu + (p - 3H\eta_v)h_{\mu\nu} - 2\eta_s \sigma_{\mu\nu}. \tag{7}$$

Here H is the Hubble variable, and $\sigma_{\mu\nu}$ denotes the shear tensor,

$$\sigma_{\mu\nu} = \theta_{\mu\nu} - Hh_{\mu\nu}, \tag{8}$$

with

$$\theta_{\mu\nu} = h_\mu^\alpha h_\nu^\beta U_{(\alpha;\beta)} \tag{9}$$

being the expansion tensor.

Let now n denote the total number density of particles in the local rest frame, and let σ be the nondimensional entropy per particle. The dimensional entropy per unit volume is thus

$S = nk_B\sigma$. The entropy current four-vector is

$$S^\mu = nk_B\sigma U^\mu, \tag{10}$$

whose covariant divergence is

$$S^\mu{}_{;\mu} = \frac{9\eta_v}{T} H^2 + \frac{2\eta_s}{T} \sigma_{\mu\nu} \sigma^{\mu\nu}. \tag{11}$$

The energy conservation for energy

$$\dot{\rho} + 3H(\rho + p) = 9\eta_v H^2 \tag{12}$$

now gives, together with the conservation equation for particle number,

$$(nU^\mu)_{;\mu} = 0, \tag{13}$$

that $na^3 = \text{constant}$ in the comoving frame. Setting $\eta_s = 0$, this leads to

$$\dot{\sigma} = \frac{9\eta_v}{nk_B T} H^2, \tag{14}$$

which is the desired result. This expression holds also in dimensional units, where c is restored (i.e. the rest of our paper).

If we add the calculation for bulk viscosity done by Husdal (2016b) we find the following result for the total entropy production, $\Delta\sigma$:

$$\begin{aligned} \Delta\sigma &= \int_{t_0}^{t_1} \dot{\sigma} dt = \int_{T_0}^{T_1} \dot{\sigma} \frac{dt}{dT} dT \\ &= \int_{T_0}^{T_1} \frac{9\eta_v H^2}{nk_B T} \frac{dt}{dT} dT. \end{aligned} \tag{15}$$

Before we can calculate this integral we need to write the variables as temperature dependent. Using Friedmann's first equation (Eq. (3)) as well as number density and energy density from Eqs. (1), (2) we get:

$$\Delta\sigma = \frac{9}{k_B} \int_{T_0}^{T_1} \eta_v \frac{8\pi G}{3c^2} g_{*\epsilon} \frac{\pi^2 (k_B T)^4}{30 (\hbar c)^3} \frac{dt}{dT} dT \tag{16}$$

$$= \frac{4\pi^5 G}{5\zeta(3)c^2} \int_{T_0}^{T_1} \eta_v(T) \frac{g_{*\epsilon}(T)}{g_{*n}(T)^3} \frac{dt}{dT} dT. \tag{17}$$

η_v , $g_{*\epsilon}$, and g_{*n} are functions of temperature and need to be calculated numerically. Also, dt/dT needs to be calculated numerically.

6 Results

The main amount of entropy production happens just before the neutrinos decouple. The main factors of the entropy production come from the viscous term (η_v) and dt/dT , which

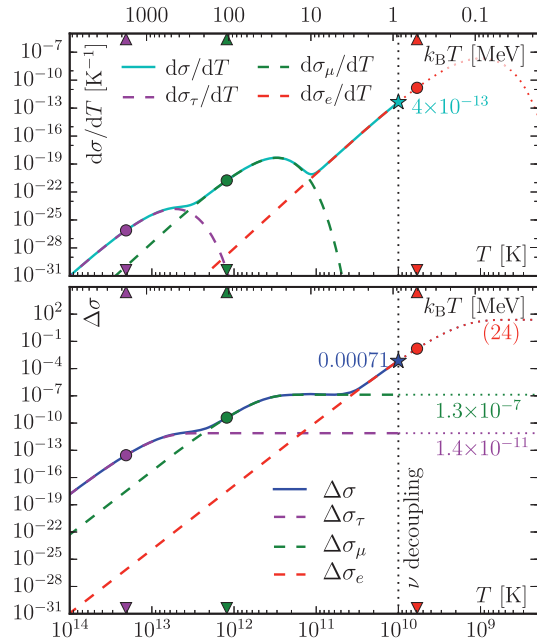


Fig. 3 Upper plot: entropy production as function of temperature ($d\sigma/dT$). For high temperatures this grows as T^{-8} , before slowing down and reaching local maxima at around $k_B T = mc_x^2/3$. Lower plot: the total (accumulated) increase in entropy ($\Delta\sigma$), which grows as T^{-7} for high temperatures. In both panels we have plotted the individual contributions by the τ^\pm , μ^\pm , and e^\pm in dashed magenta, green and red colors. At a decoupling temperature of 10^{10} K the entropy production is $4.4 \times 10^{-11} \text{ K}^{-1}$, resulting in a total increase of $7.1 \times 10^{-4} = 0.071 \%$

at high temperature ($k_B T \gg mc^2$) are proportional to T^{-5} and T^{-3} . Disregarding neutrino decoupling leads to unphysical and extreme values for the entropy production. We include values at temperatures below this point in our plots, but clearly marked the neutrino decoupling, which, if not stated otherwise, is taken to occur at 10^{10} K.

6.1 Entropy production for all charged leptons

The main result is shown in Fig. 3. The upper plot shows the entropy production as a function of temperature, $d\sigma/dT$. The lower plot shows the total (accumulated) entropy production, $\Delta\sigma$. We clearly see how the three different massive lepton-pairs dominate the entropy production at different times. The added curves (shown in dashed magenta, green, and red) show each of the charged leptons contributions to $d\sigma/dT$ and $\Delta\sigma$. As seen in Table 1, the final contribution of each lighter lepton pair outweighs those of the more massive ones. The final value of $\Delta\sigma$ depends on the neutrino decoupling temperature.

Table 1 Entropy production, $d\sigma/dT$, and total increase in entropy, $\Delta\sigma$, caused by the different charged leptons. As the maximum for the electron-pair contribution is lower than the decoupling temperature, their actual contribution is that at $T = 10^{10}$ K. The last row in our table is that for all particles at the decoupling (dc) temperature. In the first column the temperature is that of the local maxima for entropy production

	Temp. [K]	max($d\sigma/dT$) [K^{-1}]	Final $\Delta\sigma$
Taus	5.26E+12	1.52E-24	1.35E-11
Muons	3.04E+11	4.68E-19	1.34E-7
Electrons	9.93E+8	2.18E-8	2.39E+1
All at dc	1.00E+10	4.38E-13	7.10E-4

If we look more closely at $d\sigma/dT$ in the upper panel of Fig. 3 we see that the entropy production shares shape with the bulk viscosity plot in Fig. 2, but with an additional T^{-3} factor. As expected, the entropy production has local maxima slightly to the colder end of the scale compared to the bulk viscosity. We find the local peaks for the tau and muon and neutrino roughly one-fourth that of their mass equivalent. For the hypothetical electron peak, this is roughly a sixth of its mass equivalent. The local peak values of $d\sigma/dT$ increases roughly as $T^{-4.4}$ ($T^{-4.43}$ between the tau and muon peaks, and $T^{-4.29}$ between the muon and electron peaks).

6.2 Entropy production at different decoupling temperatures

The total entropy production during the lepton era is extremely dependent on the temperature at the neutrino decoupling. If the neutrinos decouple at $T = 10^{10}$ K we get an increase of entropy by about 0.071 %. Using a colder decoupling temperature of $k_B T = 1$ MeV ($T = 1.16 \times 10^{10}$ K) we get a much smaller value, with $\Delta\sigma = 0.017 \%$. Figure 4 shows the entropy production at different decoupling temperatures.

6.3 Entropy production at high temperatures

In Fig. 5 we plot the evolution of the entropy production by temperature ($d\sigma/dT$), and total entropy production ($\Delta\sigma$) due to the three charged lepton pairs multiplied by T^8 and T^7 . For high temperatures where the particle ratio³ is essentially constant, the entropy production grows steadily as T^{-8} . We see some deviations of this trend for the neutrino-electron produced entropy (and slightly for the neutrino-muon equivalent). This has two reasons. Firstly, the temperature decreases slower when the effective degrees of

³I.e. when the creation rate and annihilation rate of the massive charged leptons are the same.

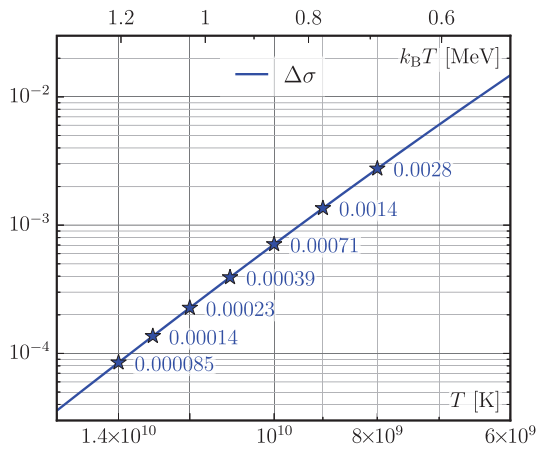


Fig. 4 A closer look at the total increase in entropy ($\Delta\sigma$) zoomed in around the decoupling temperature. The total increase in entropy grows roughly as $T^{-6.2}$ around $T = 10^{10}$ K. The final value of $\Delta\sigma$ is therefore very sensitive to the actual temperature at decoupling. $\Delta\sigma$ for different decoupling temperatures at intervals of 1 billion kelvins are marked with blue stars

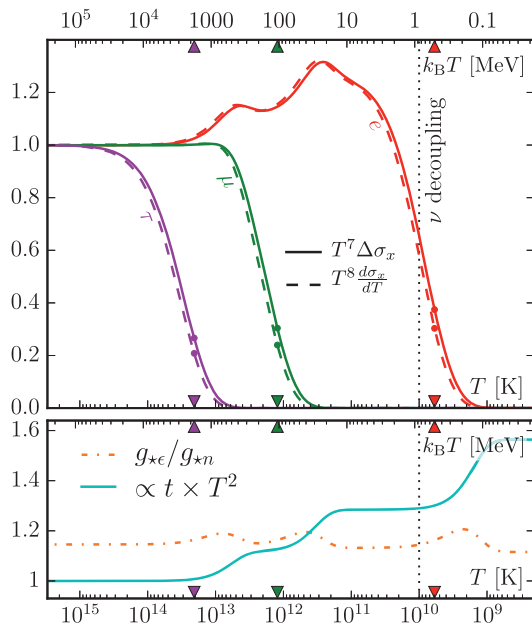


Fig. 5 Upper panel: the rate of change for $T^8 d\sigma/dT$ (shown in dashed lines) and $T^7 \Delta\sigma$ (shown in solid lines) is constant for high temperatures, and are here normalized to one. We have here plotted the contributions due to the different charged leptons in magenta (taus), green (muons), and red (electrons). The fluctuations we see in the electron (and barely in the muon) case are due to changes in $g_{*ε}/g_{*n}$ and the time-temperature relation during particle annihilations. During this process $g_{*ε}$ decreases and the temperature decreases slower with time. These two effects are shown specifically in the lower panel

freedom ($g_{*ε}$) decreases, and secondly the energy per particle first increases (because of the rest mass contribution of the massive particles) and then decreases (when the massive particles disappear). These two effects are shown in the lower plot in Fig. 5.

6.4 Calculation method

Our results are based on the viscosity calculated by Husdal (2016b). These are calculated for 105 different temperatures, with higher densities at regions with higher particle annihilation rates, and around the neutrino decoupling temperature as this is when the entropy production is at its highest. These points are interpolated using Python's SciPy package of the cubic kind. The number of steps for our numerical integration was crucial. Smaller steps equaled a smaller entropy production. Our experience was a convergence towards $\Delta\sigma = 0.071\%$ with 1000 steps per decade. 10 steps per decade would give us $\Delta\sigma = 0.30\%$. We used 100000 steps per decade from temperatures of 10^{16} K to 1.6×10^8 K.

6.5 Difference from the Caderni and Fabbri paper

Our entropy is lower than that by Caderni and Fabbri (1977) by about two-thirds. This is uneasy because our viscous factor is 5 times as large. Using the viscosity as given by Caderni and Fabbri (1977) in our model for calculating entropy we get an end-result of 0.015 %, roughly 7 times smaller than their value of 0.11 %. Our numerical integration required a relatively high precision before converging to our given value. Using 10 steps per decade of temperature gave us an end result roughly five times larger than our high precision integration. If $\Delta\sigma$ would continue to grow as T^{-7} (in the e^+e^- case) its value would be roughly twice as large. Whether or not these arguments were considered by the Caderni and Fabbri (1977) unclear to us. However, we note that the sensitivity around the decoupling temperature requires a high precision numerical integration in this region. The differences from including the muon and tau particles is small (almost negligible) for the $\Delta\sigma$ value at the time of neutrino decoupling.

7 Conclusions

For high temperatures with a stable particle ratio, the entropy production ($d\sigma/dT$) grows as T^{-8} , while the total increase in entropy ($\Delta\sigma$) grows as T^{-7} . At the time of neutrino decoupling $\Delta\sigma$ grows roughly as $T^{-6.2}$. The time of decoupling and how this happens is, therefore, essential to get a precise value for $\Delta\sigma$. Our model shows an increase in the entropy by 0.071 % at $T = 10^{10}$ K, but this value will change a lot for small changes in the decoupling temperature. Using a decoupling temperature of 1 MeV we get

$\Delta\sigma = 0.027\%$. Our result is two-thirds of that found by Caderni and Fabbri (1977). This is a bit peculiar as our (and Hoogeveen et al.'s) viscous term is roughly 5 times larger. For a more precise estimate of the entropy production during the lepton era, a rigorous theory of the decoupling should be used.

Acknowledgements We would like to thank Kåre Olaussen for inspiration and Eirik Løhaugen Fjærbu for help with Python coding.

References

- Bennett, C.L., et al.: *Astrophys. J. Suppl. Ser.* **208**, 20 (2013). doi:10.1088/0067-0049/208/2/20
- Brevik, I., Heen, L.T.: *Astrophys. Space Sci.* **219**, 99 (1994). doi:10.1007/BF00657862
- Caderni, N., Fabbri, R.: *Phys. Lett. B* **69**, 508 (1977). doi:10.1016/0370-2693(77)90856-5
- de Groot, S.R., van Leeuwen, W.A., van Weert, C.G.: *Relativistic Kinetic Theory: Principles and Applications*. North-Holland, Amsterdam (1980)
- Dobado, A., Llanes-Estrada, F.J., Rodriguez-Fernandez, D.: *Int. J. Mod. Phys. A* **31**(20n21), 1650118 (2016). arXiv:1507.06386. doi:10.1142/S0217751X16501189
- Hoogeveen, F., Van Leeuwen, W.A., Salvati, G.A.Q., Schilling, E.E.: *Physica A* **134**(2), 458 (1986). doi:10.1016/0378-4371(86)90059-2
- Husdal, L.: *Galaxies* **4**, 78 (2016a). doi:10.3390/galaxies4040078
- Husdal, L.: *Astrophys. Space Sci.* **361**(8), 1 (2016b). doi:10.1007/s10509-016-2847-4
- Kapusta, J., Muller, B., Rafelski, J.: *Quark Gluon Plasma: Theoretical Foundations: An Annotated Reprint Collection*. Elsevier, Amsterdam (2003)
- Olive, K.A., et al.: *Chin. Phys. C* **38**, 090001 (2014). doi:10.1088/1674-1137/38/9/090001
- van Erkelens, H., van Leeuwen, W.A.: *Physica A* **91**(1–2), 88 (1978). doi:10.1016/0378-4371(78)90059-6
- van Erkelens, H., van Leeuwen, W.A.: *Physica A* **101**(1), 205 (1980). doi:10.1016/0378-4371(80)90109-0
- van Leeuwen, W.A., Salvati, G.A.Q., Schelling, E.E.: *Physica A* **136**(2–3), 417 (1986). doi:10.1016/0378-4371(86)90259-1
- Weinberg, S.: *Astrophys. J.* **168**, 175 (1971). doi:10.1086/151073